

A Hybrid Approach to Improve the Design of Stilling Basin



A Hybrid Approach to Improve the Design of Stilling Basin

By

Abdelazim M. Ali
Ahmed El-Belasy
Mohamed Roushdy
Mohamed Bahgat
Abdelhamid Abdelhaq
Karima Attia
Medhat Aziz
Mohamed Ali Hamed
Heba El Sersawi
Sonia El-Serafy
Peter Ryad
Mohamed El-Zeir
Moahmed Sobeih
Essam El-Din

Coordinated by

**Dr. Ahmed Sayed Mohamed Ahmed
Hydraulics Research Institute**

NBCBN Egypt Node
Hydraulics Research Institute

Country Coordinator
Prof. Dr. Fathi El-Gamel

2010

Produced by the
Nile Basin Capacity Building Network
(NBCBN-SEC) office

Disclaimer

The designations employed and presentation of material and findings through the publication don't imply the expression of any opinion whatsoever on the part of NBCBN concerning the legal status of any country, territory, city, or its authorities, or concerning the delimitation of its frontiers or boundaries.

Copies of NBCBN publications can be requested from:
NBCBN-SEC Office
Hydraulics Research Institute
13621, Delta Barrages, Cairo, Egypt
Email: nbcbn-sec@nbcbn.com
Website: www.nbcbn.com

Project Title**Knowledge Networks for the Nile Basin**

Using the innovative potential of Knowledge Networks and CoP's in strengthening human and institutional research capacity in the Nile region

Implementing Leading Institute

UNESCO-IHE Institute for Water Education, Delft, The Netherlands (UNESCO-IHE)

Partner Institutes

Ten Selected Universities and Ministries of Water Resources from Nile Basin Countries

Project Secretariat Office

Hydraulics Research Institute – Cairo - Egypt

Beneficiaries

Water Sector Professionals and Institutions in the Nile Basin Countries

Short Description

The idea of establishing a Knowledge Network in the Nile region emerged after encouraging experiences with the first Regional Training Centre on River Engineering in Cairo since 1996. In January 2002 more than 50 representatives from all ten Nile basin countries signed the Cairo Declaration at the end of a kick-off workshop was held in Cairo. This declaration in which the main principles of the network were laid down marked the official start of the Nile Basin Capacity Building Network in River Engineering (NBCBN-RE) as an open network of national and regional capacity building institutions and professional sector organizations.

NBCBN is represented in the Nile basin countries through its nine nodes existing in Egypt, Sudan, Ethiopia, Tanzania, Uganda, Kenya, Rwanda, Burundi and D. R. Congo. The network includes six research clusters working on different research themes namely: Hydropower, Environmental Aspects, GIS and Modelling, River Morphology, flood Management, and River structures.

The remarkable contribution and impact of the network on both local and regional levels in the basin countries created the opportunity for the network to continue its mission for a second phase. The second phase was launched in Cairo in 2007 under the initiative of; Knowledge Networks for the Nile Basin. New capacity building activities including knowledge sharing and dissemination tools specialised training courses and new collaborative research activities were initiated. The different new research modalities adopted by the network in its second phase include; (i) regional cluster research, (ii) integrated research, (iii) local action research and (iv) Multidisciplinary research.

By involving professionals, knowledge institutes and sector organisations from all Nile Basin countries, the network succeeded to create a solid passage from potential conflict to co-operation potential and confidence building between riparian states. More than 500 water professionals representing different disciplines of the water sector and coming from various governmental and private sector institutions selected to join NBCBN to enhance and build their capacities in order to be linked to the available career opportunities. In the last ten years the network succeeded to have both regional and international recognition, and to be the most successful and sustainable capacity building provider in the Nile Basin.

1	INTRODUCTION	1
1.1	General.....	1
2	OVERVIEW ON THE HYDRAULIC PERFORMANCE OF THE STILLING BASIN.....	2
2.1	The Stilling Basins – An Overview	2
2.2	Hydraulic Jumps – Definition Sketch.....	2
2.2.1	Historical background of hydraulic jumps	2
2.2.2	Functions of hydraulic jumps	3
2.2.3	Parameters defining the hydraulic jumps	3
2.2.4	Types of hydraulic jumps	4
2.2.5	Control of jumps using stilling basins	5
2.3	Stilling Basins - Technical Data	6
2.3.1	Definition.....	6
2.3.2	Historical background on stilling basins in Egypt.....	7
2.3.3	Stilling basins types.....	12
3	PHYSICAL MODELING OF THE STILLING BASIN	15
3.1	General.....	15
3.1.1	Procedures for designing the physical model.....	15
3.1.2	Classification of physical models.....	16
3.2	Physical Model Experiments of Stilling Basins.....	16
3.2.1	Hydraulic Jump Experiments	16
3.2.2	Scour Downstream Hydraulic Structures Experiments.....	17
3.2.3	Summary	19
3.3	Stilling Basin of Egyptian Barrages.....	19
3.4	Identification of the Problem	20
3.5	Objectives of the Study	20
3.6	Methodology	20
3.7	Execution	20
3.8	Model Similarity	21
3.9	The Experimental Installation	22
3.10	Construction of the Physical Model.....	25
3.11	Measuring Devices	30
3.12	Calibration of the Measuring Devices.....	32
3.13	Model Test Program	34
3.14	Geometric Variables.....	34
3.15	Hydraulic Variables.....	35
3.16	Test Series Description.....	36
3.17	Test Procedures	39
3.18	The Undertaken Measurements.....	39
3.19	Velocity Measurements	39
3.20	Scour Profile Determination.....	40
3.21	Characteristics of the Flow under gate and Hydraulic Jump.....	40
3.22	Measuring the Length of the Reverse Flow Lrf	41
3.23	Results.....	41
3.23.1	The velocity distribution	42
3.23.2	The near bed velocity	44
3.23.3	Scour downstream the apron	44
3.23.4	The characteristics of the submerged hydraulic jump.....	44
4	NUMERICAL MODEL SIMULATIONS OF STILLING BASIN.....	46
4.1	Introduction.....	46

4.3	General.....	48
5.3	Problem definition and analysis.....	48
4.4	Objectives	48
4.5	Physical & Numerical models	48
4.6	The Case Study	49
4.7	The Numerical Model (Delft 3D) Setup and Operation	50
4.8	Results and Analysis	52
4.8.1	Fully Open Gates and Uncontrolled Upstream Water Level	52
4.8.2	Discharge Capacity (Rating Curve)	53
4.8.3	Water Levels.....	53
	Velocities near the variable bed along the longitudinal section	61
4.9	Partially Open Gate.....	64
4.10	Test Procedure	74
4.11	Gate openings calibration using the new option (Barrier).....	78
4.12	Results and Analysis	81
	Velocities Profiles	81
4.12.1	Sensitivity Analysis.....	84
5	DISCUSSION AND REMARKS.....	115
5.1	General.....	115
5.2	Comparison of Physical & Numerical models.....	115
5.3	Limitations of the models	115
6	CONCLUSIONS AND RECOMMENDATIONS.....	117
6.1	Conclusions.....	117
6.2	Recommendations.....	118
7	REFERENCES	119

LIST OF RESEARCH GROUP MEMBERS

LIST OF FIGURES

Figure 2-1:	Definition sketch of the hydraulic jump	2
Figure 2-2:	Length in Terms of Sequent Depth [Bureau of Reclamation (1955)]	4
Figure 2-3:	Classifications of Hydraulic Jumps	5
Figure 2-4:	Longitudinal Section of the New Esna Spillway Stilling Basin, Sogreah 1984	8
Figure 2-5:	Longitudinal Section of the New Naga Hammadi Spillway Stilling Basin, Lahmeyer (1997)	8
Figure 2-6 :	Experimental relations for sharp crested weir [Chow (1988)]	9
Figure 2-7:	Broad crested weir [Chow (1959)]	10
Figure 2-8:	The relations between f_1 , y_3/y_1 , and z/y_1 for abrupt rise	10
Figure 2-9:	The effect of negative step on hydraulic jumps	11
Figure 2-10:	Experimental and analytical relations for abrupt drop.....	11
Figure 2-11:	Counter flow	12
Figure 2-12:	Definition sketch for stilling basins	13
Figure 2- 13:	USBR TYPE III stilling basin	13
Figure 2-14:	USBR TYPE IV stilling basin	14
Figure 2-15:	SAF stilling basin (Blaisdell, 1959)	14
Figure 3-1:	Details of the flume and model arrangements	23
Figure 3-2:	Flume entrance	24
Figure 3-3:	Flume exit	25
Figure 3-4:	Sieve analysis of sand, filter, and rip rap materials	28
Figure 3-5 a:	Model Construction	29
Figure 3-5 b:	Model Construction	30

Figure 3- 6: Sluiceway stilling basin with parabolic slope, test series A	37
Figure 3-7: Sluiceway stilling basin with linear slope, test series B	37
Figure 3-8: Sluiceway stilling basin with double parabolic slope, test series C.....	38
Figure 3-9: Sluiceway stilling basin with horizontal apron, test series D	38
Figure 3-10: Sluiceway stilling basin with linear slope and raised apron	39
Figure 3-11: locations of the velocity measurements	40
Figure 3-12: Typical scour profile downstream apron	40
Figure 3-13: The measured flow and the submerged hydraulic jump parameters.....	41
Figure 3-14: Length of the reverse flow	41
Figure 3-15: Velocity distribution downstream the gate, test No. 4, series A.....	42
Figure 3-16: Velocity distribution downstream the gate, test No. 4, series B	42
Figure 3-17: Velocity distribution downstream the gate, test No. 4, series C	42
Figure 3-18: Velocity distribution downstream the gate, test No. 4, series D.....	42
Figure 3-19: Velocity distribution downstream the gate, test No. 5, series A.....	43
Figure 3-20: Velocity distribution downstream the gate, test No. 5, series B	43
Figure 3-21: Velocity distribution downstream the gate, test No. 5, series C	43
Figure 3-22: Velocity distribution downstream the gate, test No. 5, series D.....	43
Figure 3-23: the near bed velocity distribution downstream the gate, series A.....	44
Figure 3-24: the scour profiles downstream the apron, test No. 4, series A.....	44
Figure 4-1: Longitudinal Section of the New Naga Hammadi Spillway Stilling Basin (HRI 1998)	49
Figure 4-2: Location of New Naga Hammadi Barrage	50
Figure 4-3: The observation points along the horizontal grid	52
Figure 4-4: Rating curves using 1D Model and d' Aubuisson Formula.....	53
Figure 4-5: Upstream water levels.....	55
Figure 4-6: water levels upstream the sill and water levels over the sill (52.80)	56
Figure 4-7: Water drop over sills (52.80) and (53.45).....	57
Figure 4-8: Water drop over sills (52.80) & (53.45)	57
Figure 4-9: Total Head loss for sill levels (52.80) & (53.45).....	59
Figure 4-10: total head losses for different models	59
Figure 4-11: Velocities at u/s and d/s gauge stations, sill level (52.80)	60
Figure 4-12: Velocities at u/s and d/s gauge stations, sill level (53.45)	60
Figure 4-13: Tailwater and conjugate depth.....	65
Figure 4-14: The hydraulic jumps according to Z Grid (Q = 4000 m ³ /s)	66
Figure 4-15: The velocity distribution at section X-X (Z-Grid).....	66
Figure 4-16: Froude Number at the Vena-Contracta.....	67
Figure 4-17: Head Losses in partially open gate	69
Figure 4-18: Discharge Coefficients for submerged hydraulic jump (US Army)	71
Figure 4-19: The new studied profile (Abdel Azim, 2005)	72
Figure 4-20: The new bathymetry	73
Figure 4-21: The roughness map	74
Figure 4-22: Gate openings vs. the discharges for constant head (H = 6.93 m).....	77
Figure 4-23: A definition sketch for partially open gate	78
Figure 4-24: losses coefficients in case of 1D model	79
Figure 4-25: losses coefficients in case of 2DV models.....	81
Figure 4-26: The different locations for the velocity measurements in the flume	81
Figure 4-27: Velocity profiles for test group A1	82
Figure 4-28: Velocity profiles for test group A7	82
Figure 4-29: The submerged hydraulic jump	112
Figure 4-30: The submerged jump length	112
Figure 4-31: approximate estimation for the submerged jump length	113
Figure 4-32: the submerged jump length.....	114

LIST OF TABLES

Table 2-1: Classification of Jump According to Mccorquodale (1986)	6
Table 2-2: Structures Along the Nile River	7
Table 3-1: Properties of the sand base	26
Table 3-2: Sieve analysis of the sand base	26
Table 3-3: Sieve analysis of the filter	27
Table 3-4: Sieve analysis of the rip rap layer	28
Table 3-5: Summary of the material characteristics	28
Table 3-6: Geometric variables of the tested stilling basin	35
Table 3-7: The Hydraulic Variables	36
Table 3-8: The test programme applied for all test series	36
Table 3-9: Results of the Submerged Hydraulic Jump Parameters	45
Table 4-1: Summary for the important computational parameters	51
Table 4-2: The Flume Data	52
Table 4-3: Water levels from the flume Data in case of fully open gate and sill level (52.80)	53
Table 4-4: Upstream water levels	55
Table 4-5: Water drop over sills	56
Table 4-6: Total Head loss between sections CS1 and CS2	58
Table 4-7: Velocities at u/s and d/s gauge stations at one meter above the bed	60
Table 4-8: Upstream Velocity Measurements above variable bed for Fully Open Gate	61
Table 4-9: Downstream Velocity Measurements above variable bed for Fully Open Gate	63
Table 4-10: Measured and calculated parameters	65
Table 4-11: Froude Number at the Vena-Contracta	67
Table 4-12: Head Losses in partially open gate	68
Table 4-13: Head losses in partially and fully open gates	69
Table 4-14: Energy losses in partially open gates	70
Table 4-15: Gate openings from the 1D model and theoretical analysis	71
Table 4-16: some of the new obtained flume results	74
Table 4-17: The Prototype Results	76
Table 4-18: Gate Calibration in case of 1D Model	78
Table 4-19: Gate Calibration in case of 2DV Model	80
Table 4-20: the velocity values in the flume	82
Table 4-21: the velocity values in the prototype	83
Table 4-22: Velocity profiles in the Vertical Direction ($Q = 383.97 \text{ m}^3/\text{s}$)	85
Table 4-23: Velocities in the longitudinal direction ($Q = 383.97 \text{ m}^3/\text{s}$)	87
Table 4-24: Velocity profiles in the Vertical Direction downstream the sill (for $Q = 383.97 \text{ m}^3/\text{s}$ only)	91
Table 4-25: Velocities in the longitudinal direction downstream the sill (for $Q = 383.97 \text{ m}^3/\text{s}$ only)	93
Table 4-26: the velocity profiles in the vertical direction	98
Table 4-27: Velocities in the Longitudinal Direction	107
Table 4-28: calculation of the submerged jump length theoretically	113
Table 4-29: a summary table for all the results regarding the jump length	114
Table 5-1: Limitations of Physical and Numerical Models	116

LIST OF PHOTOS

Photo 3-1: General view of the flume	24
Photo 3-2: The electromagnetic flowmeter	33
Photo 3-3: The ultrasonic flowmeter	33
Photo 3-4: The electromagnetic currentmeter	33
Photo 3-5: point gauge	34
Photo 3-6: used digital camera	34
Photo 3-7: Data Acquisition systems and the data logger	35

This report is one of the final outputs of the research activities under the second phase of the Nile Basin Capacity Building Network (NBCBN). The network was established with a main objective to build and strengthen the capacities of the Nile basin water professionals in the field of River Engineering. The first phase was officially launched in 2002. After this launch the network has become one of the most active groupings in generating and disseminating water related knowledge within the Nile region. At the moment it involves more than 500 water professionals who have teamed up in nine national networks (In-country network nodes) under the theme of “Knowledge Networks for the Nile Basin”. The main platform for capacity building adopted by NBCBN is “Collaborative Research” on both regional and local levels. The main aim of collaborative research is to strengthen the individual research capabilities of water professionals through collaboration at cluster/group level on a well-defined specialized research theme within the field of River and Hydraulic Engineering.

This research project was developed under the “Local Action Research Modality” which has a main objective to contribute to the capacity building process at local level and enhance the collaboration among the researchers and institutions in the same country. This activity is the core activity of all NBCBN nodes and is contributing to the establishment of the in-country network.

This report is considered a joint achievement through collaboration and sincere commitment of all the research teams involved with participation of water professionals from all the Nile Basin countries, the Research Coordinators and the Scientific Advisors. Consequently the NBCBN Network Secretariat and Management Team would like to thank all members who contributed to the implementation of these research projects and the development of these valuable outputs.

Special thanks are due to UNESCO-IHE Project Team and NBCBN-Secretariat office staff for their contribution and effort done in the follow up and development of the different research projects activities.

Ir. Jan Luijendijk

Project Director
UNESCO-IHE
j.luijendijk@unesco-ihe.org

Eng. Amel M. Azab

Network Manager
NBCBN-SEC. Office
a_azab@nbcbn.com

The research group would like to acknowledge the contribution of Mr. Peter Riyad in this research. Chapter 4 of this report includes the main contribution by Mr. Ryad who successfully graduated from his MSc course at UNESCO_IHE in Delft, The Netherlands. His thesis has been elaborated in a sandwich program. During the periods spent at HRI he was closely working with HRI staff and with the members of the local action team. A part of his work has also been presented during the international conference Hydropower 2008, Slovenia, October 2008.

1

INTRODUCTION

1.1 General

In the framework of activating and improving the collaboration between local institutions in each Nile Basin Countries, the Nile Basin Capacity Building Network (NBCBN) has initiated and supports a research program with a so-called local action research project that has been activated during the workshop organized in Cairo from 5-7 March 2007. Amongst this program is to strengthening the collaborative work between the Egyptian institutions working in the water sector. The involved Egyptian institutions are as follows:

- 1- Ain Shams University
- 2- Hydraulics Research Institute, National Water Research Center
- 3- Menia University
- 4- Menofia University
- 5- Nile Research Institute, National Water Research Center

The research point was properly selected to meet the most critical research interest for most of the involved institutions in order to make sure that the professional experience of the above mentioned institutions are fully utilized. It is intended that the selected research topic represents a practical problem that can be applied to many of the Nile Basin Countries. This includes the design of an energy dissipating structure which is called the stilling basin. The research topic pertaining to stilling basin has been described in the research methodology that is divided into stages. These stages are to:

- Provide an overview on the stilling basin,
- collect the available data,
- construct and conduct a physical model study,
- develop or adopt a numerical model

The developed or adopted numerical model would eventually be utilized to investigate the flow field in the stilling basin and derive the flow conditions that will be employed in designing the stilling basin.

This report covers all tasks of the project that are summarized in chapter as follows:

- Chapter 2: provides an overview on the stilling basin,
- Chapter 3 discussed all related physical model simulations on stilling basin as well as the flume experimental works.
- Chapter 4 explains the numerical model simulations on stilling basin and its hydraulic performance. This chapter includes also description of the utilized numerical model, the case study and numerical model results.

2

OVERVIEW ON THE HYDRAULIC PERFORMANCE OF THE STILLING BASIN

2.1 The Stilling Basins – An Overview

This chapter thus introduces, in details, the following:

- Hydraulic jumps in technical terms
 - historical background of hydraulic jumps
 - functions of hydraulic jumps
 - parameters defining the hydraulic jumps
 - types of hydraulic jumps
 - control of jumps using stilling basins
- Stilling basin in technical terms
 - historical background of stilling basins
 - stilling basins types

2.2 Hydraulic Jumps – Definition Sketch

Hydraulic jumps are natural phenomena that occur due to the conflict between the upstream and downstream controls influencing the same reach of a channel, Fig. (2-1). For example, if the upstream control causes supercritical flow, then a hydraulic jump is the only mean to resolve this transition by forming significant turbulence and dissipating the energy.

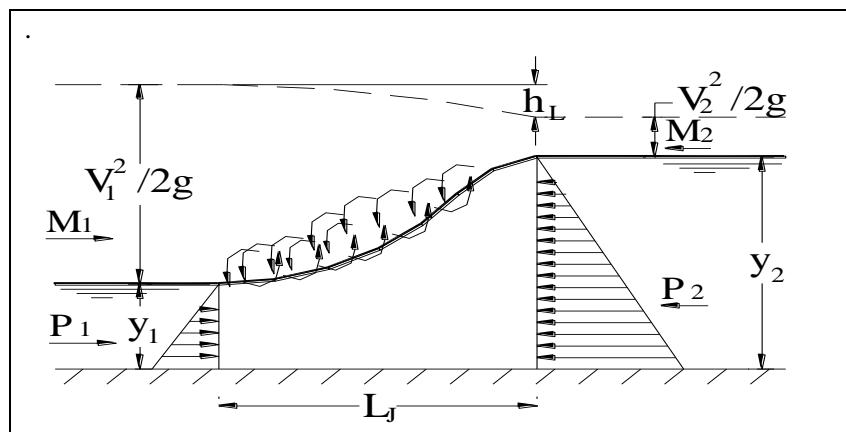


Figure 2-1: Definition sketch of the hydraulic jump

2.2.1 Historical background of hydraulic jumps

Talking about the historical background of the hydraulic jumps, one has to mention the following names and their achievements:

- *Leonardo Da Vinci (1480)* was the first one to observe the hydraulic jump, Rouse and Simon (1957).

- **Venture (1797)** was also among the early researchers who dealt with the jumps where he mentioned that a hydraulic jump can be used only to raise the water depth for drainage problems, Rouse and Simon (1957).
- **Bidone (1820)** was also the first one to mention it in his memoirs, Bakhmeteff and Matzke (1935).
- **Belanger (1828)** was the first one to find a theoretical solution for the relative depth of the jump using the momentum and the continuity equations, for a steady flow in horizontal channel with constant bed width.

Since then, many researchers have studied this phenomenon trying to study all the cases and types of jumps and the different ways to control the hydraulic jumps and also they tried to indicate how to use them as energy dissipaters.

2.2.2 Functions of hydraulic jumps

The hydraulic jump has many applications. Chow (1959) and (1988) cited them in the field of open channel flow that they can:

- dissipate energy in hydraulic structures thus preventing scour at their downstream
- reduce the net uplift pressure under the hydraulic structures
- raise the water level on the downstream side of the structures
- increase the discharge of a sluice gate
- aerate flows and de-chlorinate wastewaters
- remove air pockets from open channel flows
- mix chemicals used for water purification

2.2.3 Parameters defining the hydraulic jumps

Many parameters define the hydraulic jump properties. Also, many equations were set to inter-relate these parameters. These are some of them:

- **Belanger (1828)** interrelated the depths upstream and downstream of the hydraulic jump by a simplified equation, as follows:

$$\frac{y_2}{y_1} = 0.5 \left(\sqrt{1 + 8F_1^2} - 1 \right) \quad (2-1)$$

where:

y_1 and y_2 : are the initial and sequent depth
 F_1 : the initial Froude number

- **Chow (1959) and (1988)** presented the following formula to express the energy loss as:

$$DE = E_1 - E_2 = \frac{(y_2 - y_1)^3}{4y_1 y_2} \quad (2-2)$$

where:

E_1, E_2 : specific energy before and after the jump

- **Subramania (1982)** gave an equation to estimate the energy loss as a function of the initial Froude number as:

$$\frac{\Delta E}{E_1} = \frac{\left(-3 + \sqrt{1 + 8F_1^2} \right)^3}{8(2 + F_1^2) \left(-1 + \sqrt{1 + 8F_1^2} \right)} \quad (2-3)$$

- **Chow (1959)** expressed the efficiency of the jump as follows:

$$\eta = \frac{E_2}{E_1} = \frac{(8F_1^2 + 1)^{3/2} - (4F_1^2 - 1)}{8F_1^2(2 + F_1^2)} \quad (2-4)$$

- **Chow (1959)** derived a formula for the height of the hydraulic jump, as follows:

$$\frac{H_J}{E_1} = \frac{y_2 - y_1}{E_1} = \frac{\sqrt{1 + 8F_1^2} - 3}{F_1^2 + 2} \quad (2-5)$$

- **The Bureau of Reclamation (1955)** presented a plot to L_j/y_2 versus F_1 as shown in Fig. (2-2). Also, the length of the jump cannot be determined theoretically, but it was investigated experimentally as:

$$L_j = 6.9 (y_2 - y_1) \quad (2-6)$$

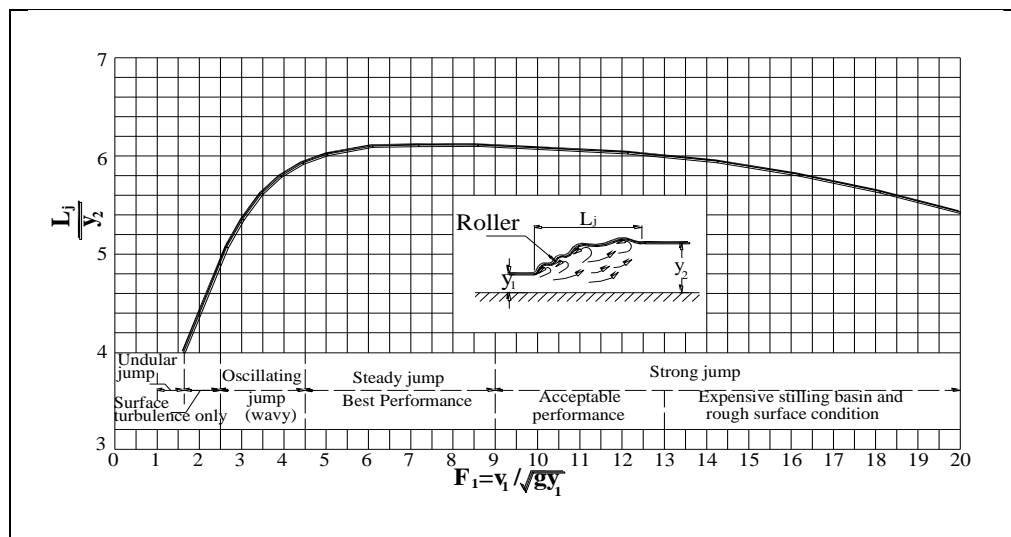


Figure 2-2: Length in Terms of Sequent Depth [Bureau of Reclamation (1955)]

2.2.4 Types of hydraulic jumps

As a result of extensive studies, different researchers gave different classification to hydraulic jumps:

- **Bradley and Peterka (1957)** classified the hydraulic jumps into five categories based on the value of the initial Froude number F_1 . These five categories are illustrated in Fig. (2-3). Descriptions of the classifications are described as follows:
 - Undular Jump ($1.0 < F_1 \leq 1.7$)
 - Weak Jump ($1.7 < F_1 \leq 2.5$)
 - Oscillating Jump ($2.5 < F_1 \leq 4.5$)
 - Steady Jump ($4.5 < F_1 \leq 9.0$)
 - Strong Jump ($F_1 > 9.0$)
- **McCorqudale, (1986)** presented another classification of the hydraulic jumps based on the different circumstances, Table (2-1). These are:
 - bed slope (horizontal or sloping)

- plan or shape of the boundary (rectangular – radial diverging – radial converging – abrupt expansion)
- submergences (emerged – submerged)
- appurtenances (unforced – forced)

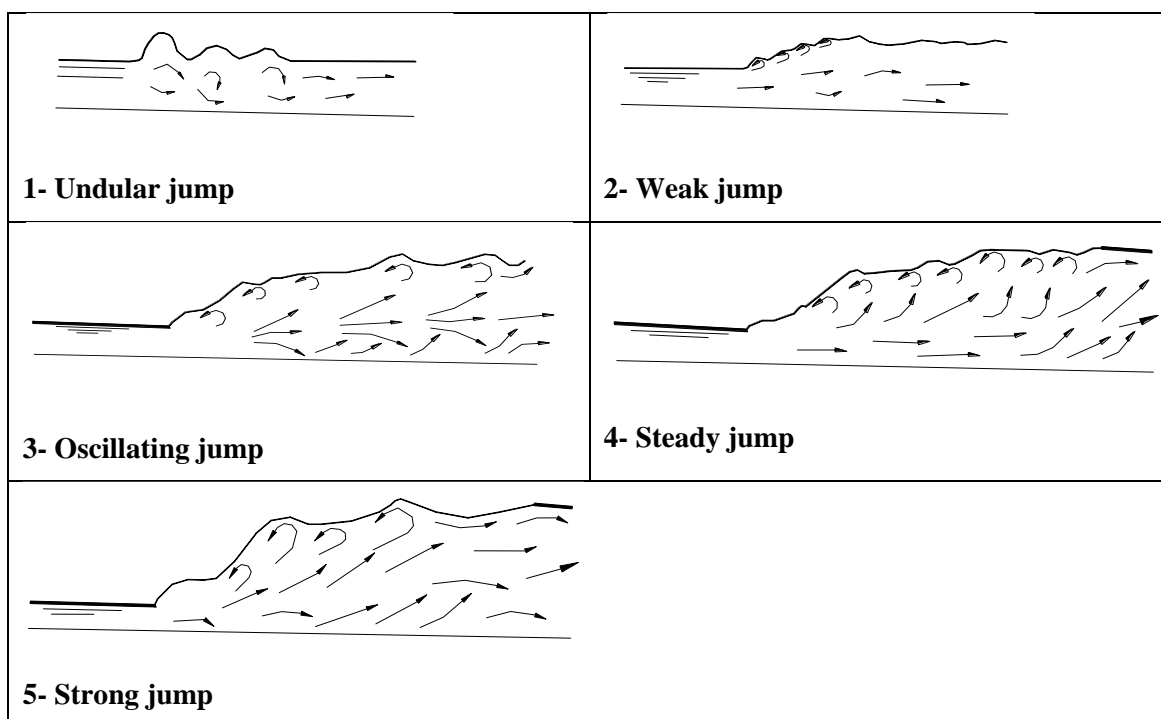


Figure 2-3: Classifications of Hydraulic Jumps

2.2.5 Control of jumps using stilling basins

The hydraulic jump can be controlled by different methods. The function of these methods is to ensure the formation of a jump within the stilling basin and to control its position under all probable operating conditions.

In other words, "to control" means to force the occurrence of the jump and to control its position, hence, reducing the risk of bed scour after the hydraulic structures. The design of such controlling structures should consider three interrelated parameters:

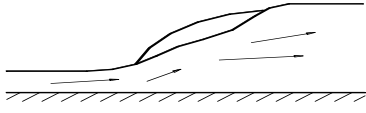

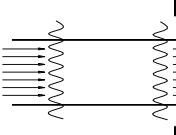
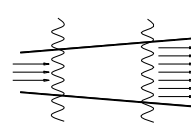
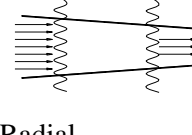
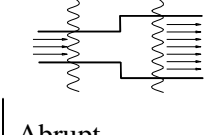
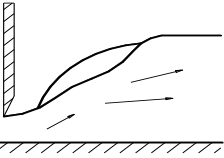
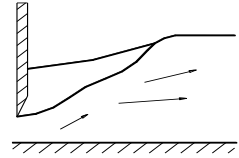
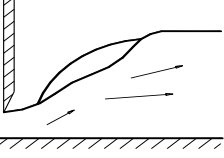
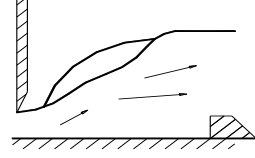
- jump position
- tail water level
- jump type

Mainly, there are two different categories to control the hydraulic jump:

- control by adding structures in the stilling basin
- control by stilling basin modifications

This will lead us to present the stilling basin in technical terms.

Table 2-1: Classification of Jump According to Mccorquodale (1986)

Feature	Examples		
Bed slope	 Horizontal	 Sloping	
Plan or shape of boundary	 Rectangular	 Radial diverging	
		 Radial converging	 Abrupt expansion
Submergence	 Un-submerged (free)	 Submerged	
Appurtenances	 Unforced (free)	 Forced	

2.3 Stilling Basins - Technical Data

2.3.1 Definition

Stilling basins with all its types (USBR, SAF) are external energy dissipaters placed at the outlet of a culvert, chute, or rundown. These basins are characterized by some combination of chute blocks, baffle blocks, and sills designed to trigger a hydraulic jump in combination with a required tail water condition.

The *selection* of a stilling basin depends on several considerations including:

- hydraulic limitations
- constructability
- basin size
- cost

With the required tail water, velocity leaving a properly designed stilling basin is equal to the velocity in the receiving channel. It can be further said that depending on the specific design, they operate over a range of approach flow Froude numbers from 1.7 to 17 according to their type. The range for the USBR Type III is 4.5-17, while that of the USBR Type IV is 2.5-4.5. On the other hand, for the SAF, this range is 1.7 to 17.

To ensure that a stilling basin performs its function efficiently, it should be designed in such a way that the elevation of the tail water depth at the downstream channel is relatively equal to the conjugate depth of jump. Otherwise, the jump will be swept out of the basin or the jump will be drowned. This will lead to the loss of

its function as an energy dissipater. The higher the Froude numbers at the entrance to a basin, the more efficient the hydraulic jump and the shorter the resulting basin. To increase the Froude number, many methods are available, among them, for example, adding an expansion and depression. The expansion and depression converts depth, or potential energy, into kinetic energy by allowing the flow to expand, drop, or both. The result is that the depth decreases and the velocity and Froude number increase.

2.3.2 Historical background on stilling basins in Egypt

As for the historical background of stilling basins in Egypt, many are available in front of the hydraulic structures that are constructed along the Nile River. These structures include dams and storage reservoirs, such as the Old Aswan Dam, Aswan High Dam, Esna Barrage, Naga Hammadi Barrage, Assuit Barrage, Delta Barrage, Zefta Barrage, Idfena Barrage, table 2-2. The following figures describe these existing structures:

Table 2-2: Structures Along the Nile River

Date of Construction	Name	Location(km)	No. of Opening	Water head (m)
1898-1902	Old Aswan Dam	6.5	180	35
1990-1994	New Esna	167.85	11	9.1
1927-1930	Nag Hammadi	359.45	100	4.3
1898-1902	Assiut	544.75	111	4.3
1939	Delta	953.2-	34	3.8
1939	(Damietta) Delta (Rosetta)	953.76	46	3.8
1901-1903	Zefta	1046.7	50	4.0
1985-1988	Faraskour	1164.0	5	2.2
1951	Edfina	1159.0	46	2.7

Some of these barrages suffer from scouring downstream the apron due to the extra head more than the design values. These barrages were rehabilitated and new stilling basins were added. Among these are:

- **New Esna Spillway Stilling Basin:** The spillway of new Esna barrage consists of 11 vents each of 12m in width. Each vent is equipped by radial gate with radius of 14m. There is a raised sill under the gate with elevation of (66.00), followed by a sloping apron with a slope of 1: 5 (the middle apron). The rear apron is with a horizontal length of 25m from the downstream nose of the piers and its elevation is (61.50). There is an end sill with an elevation of (62.00) and the face slope is 1:3. The design overall length of the stilling basin is 60m. Also, the riprap protection was used immediately downstream the apron ranging from 0.20 to 0.50m. During the model tests to the New Esna Barrage, it has been observed that significant scour occurred immediately downstream the stilling basin and exceeded the expected values. Therefore, the physical model was used to improve the stilling basin and the bed protection. Based on the results of the model tests, the stilling basin was then extended by 15m and the bed protection was modified and changed to range between 0.50 and 0.70m.
- **New Naga Hammadi Spillway Stilling Basin:** The spillway of new Naga Hammadi barrage consists of seven vents each of 17m in width. Each vent is equipped with a radial gate with 11m radius. There is a raised sill under the gate with an elevation of (52.80) (for apron), followed by a sloping apron with slope 1: 5 (the middle apron) and the rear apron with a horizontal length of 30m from the

downstream nose of the piers and its elevation is (48.80). The design overall length of the stilling basin is 64m. Also, the riprap protection, which is used immediately downstream the apron, is with D_{50} of 0.39m. During the physical model tests of the New Naga Hammadi Barrage, it has been observed that the significant scour occurred immediately downstream the stilling basin and exceeded the expected values. Therefore, the physical model was used to improve the stilling basin and the bed protection. Based on the results of the model tests, the stilling basin was extended by 24.8m and the bed protection was modified and replaced by $D_{50} = 0.75\text{m}$, Fig. (4).

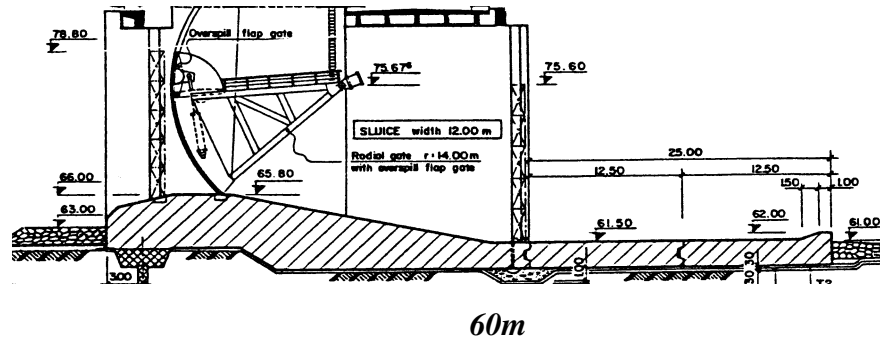


Figure 2-4: Longitudinal Section of the New Esna Spillway Stilling Basin, Sogreah 1984

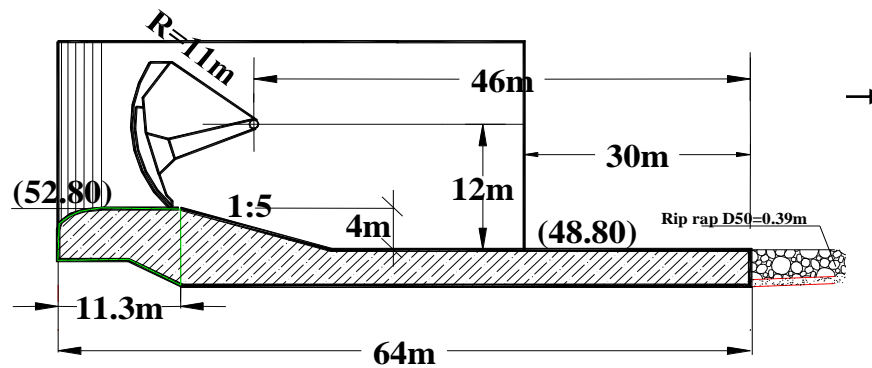


Figure 2-5: Longitudinal Section of the New Naga Hammadi Spillway Stilling Basin, Lahmeyer (1997)

Since stilling basins were originally implemented, they have been modified gradually either by:

- adding structures in the stilling basin
 - sharp crested weir (sill)
 - broad crested weir

Or by:

- modifying the stilling basin
 - rise in bed level (positive step)
 - drop in bed level (negative step)
 - expansion in bed width (gradual or sudden)
 - counter flow
 - rough bed
 - bed slope

Regarding the *sharp crested weir (sills)*, several investigators studied the incorporated parameters in the design and ended to the following relationship,

$$\frac{z_1}{y_1} = \varphi \left(F_1, \frac{X}{y_2}, \frac{y_3}{y_1} \right) \quad (2-7)$$

This equation was further developed by Rageh (1999) who used a continuous sill to reduce the length of jump up to 25% compared with the radial jump without sill. He gave the following relationship:

$$\frac{L_j}{y_1} = 0.61 F_1^{1.4} \left(\frac{X}{Z} \right)^{0.32} \left(\frac{r_2}{r_1} \right)^{0.42} \quad (2-8)$$

where:

- F_1 : Froude number
- z_1 : the height of the sill
- y_1 : the approaching depth
- y_2 : the water depth upstream the sill
- X : the distance from the toe of the jump to the sill
- y_3 : the downstream water depth
- x : the sill location related to the jump upstream end
- r_1, r_2 : are the radius of basin at the beginning and end of jump

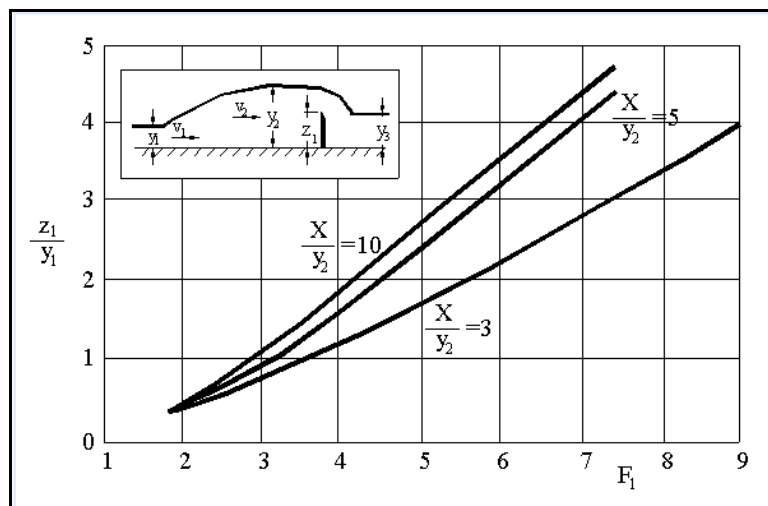


Figure 2-6 : Experimental relations for sharp crested weir [Chow (1988)]

As for controlling by adding broad crested weir, this can only be achieved if the downstream depth is lower than the critical depth on top of the weir. That is, if $y_3 < (2y_2 + z_1)/3$, the tail water will not affect appreciably the relationship between the head water elevation and the discharge. For this condition, a relationship between F_1 and z_1/y_1 can be established, Fig. (2-6), where the length X is given by:

$$X = 5(z_1 + y_3) \quad (2-9)$$

As a comment to end up with, it is said that a broad-crested weir has certain advantages in comparison with some other types of control. It has a greater structural stability than a sharp-crested weir and usually requires lower cost of excavation than an abrupt rise, Chow (1959).

Regarding the modification by adding a rise in bed level (positive step), several investigators studied it. Among them are Foster and Skrinkd (1950) and Chow (1959). They reported that they developed a diagram giving a relationship for F_1 , y_3/y_1 , z_1/y_1 for an abrupt rise of $x = 5(z + y_3)$, where x is the distance from the initial depth to the rise, y_3 is the water depth over the step, and z_1 is the step height, Fig. (7).

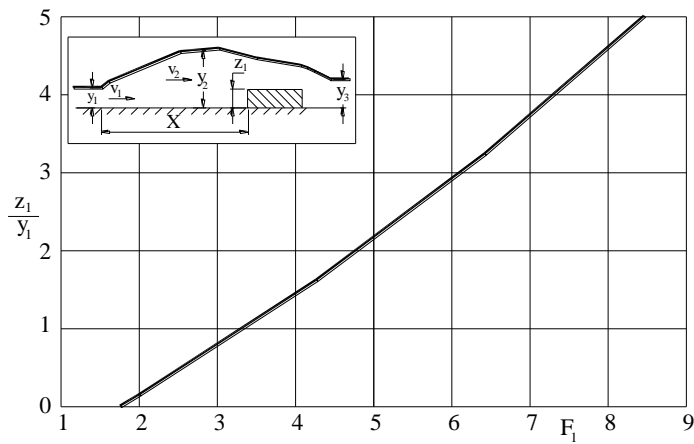


Figure 2-7: Broad crested weir [Chow (1959)]

As for the addition of a *drop in the bed level (negative step)*, Chow (1959) showed that if the downstream depth is larger than the normal depth for a normal jump, a drop in the channel floor must be provided to ensure formation of jump. This condition occurs generally at the end of expansion of a super critical flow, Fig. (9). Also, some experimental studies were carried out and a chart was produced to design the relative height of the drop, Fig. (2-8) and Fig. (2-10).

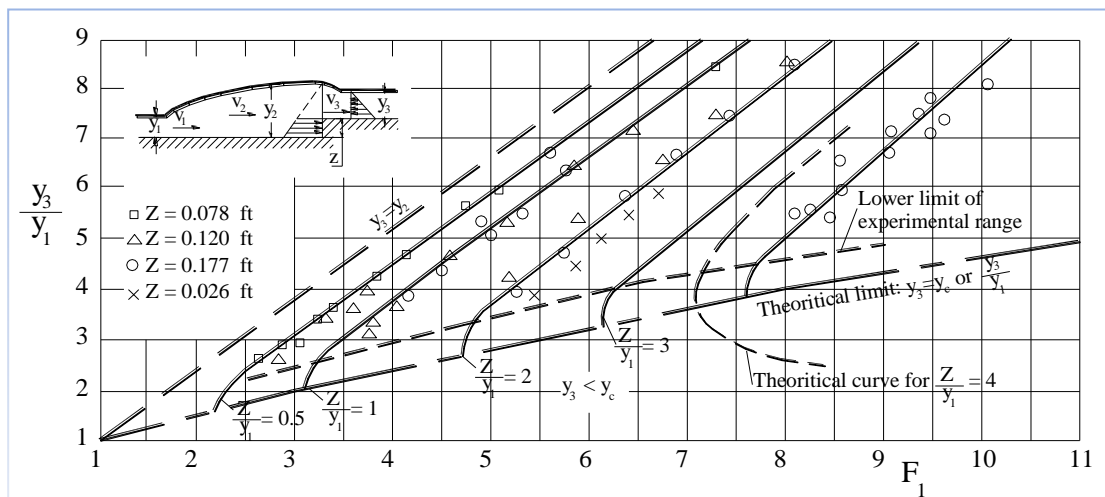


Figure 2-8: The relations between F_1 , y_3/y_1 , and z/y_1 for abrupt rise

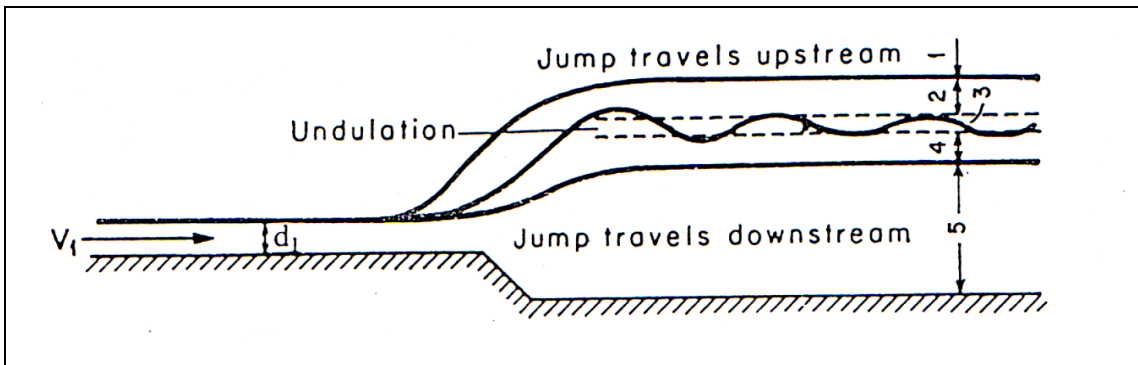


Figure 2-9: The effect of negative step on hydraulic jumps

Also, adding an *expansion in the bed width* is used quite often. The expansion in the bed width in the stilling basin can be gradual or sudden. The sudden expansion may be considered, from the geometric point of view, as a special case from gradual expansion, Herbrand (1973), Khalifa and McCorquodale, (1979) and (1983), Nettleton and McCorquodale (1983), Hager (1985), Abdel-Aal (2000) and Negm (2000).

Regarding the addition of *counter flow*, energy can be dissipated by splitting it into two or more jets and directing them against the original flow, Fig. (2-11). Using counter flows induce many problems, such as the difficulty of field construction, and the possibility of being blocked Vicher and Hager (1999).

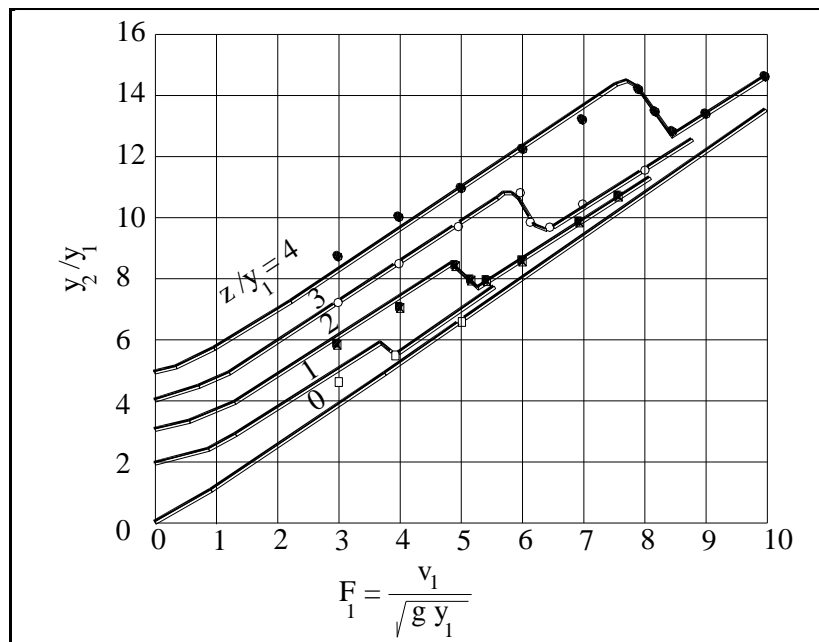


Figure 2-10: Experimental and analytical relations for abrupt drop

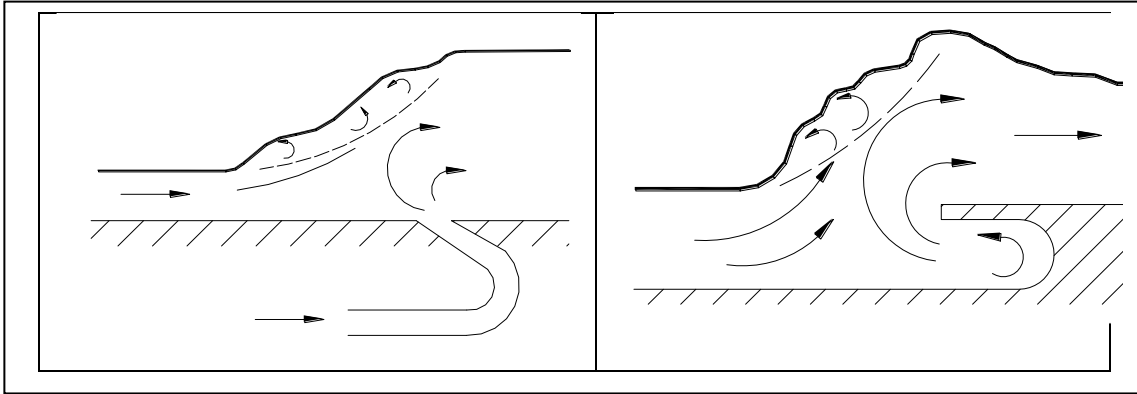


Figure 2-11: Counter flow

As for modifying the basin by *roughening the channel walls* or bed or both is an effective method for controlling the hydraulic jump. There are many methods for roughening the bed or sides. Using baffled apron, series of blocks, series of drops or lateral sill or sills can control the hydraulic jump as well, Hughes W.C. and Ernest Flack (1984). Also, Nettleton and Mc Corquodale (1989) gave a relation to determine the most effective location of baffle blocks as follows:

$$R_b = \frac{r_b}{r_1} = 1 + 0.5 \frac{L_j}{y_1} \quad (2-10)$$

where:

r_b : the radius to the beginning of the baffle blocks

r_1 : the radius to the beginning of the jump

Mohammed (1991) and Hager (1995) did also distinguished work in that field.

Regarding the modification by *adding sloping floor*, Ohtsu and Yasuda (1991) studied the range 0° to 60° of bed slopes, and Froude number that ranged from 1.40 to 4.0. Also, Ahmed et al, (1993) studied the hydraulic characteristics of a B-jump on a sloping channel using three different bed slopes and a range of initial Froude number from 2.4 to 7.4. On the other hand, McCroquodale and Mohamed (1994), Stefano and Alessandro (2000), Eid and Rajaratnam (2002) and Abdel Wehab A. (2002), were among the researchers that studied the addition of sloping floor.

2.3.3 Stilling basins types

Usually, stilling basins are basically defined according to Fig. (2-12). Many researchers then introduced many types of basins. This section introduces some of the types of stilling basins. These are:

- USBR Type III
- USBR Type IV
- SAF

The USBR Type III stilling basins were developed by the United States Bureau of Reclamation (USBR) based on model studies and evaluation of existing basins (USBR, 1987). The USBR Type III stilling basin (USBR, 1987) employs chute blocks, baffle blocks, and an end sill as shown in Fig. (2-13). The basin action is very stable with a steep jump front and less wave action downstream than with the free hydraulic jump. The position, height, and spacing of the baffle blocks should be carefully designed. For example, if the baffle blocks are placed too far at the upstream, wave action in the basin will result. On the other hand, if they were put too far at the downstream, a longer basin will be required. Also, if they were too high, waves can be produced; and if they were too low, the jump will sweep out or rough water may result. The baffle blocks may

be shaped as cubes or sloping cubes. The corners should not be rounded as this reduces energy dissipation. The recommended design of this type is limited to the following conditions:

- The maximum unit discharge should be $18.6 \text{ m}^3/\text{s}/\text{m}$.
- The velocities, entering the basin, should be up to 18.3 m/s .
- The Froude number, entering the basin, should be between 4.5 and 17.
- The tail water elevation should be equal to or greater than the full conjugate depth elevation.

The basin sidewalls should be vertical rather than trapezoidal to insure proper performance of the hydraulic jump.

The USBR Type IV stilling basin (USBR, 1987), Fig. (2-14), is intended for use in the Froude number ranges from 2.5 to 4.5. In this low Froude number range, the jump is not fully developed and the downstream wave action might be a problem. For the intermittent flow encountered at most highway culverts, wave action is not judged to be a severe limitation. The recommended design of this type is limited to the following conditions:

- The basin sidewalls should be vertical rather than trapezoidal to insure proper performance of the hydraulic jump.

Tail water elevation should be equal to or greater than 110 % of the full conjugate depth elevation. The additional tail water improves the jump performance and reduces the wave action (the hydraulic jump is very sensitive to the tail water depth at low Froude numbers for which the basin is applicable).

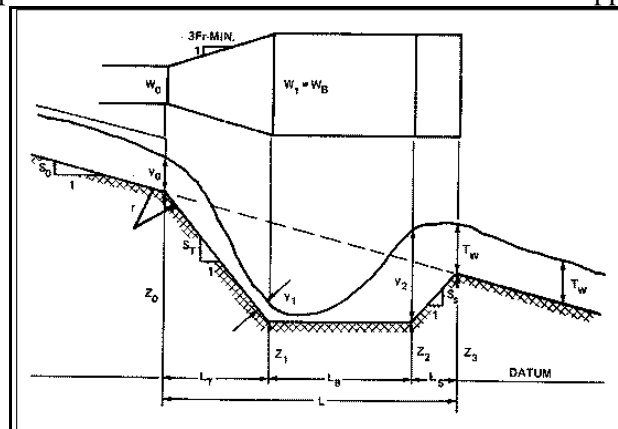


Figure 2-12: Definition sketch for stilling basins

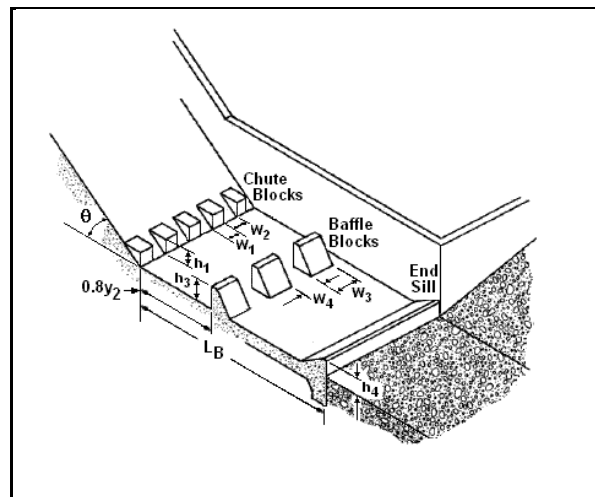


Figure 2-13: USBR TYPE III stilling basin

The St. Anthony Falls (SAF) stilling basin, Fig. (2-15), is based on model studies conducted by the Soil Conservation Service at the St. Anthony Falls Hydraulic Laboratory of the University of Minnesota (Blaisdell, 1959). The Saint Anthony Falls (SAF) stilling basin provides chute blocks, baffle blocks, and an end sill that allows the basin to be shorter than a free hydraulic jump basin. It is recommended for use at small structures such as spillways, outlet works, and canals where the Froude number at the dissipator entrance is between 1.7 and 17. The reduction in basin length achieved through the use of appurtenances is about 80% of the free hydraulic jump length. The SAF stilling basin provides an economical method of dissipating energy and preventing stream bed erosion.

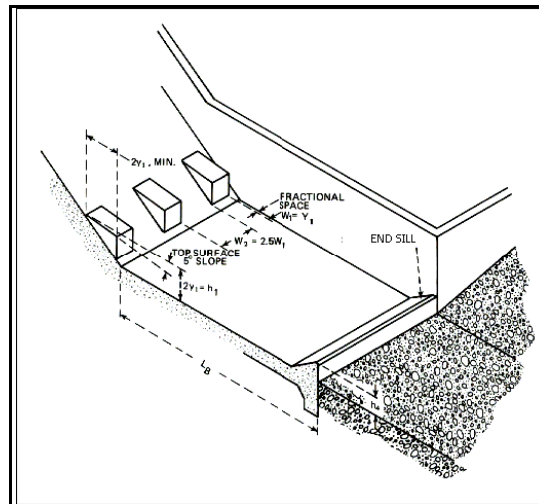


Figure 2-14: USBR TYPE IV stilling basin

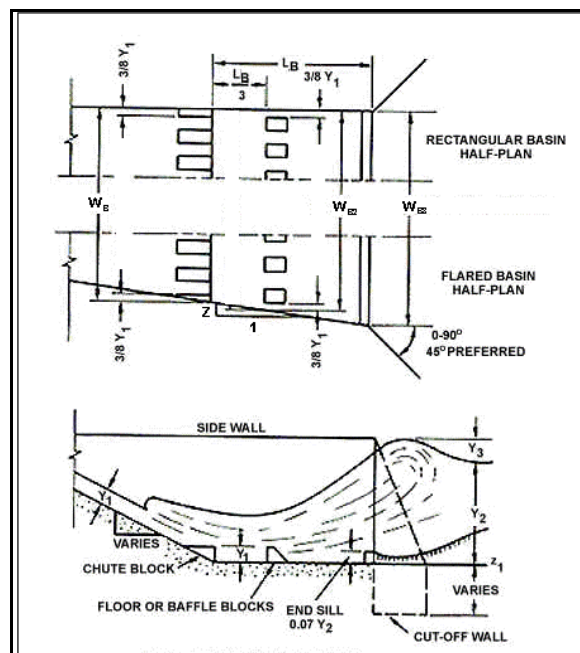


Figure 2-15: SAF stilling basin (Blaisdell, 1959)

3

PHYSICAL MODELING OF THE STILLING BASIN

3.1 General

Since the beginning of the twentieth century, the engineers were engaged on designing the hydraulic structures (such as dams, spillways, stilling basins, or barrages). Consequently, a new and scientific method to predict the performance of these structures was developed. This is performed by preparing physical models in experimental laboratories so as to form some opinion about the working and the behavior of the proposed hydraulic structures. However, the physical models have some advantages.

The advantages of physical models are as follows:

- The hydraulic performance and the working details of hydraulic structures can be visualized and be predicted.
- The boundary conditions can be easily applied
- With the help of physical models, a lot of alternative designs can be simulated and studied. So that the most economical, accurate, safe and applicable design could be selected
- They help in detecting and overcoming the defects in the hydraulic structures

However, these physical models may inhibit some limitation and drawbacks which are described as follows:

- The model scale depends many on the laboratory facilities (space, pump capacity, measuring tools)
- If the physical model is not designed or constructed properly, the results will be vague and inaccurate. For example, if the bathymetric around the structures or headlands at the riverbanks are not represented, the flow field would be totally different compared to the reality.
- The results of the physical models are affected by the similarity scale, which means if the turbulence flow is not represented well, the viscous force may produce an inaccurate results.

3.1.1 Procedures for designing the physical model

The general procedure that is usually carried out for the physical model design involves the following steps:

1. selecting the suitable scale of the physical model
2. constructing the model
3. testing the model
4. correcting the prediction

As for selecting the suitable scale of the physical model, The planning of the model is very important point. Though the selection of scale depends on many factors, these are:

1. availability of fund
2. availability of time
3. availability of place
4. availability of water supply
5. desired results
6. importance of the model
7. availability of constructing materials

After selecting the suitable material type for constructing the model, the next step is the construction of the model. All dimensions and levels should be very accurate.

After obtaining the precise measurements of hydraulic quantities of a model, the next step is correcting the prediction based on the practical and field experience.

3.1.2 Classification of physical models

All physical models are classified into:

1. undistorted or distorted models
2. fixed or moveable bed models
3. large or small scale models

3.2 Physical Model Experiments of Stilling Basins

3.2.1 Hydraulic Jump Experiments

Hager and Sinniger (1985) studied by an elementary hydraulic approach the characteristics of the hydraulic jump in a stilling basin with an abrupt rise. Results obtained included an expression for the sequent flow depth, the head loss due to the hydraulic jump formation and the length characteristics in terms of the inflow Froude number and the step height. They found that the pressure distribution just in front of the steps is not hydrostatic, but must be augmented by dynamic pressure head. For a given energy head and Froude number at the upstream zone of stilling basin, the dissipated energy is independent of the step height and corresponds to the value of the hydraulic jump on a horizontal bottom. The length of the roller and the jump were slightly longer in stilling basins with positive steps than that for ordinary hydraulic jumps on horizontal bottoms.

Joe and Edward (1989) studied the extreme pressure in the hydraulic jump stilling basin with and without chute blocks and intermediate blocks, jump locations on the chute as well as at the toe of the chute, and sill. The peak value of the pressure depends on the location of the hydraulic jump, chute slope, incident Froude number, incident flow development, and the length of test run. They concluded that the maximum fluctuation on the floor usually occurs at about one-third of the distance through the jump. The magnitude of maximum pressure fluctuations is not significantly affected by inflow development conditions.

Khalifa and McCorquodale (1979) studied the radial hydraulic jump that occurs in a stilling basin with diverge side wall. They concluded that, the sequent water depth ratio of the radial hydraulic jumps is less than that of rectangular jump, and the length of radial jumps is about 70% of rectangular jumps under the same flow conditions. Also, the energy losses in radial hydraulic jumps are 15% higher than in case of rectangular jumps.

Mohammed (1991) studied the rectangular hydraulic jump downstream low head irrigation structures on a rough channel bed under different flow conditions to obtain the optimum length of roughness from both the hydraulic and economical point of view. The experimental investigations were conducted under different flow conditions. He concluded that:

- The length of the hydraulic jump was reduced when cube roughness were used, and gave more reduction for values of Fr_1 less than 6.0.
- Decreasing L_R / h_b improved the efficiency of the stilling by decreasing the relative length of the jump, where L_R is the roughness length and h_b is the roughness height.
- The percentage reduction in length of the jump using bed roughness was decreased as Fr_1 was increased.

Hager and Li (1992) studied the effect of a continuous, transverse sill on the hydraulic jump in a rectangular channel. A novel normalization procedure was introduced by referring to the roller length of classic jump. Furthermore, they discussed the two and three-dimensional flow patterns. They also found that, the sill-controlled stilling basin is more efficient depending on the quantity of Tailwater depth.

Ezzeldeen, et al. (2000) studied experimentally the basic characteristics of the forced hydraulic jump. The effects of sill height, sill spacing, and channel bottom slope on the basic characteristics of the forced hydraulic

jump were examined for different initial supercritical flow conditions. Also, the variation in drag coefficient resulting from using double rows of continuous sill of a given height with different spacing was inspected and compared to the results of using single continuous sill of the same height.

The study showed that, both relative height of the sill and relative spacing of the sill have a considerable effect on the characteristics of the jump.

Negm (2003) studied experimentally the formulation of hydraulic jump in sloping rectangular closed conduits. Both positive and negative slopes were considered. The results were analyzed in terms of inlet Froude number, Fr_1 , the bottom slope, and the inflow depth ratio where the inflow depth ratio was the ratio between the initial depth and the conduit height. The analysis of the results indicated that, both the inlet Froude number and the bottom slope have major effects while the inflow depth ratio had a minor effect on the depth ratio of the jump at the outlet.

Prediction model was formulated and compared with the measurements as well as the results of the previously developed prediction models. He concluded that, the jump depth ratio (where the jump depth ratio was the ratio between the depth of flow at the outlet and the initial depth) was increased with the increase of Fr_1 and increases with the increase of the bottom slope of the conduit. The negative bottom slope produces values of the jump outlet depth ratio lower than those produced by the positive bottom slope and the values of horizontal slope were between the values of the negative slope and those of positive slope.

3.2.2 Scour Downstream Hydraulic Structures Experiments

The problem of scour is extremely complex since the flow conditions within the scour hole are difficult to evaluate. Even when this is possible, the interaction between the sediments and the flow characteristics are not easily quantified. Thus, theoretical analysis of local scour is in a rudimentary stage, and so far prediction of the extent of scour is mostly based on the empirical results.

Rajaratnam and Macdougall (1983) studied experimentally erosion of sand bed by plan turbulent wall jets. They concluded that, the maximum equilibrium scour depth is a function of density metric Froude number

" F_o " which was defined as $\frac{V_i}{\sqrt{gd_{50}(\gamma-1)}}$ where " v_i " is jet velocity, d_{50} the median diameter of the bed

material, and " γ " is the specific gravity of the bed sediments. Their experiments showed that, the location of the maximum scour depth moved towards downstream direction as the Tailwater was increased.

El-Masry (1984) studied the effect of discharge, gate opening, length of solid floor, and downstream water depth on scour hole parameters downstream sluice gate. It was found that the relationship between the scour depth and the length of rear apron, for different values of Froude number, indicated a negative linear correlation.

Nik Hassan and Narayanan (1985) studied the rate of scour downstream of a rigid apron due to a jet of water issuing through a sluice gate opening. Experiments were carried out for various sand sizes, sluice gate opening, efflux velocities, and lengths of apron. It was concluded that:

- The flow over the rigid apron downstream of the sluice gate was similar to a wall jet modified by the existence of the reverse flow.
- The mean velocity distributions measured in the rigid model was used to develop a semi-empirical theory to predict the temporal rate of scour depth for wall jet issuing on a bed of sand.
- Introducing Froude number could achieve dynamic similarity for modeling of technique local scour.

Uyumaz (1988) dealt with the scour phenomenon in non-cohesive soil below the vertical gates. The vertical gate was investigated in case of simultaneous flow over and under the gate. In the experiments, two different

bed materials of homogeneous noncohesive soil were used. He developed an empirical equation for estimating scour depth in terms of grain size, height of water at the outlet, total discharge, and head

Nashat (1995) studied the local scour behind sluice gate utilizing erodible sand basin. A single vent regulator model was selected to study the influence of some relevant parameters on the scour reach of solid apron behind a sluice gate.

The experiments were carried out to determine the minimum values of the scour length under the condition of submerged jump. The tested parameters were head, longitudinal bed slope, and the bed material characteristics. Also, he made a comparison between the experimental results and the existing ones in the field. He summarized the conclusions in to the following remarks:

- Longitudinal slope of channel bed and Froude criterion had weightless effect on the scour reach downstream a sluice gate.
- The scour reach on solid apron was found to be a function of the differential head between upstream and downstream water levels of the gate and the downstream water depth.

Yassin, et al. (1995) studied the scour length downstream of the fall hydraulic structures. The model was a clear over fall weir. The study was based upon the fact that, the local scour is a function of the velocity distribution, the amount of turbulence existing in its locality and the magnitude of maximum and mean velocity. It was found that, the scour length on the center line of the model was greater than that of the other axes. The following empirical equations were obtained:

$$L_s = 19.3 (h_{wd})^{0.25} (Q^{0.35}) \quad (11)$$

$$L_s = 27.7 (H)^{0.167} (Q^{0.35}) \quad (12)$$

$$L_s/Y_o = 6.8 (h_{wd}/h_{wu})^{0.22} \quad (13)$$

$$\text{For } 0.169 \geq Fr \geq 0.157, \text{ and} \\ L_s = 7.4(q.Y)^{0.4} [h_{wd}/h_{wu}]^{0.22} \quad (14)$$

For other values of Froude number in which

L_s	Predicted scour length,
h_{wd}	The fall height,
Q	Water discharge over the weir,
H	Total energy head,
h_{wu}	The difference between sill level of the weir and upstream bed level of the channel,
Fr	Froude number,
Y_o	Downstream uniform depth in the channel, and
Y	Downstream water depth.

Baghdedi (1997) studied scour hole downstream of drop structures theoretically and experimentally. He examined the effect of the inclination of the sloping face, the difference between the upstream and downstream water level, and Froude number of the downstream flow on the dimensions of the scour hole. It was found that the dimensions of the scour hole decreased with the increase of the Tailwater depth and increased with the increase of the inclination angle of the sloping face of the drop structure, Froude number, the height of the drop structure and the impinge jet velocity.

It was also mentioned that when there was a significant abrupt drop, in bed channel level and the downstream flow level was less than the upstream bed level, the flow would leave the upstream bed forming a jet. This jet impinged the downstream channel with a velocity " V_i " and angle of inclination equaled the angle of inclination of the upstream face of the drop structure " α ". The jet velocity would be diffused in the tailwater depth and will intrude the downstream bed level with a velocity " V_s ". The following equation was also developed:

$$D_s = 0.8503 \left(\frac{\gamma}{\tau_{cr}} \right) \left(\frac{v_i^2 Y_i}{g} \right)^{0.205} \sin \alpha - Y_{D,s} \quad (15)$$

in which

D_s	Maximum scour depth
γ	Specific gravity of fluid,
τ_{cr}	Critical shear stress,
v_i	Impinge average jet velocity,
Y_i	Thickness of the jet at the tailwater level,
g	Gravitational acceleration,
α	Angle of inclination of the sloping face of the drop structure, and
$Y_{D,s}$	Depth of flow downstream the drop structure.

Also it was concluded that:

- The dimensions of the equilibrium scour hole decreased with the decrease of the angle of inclination of the drop structure face.
- The maximum scour depth increased with the increase of Froude number of the downstream flow.
- The increase of the Tailwater depth decreased the value of the maximum equilibrium scour depth.

3.2.3 Summary

Based on the above, it can be concluded that many researchers performed numerous experimental works to investigate the hydraulic performance of the stilling basin with various structure – end sill, chute blocks or baffle blocks, to help producing better energy dissipation and to control the dimensions of the hydraulic jump. Others focused on quantifying experimentally and then with empirical formulae the scour hole characteristic based on the hydraulic and structure parameters.

Many others also conducted experimental researches but because of the complexity in nature of the turbulence production and diffusion process, numerous investigations have been made mainly towards the understanding of their macroscopic structures. However, the development of Laser Doppler Anemometry (LDA) and the advance in numerical techniques have made it feasible for further study of their internal turbulence structure.

3.3 Stilling Basin of Egyptian Barrages

The Nile River is much more than a waterway to Egypt. It is the fountainhead of all activities and life. It comprises over 95% of the total water resources of the country which predominantly depends on agriculture. Prior to the construction of the Aswan High Dam (AHD), the flow of water in the Nile River was characterized by extreme seasonal variation. During the flood period, from August to November, the discharges exceeded the irrigation requirements. During the rest of the year, the discharge was inadequate for the irrigation needs.

The Ministry of Water Resources and Irrigation (MWRI) has taken the responsibility of safeguarding the water resources of the river. Therefore, over the last century a number of barrages and dams have been constructed to improve the diversion of water into the irrigation canals and to modify seasonal variation in the river Nile flows, Electric power generation has been another benefit of these barrages. The number of the constructed barrages along the Nile and its two branches reached to seven.

Since the construction of the AHD the river channel has been seeking to establish a new regime to cope with the drastic change in the inflow rates related to water and sediment. As a result, a remarkable alteration in the river geometry is attempted to reach an eventually stable condition. The channel widths are reduced, new lower islands are created and back channels are abandoned so that many older islands are attached to the main flood plain. The adjustment of geometry is accomplished by erosion and deposition processes that tend to

deepen, flatten, meander and widen the river. This situation has a direct effect on the constructed barrages which led the MWRI to take the responsibility to rehabilitate the existing barrages along the Nile River. The main reason for this rehabilitation is the continuous increase of the barrage head difference. Some problems pertaining to the stability of the structure are also observed.

3.4 Identification of the Problem

Seepage and uplift pressures under the barrages have increased due to degradation in the river bed at downstream side since the closure of the Aswan High Dam (AHD) in 1968. Age is also a factor that should be considered in the barrage stability. It is now facing major problems in connection with the ageing of the construction material. Furthermore, the progressive development of scour holes downstream of the apron put the barrage stability in question. The downstream concrete weir on the apron to counterbalance the hydraulic head has been washed away in several locations.

During the testing of the physical model of the New Esna Barrage, it has been observed that significant scour occurred immediately downstream the stilling basin that exceeded the expected values. This observation has been further verified during the monitoring of the structure. The same findings were repeated with the model testing of the New Naga Hammadi Barrage design. In both cases, a significant design modification has been introduced based on expert opinions. Therefore this problem highlight the need to develop some design criteria suitable for Nile River conditions to be used in the future applications.

3.5 Objectives of the Study

The aim of this study is to investigate in detail on bay of the sluiceway radial gate. The main objectives of this study are as follows:

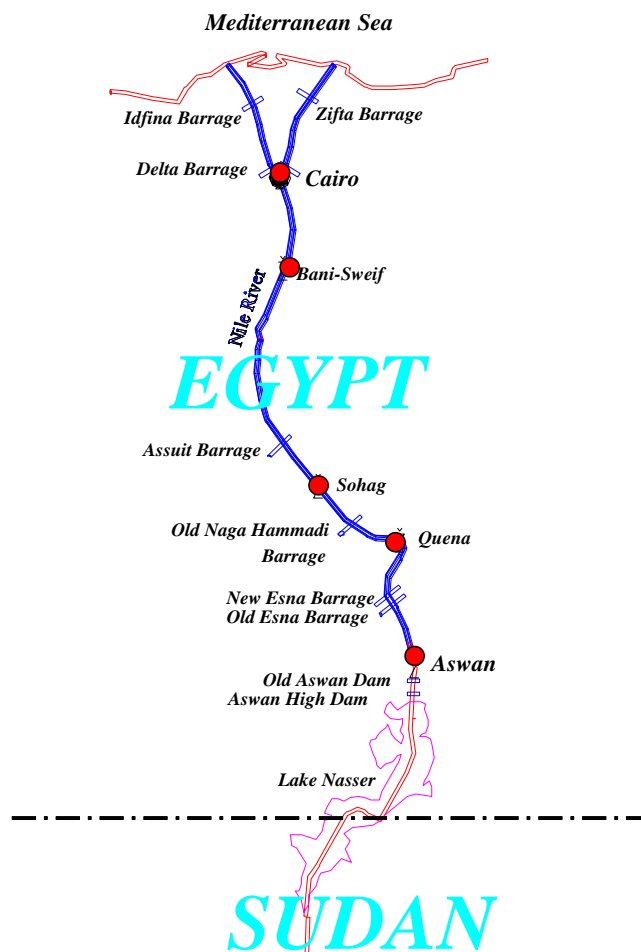
- Testing different design alternatives for stilling basins.
- The results of the physical model will be used as a database for calibrating and modifying an existing numerical model.

3.6 Methodology

A well designed 2-D hydraulic detail model of the sluiceway bay (in a flume) is the best tool to check the flow patterns upstream and downstream of the proposed structure, and to provide input for further 3-D hydraulic scale model testing of the Barrage layout. By the detailed model, the discharge capacity and hydraulic performance of the sluiceway will be tested with the aim to confirm or optimize the levels of the sluiceway sill and apron and the extension of the latter. The flume model gives direct insight into the physical processes.

3.7 Execution

Usually, spillway models in conjunction with stilling basins or energy dissipaters or other structures that discharge high-energy water are built geometrically similar to their prototypes. A 2-D model flume study with an undistorted scale of 1:21 is designed to represent 500 m of the Nile River, together with simulating one bay of the sluiceway, the sill and downstream apron, and the upstream and downstream Rip-Rap protection.



3.8 Model Similarity

For correct reproduction of the important hydraulic phenomena in a hydraulic model, a complete similarity including geometric and dynamic similarity between prototype and model must be fulfilled when determining the model scales.

Because the model has free surface flow, the inertia and gravitation forces are dominant. Therefore, for simulation, the model has to be based on Froude number equality with the prototype. To simulate the kinematics and dynamics of the flow field properly, an undistorted geometric scale model is required.

The Froude number, which represents the ratio of flow inertia forces to gravitational forces, is given by:

$$F_r = \frac{V}{\sqrt{gh}} \quad (3-1)$$

where

F_r = Froude number,
 v = average flow velocity, (m/s)
 h = characteristic depth, (m)
 g = gravitational acceleration, (m/s²).

From the condition that the Froude Number in both prototype and model should be equal, the velocity scale ratio can be determined from which the other scale ratios can be derived:

$$\begin{aligned} \text{Velocity scale ratio} &= n_v = (n_h)^{0.5}, \\ \text{Discharge scale ratio} &= n_Q = n_l n_h n_v = n_l (n_h)^{1.5}, \text{ and} \\ \text{Time scale ratio} &= n_t = n_l / n_v = n_l / (n_h)^{0.5}. \end{aligned}$$

An undistorted geometric scale of 1:21 was selected. Consequently, the ratios for the other quantities are:

$$\begin{aligned} \text{Horizontal length scale,} & n_h = 21, \\ \text{Velocity scale} & n_v = (21)^{0.5} = 4.58, \\ \text{Discharge scale} & n_Q = (21)^{2.5} = 2020.92, \text{ and} \\ \text{Time scale} & n_t = (21)^{0.5} = 4.58. \end{aligned}$$

3.9 The Experimental Installation

The used experimental arrangement is an important component in executing any physical model. It will be discussed here in details.

Flume

The experiments were conducted using a 1.0 m wide, 26.0 m long and 1.20 m deep flume. The side walls along the entire length of the flume are made of glass with steel-frames, to allow visual investigation of the flow patterns and stability of bed protection. The horizontal bottom of the flume is made of concrete and provided with a steel pipe to drain the water from the flume. The tail water depth is controlled by a tailgate located at the downstream end of the flume Figure 2.1.

The water enters the flume from a constant head tank, which is fed by a centrifugal pump with a total discharge of 0.5 m³/s (500 l/s). A recirculating discharge system was used and there was underground reservoir of a total capacity of 80 m³. Plate 2.1 shows the general view of the used flume. Also, Figure 2.1 shows the detailed component of the flume.

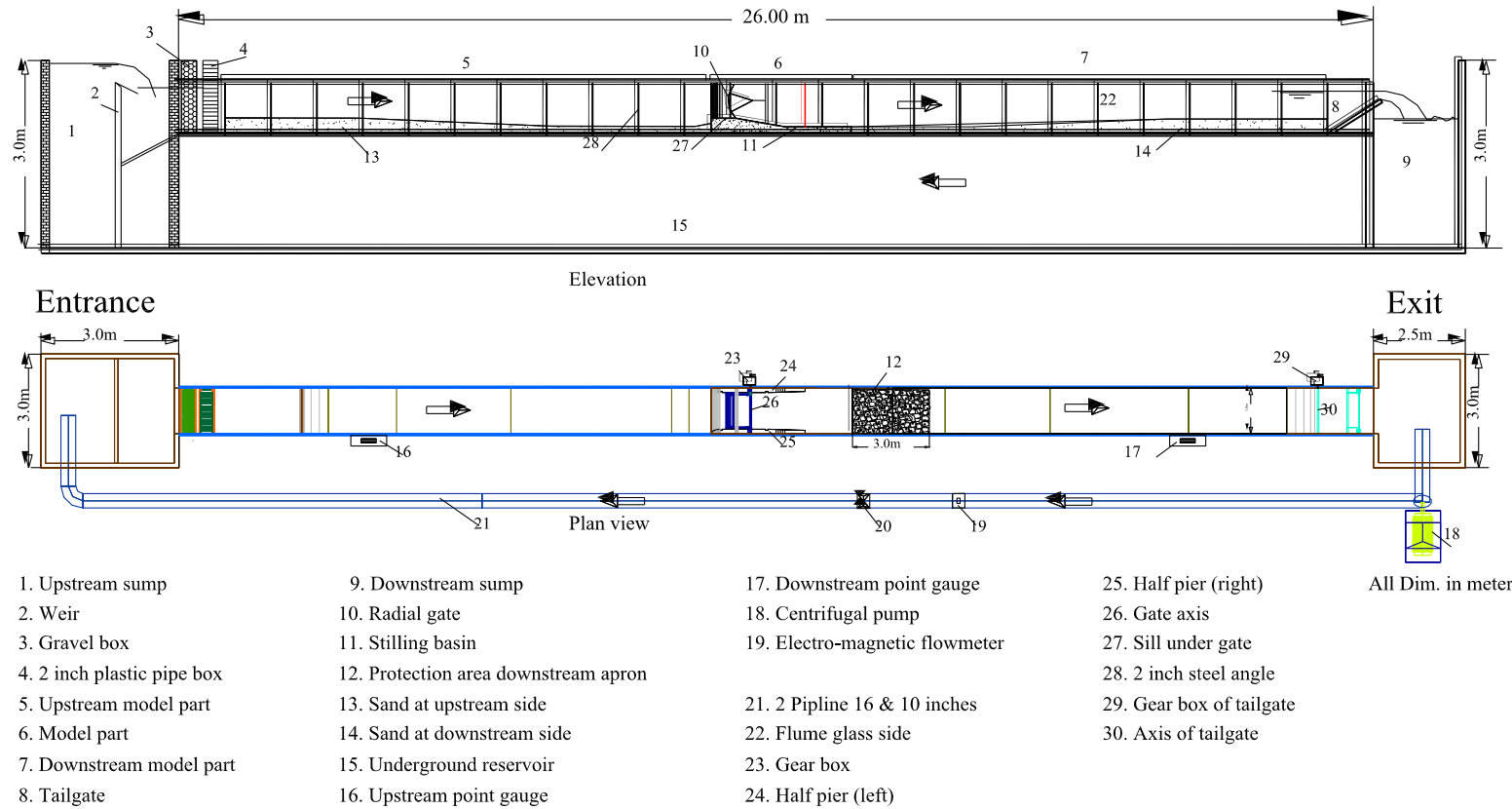


Figure 3-1: Details of the flume and model arrangements



Photo 3-1: General view of the flume

Flume Inlet

The flume inlet consists of a masonry basin of 3.0 m width, 3.0 m length and 2.5 m depth. This entrance receives the delivered water from the pump through a pipeline to dissipate the energy of the flow that enters the model and to avoid any disturbance of the flow in the flume. A weir was built at the entrance. The water passes through a screen box filled with large gravel followed by another screen box filled with 2 inch-diameter plastic pipes to dissipate the energy at the inlet to suppress any excessive turbulence. A detail of the flume inlet is shown in Figure 2.2.

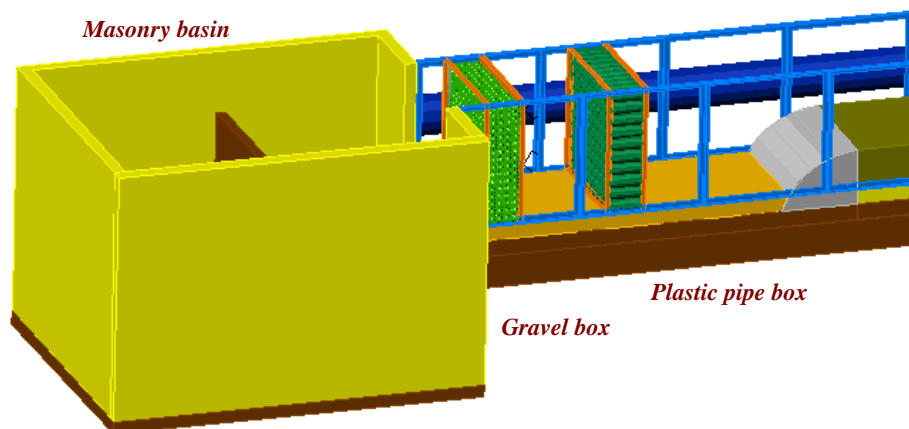


Figure 3-2: Flume entrance

Flume Exit

The flume exit consists of a basin that starts directly at the end of the simulated reach followed by a tail control gate as shown in Figure 2.3 to adjust the water surface levels in the model. A steel flap gate, hinged at the bottom to provide an adjustable inclination, is installed at the downstream end of the flume to control the downstream tailwater depth. The details of the flume exit are shown in Figure 2.3.

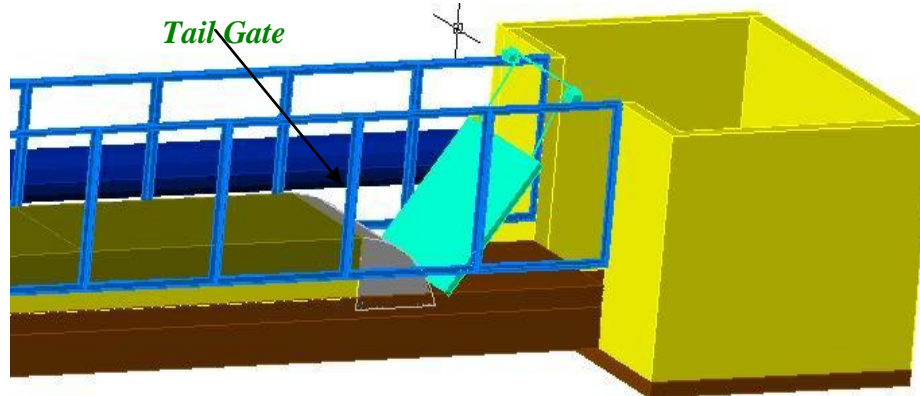


Figure 3-3: Flume exit

Flume Feeding System

The flume is provided with a recirculating system. There is two pumps with different capacities; of 500 lit./s and 150 lit./s. These two pumps are connecting with two pipelines 16 and 10 inches, respectively. The maximum feeding capacity of the system is $0.65 \text{ m}^3/\text{s}$ (650 l/s). This capacity was sufficient for all the cases of the required tests. An Ultrasonic flowmeter was installed on the feeder pipe of ten inch diameter and an electro-magnetic flowmeter was installed on the feeder pipe of 16 inch diameter. These two flowmeters are used for measuring the discharge during the tests.

3.10 Construction of the Physical Model

The physical model was constructed in two months. The technical team of the HRI contributed in the construction.

A sluiceway bay is constructed at a distance of about 12.0 m downstream the flume inlet. The sluiceway bay consists of a gated sill and two half-piers (9.5 cm thick each) symmetrically installed on both wall sides. A bras radial gate with a radius of 57.10cm is used to regulate the flow. A hand driven gearbox carries out controlling the radial gate opening. The gear system was composed of a vertical and horizontal level gears. The vertical gear was engaged with a steel rod provided with a handle. The gate will close or opened by moving the handle and the gate opening was measured by using a vertical scale. A rubber strip was fixed at both sides to be compressed to the flume sides when the gate slides. This arrangement ensured no leakage from the flume sides. The radial gate was rested on a raised sill with a length of 0.54m and width of 0.81m followed by an inclination apron with different shape. The horizontal apron was started from the end point of the inclination apron to some distance in the downstream side.

The horizontal apron was followed by a 3m long movable bed covered by rip rap with $d_{50}=1.5\text{cm}$. The upstream and the downstream parts of the radial gate are considered a part of the physical model, which was filled, with sand of 0.51 mm mean diameter. The upstream part was shaped in such way to enhance the flow and make it smooth when it approaches the gate. Also, the downstream part of the model was shaped to distribute the flow uniformly. The movable bed, at the downstream part, comprises of three different layers, sand, filter, and rip rap Layers that are defined as following:

First Layer: Sand Base

A sand layer was placed to cover the Flume floor at both upstream and downstream part. The thickness of the sand layer was differed from one place to another (0.10m directly after the apron and 0.40m at the end of the flume. The characteristics of the used sand (according to the Egyptian code) are shown in and Tables (2.1) and (2.2) and Figure 2.4.

Table 3-1: Properties of the sand base

Property		Sand base	E.S.S. 1109/1971 Limitations
Specific gravity	t/m ³	2.65	2.50 - 2.75
Volume weight	m ³	1.68	1.60 - 1.80
Fineness	-	2.54	1.50 - 3.75
Clay and fine dust	%	0.75	< 3 %
Organic impurities	-	Nil	Not allowed
Geometric mean diameter	mm	0.51	
D ₈₄ /D ₅₀	-	1.35	
D ₅₀ /D ₁₆	-	1.34	

Table 3-2: Sieve analysis of the sand base

Sieve Size (mm)	Retain weight (gm)	Finer weight (gm)	Finer percent %
1.000	0.00	340.34	100.00
0.710	27.60	312.74	91.89
0.500	134.89	177.85	52.26
0.355	136.96	40.87	12.01
0.250	30.15	10.72	3.15
0.180	4.39	6.33	1.86
0.125	1.98	4.35	1.28
0.090	1.59	2.76	0.81
0.063	1.29	1.47	0.43
0.000	1.47	0.00	0.00

Second Layer: Filter Layer

A medium fine gravel filter was used to prevent leaching of the permeable soil throughout the rip rap layer. The design specification of the filter according to the under layer permeable soil is as following:

Permeability to sand

To prevent the loss of fine material from an under laying filter layer or the subgrade, the following requirements with regard to imperviousness to sand must be met

$$\frac{d_{15} \text{ filter}}{d_{85} \text{ sand}} \leq 5$$

and

$$\frac{d_{50} \text{ filter}}{d_{50} \text{ sand}} = 5 - 60$$

Whereas, the ratio in the above equation depends on the shape and gradation of the grains as follows;

- Homogeneous round grains (gravel) 5 - 10
- Homogeneous angular grain (broken gravel, rubble) 10 - 30
- Well graded grains 12 - 60

Permeability to water

To prevent a filter layer from being lifted by water entering the channel through bottom or banks, the permeability to water must be greater than that of the under laying material. To maintain a sufficient permeability to water the following design specification must be used;

$$\frac{d_{15} \text{ filter}}{d_{15} \text{ sand}} = 5 - 40$$

Where d_{15} is the diameter of the sieve opening where 15% of the total weight of the sample passes. Depending on the shape and gradation of the grains, the following ratios can roughly be used:

- Homogeneous round grains (gravel) 5 - 10
- Homogeneous angular grain (broken gravel, rubble) 6 - 20
- Well graded grains 12 - 40

To prevent the filter from clogging, it is advisable that d_{15} of a layer must be larger than 0.75mm. The sieve analysis of the filter is shown in Tables (2.3).

Table 3-3: Sieve analysis of the filter

Sieve Size (mm)	Retain weight (gm)	Finer weight (gm)	Finer percent %
9.50	0.00	350.11	100.00
8.00	9.96	340.15	97.16
5.60	60.56	279.59	79.86
4.00	211.32	68.27	19.50
2.80	63.77	4.50	1.29
2.00	4.50	0.00	0.00

Third layer: Rip Rap Layer

The rip rap layer is 4 m long and was placed just downstream the solid apron. The geometric mean diameter of the rip rap layer d_{50} was equal 15.54 mm. It should be mentioned that the rip rap was analyzed in the sedimentation laboratory at HRI. The rip rap layer was placed over a filter layer and sand layer. It must be mentioned that the same type of rip rap was used in all the model tests. Table (3.4) shows the characteristics of the rip rap layer.

Table 3-4: Sieve analysis of the rip rap layer

Sieve Size (mm)	Retain weight (gm)	Finer weight (gm)	Finer percent %
31.50	0.00	276.89	100.00
25.00	0.00	276.89	100.00
22.40	17.93	258.96	93.52
19.00	10.87	248.09	89.60
16.00	97.93	150.16	54.23
13.20	76.64	73.52	26.55
11.2	44.85	28.67	10.35
9.50	16.88	11.79	4.26
8.00	5.78	6.01	2.17
5.60	3.92	2.09	0.75
4.00	2.09	0.00	0.00

A summary of the characteristics of the three layers is given in Table 3.5 while the sieve analysis is represented on Figure 3.4.

Table 3-5: Summary of the material characteristics

Material Characteristics	Sand	Filter	Rip Rap
D15 (mm)	0.36	3.60	11.80
D50 (mm)	0.49	4.70	15.54
D85 (mm)	0.67	6.10	18.50
D84/D50	1.35	1.29	1.19
D50/D16	1.34	1.27	1.31

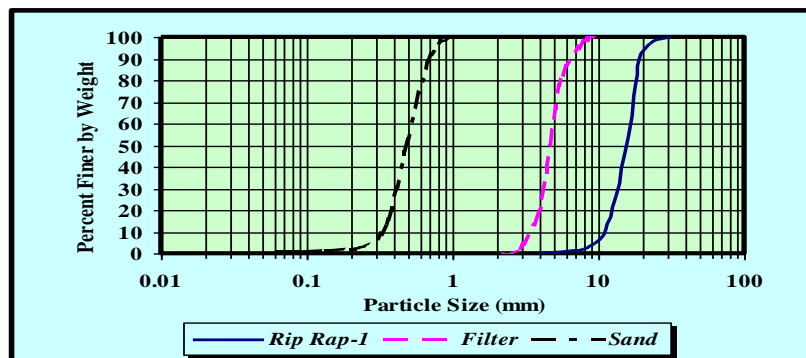


Figure 3-4: Sieve analysis of sand, filter, and rip rap materials



Figure 3-5 a: Model Construction



Figure 3-5b: Model Construction

3.11 Measuring Devices

In this section the used of measuring devices are explained. These measuring devices are the flowmeter for measuring the flow discharge, the currentmeter for measuring the flow velocity, the data logger for collecting the data and transferred it to the computer, the point gauge for adjusting the water level at both upstream and downstream the gate and measuring the scour hole and the digital camera for recording the scour downstream the apron. In the following section a detail description for each device used in this study.

Flow meters

To measure the passing discharge into the model with a reasonable accuracy, different sizes of electro-magnetic or ultrasonic flow meters were installed on all feeding pipelines to the model. The electro-magnetic and ultrasonic flow meters were installed to measure the discharge through the two 16 and 10 inch-diameter feeding pipelines, respectively. The flowmeters measure the flow rate with accuracy of $\pm 1\%$. The description of both flowmeters is presented in following sections.

Electromagnetic Flow meter

In accordance with Faraday's law of induction, a voltage is induced in a conductor that is moved through a magnetic field. In the magneto-inductive principle of measurement the flowing medium represents the moving conductor. The induced voltage proportional to the flow velocity and is fed to the measuring amplifier by a pair of electrodes. The flow volume is calculated across the cross section of the pipeline. Plate 2.2 shows the electromagnetic flowmeter in operation. The specifications of the electromagnetic flowmeter are as following:

Type	: Electromagnetic E
Power Supply	: 85-260V AC, 45-65 Hz
Full Scale Value Scaling	: 0.30-10.0 m/s
Current Output	: 0/4-20 mA
Flow Rate Unit	: m ³ /s or Lit/s
Current Span	: 0-20 mA
Pulse/ Frequency Output	: 0-10000 Hz

Ultrasonic Flowmeter

This kind of flowmeter is movable so it easy to install it in more than one pipeline. Plate 2.3 shows the ultrasonic flowmeter in operation. The specifications of the ultrasonic flowmeter are as following:

Type	: 1010P/WP
Flow Velocity Range	: ± 12.2 m/s
Flow Sensitivity	: 0.015 m/s even at zero flow
Flow Rate Unit	: m ³ /s or Lit/s
Current Output	: 4 - 20 mA
Pulse Rate	: 0 - 5000 Hz

Current-meter

Flow velocity in the model was measured using the currentmeter. The used currentmeter was measured the flow velocity in two directions, with the flow direction and perpendicular to the flow direction. The time for measuring the velocity could be controlled and also continuous readings could be obtained. In the following section a description for the used currentmeter is given.

Electromagnetic Current meter

The electromagnetic currentmeter type E.M.S. was manufactured by Delft Hydraulics, Holland. This current-meter is a well-known pipe flowmeter employing Faraday's Induction Law for velocity measurements of a conductive liquid moving through a magnetic field. Plate 2.4 shows the used currentmeter in the study. The specifications of the electromagnetic currentmeter are as following:

Sensor	: Ellipsoid 11 x 33 mm, with 10 mm rod diameter
Range	: 0 to +/- 2.5 m/s.
Output	: Approximately 0.13 mv/cm/s, a second order equation is used to calculate the accurate velocity component from the measured volt (two perpendicular components per point).
Accuracy	: ± 0.01 m/s ± 1 % of value measured
Input	: 220 VAC

Data logger

The data logger was connected with the computer and all the velocity measurements were transferred directly to the computer and stored into text format file, which can be retrieved by Excel programme.

The HP data logger (256 channels 3 wires MUX) consists of :

1. Mainframe (VXI E142B)
2. VCLink interface
3. Multimeter (5.5 digit HPE1411B)
4. Four Modules of 64 channels 3 wire MUX.

HP data logger was controlled by a program that was built in VEE 4.0 language It has two modes of operation.

- 1- Normal operation
- 2- Transient operation with 12 micro second speeds

HP VEE is (Hewlett – Packard’s Visual Engineering Environment) is a graphical programming language for creating test systems and solving engineering problems optimized for building test and measurement applications – especially programs with operator interfaces with revision 4.0,HPVEE exhibits high speed with its new compiler, and its instrument I/O is even faster than before. HP VEE integrates with textual languages including C/C++, Visual Basic, Pascal, Fortran and HP BASIC. Use HP VEE 4.0 on windows 95/ Windows NT and HP – UX workstations.

Point Gauges

To monitor water surface levels along the flume, two point gauges were installed within the stilling wells. One of these point gauges was used to adjust the water depth at the upstream side at 6.9 m from the radial gate hinge. The second at 9.75 m from the radial gate hinge for adjusting the downstream water depth. Also, this instrument was used to measure the scour of the bed downstream the apron. The accuracy of these gauges is within $\pm 0.1\text{mm}$. Plate 2.6 shows the used point gauge in the model.

Digital Camera

The digital camera was used to demonstrate the flow under the radial gate as well as the scour of bed material downstream the apron. It was also used to produce photos that show the state of flow in the whole model. These photos were used during the comparison between the different stilling basins results. Plate 2.7 shows the used digital camera in this study.

3.12 Calibration of the Measuring Devices

HRI is very well equipped with instrumentation. All equipments and instrumentations were calibrated at HRI before and during carrying out the model work. All equipments performance and accuracy were checked weekly.

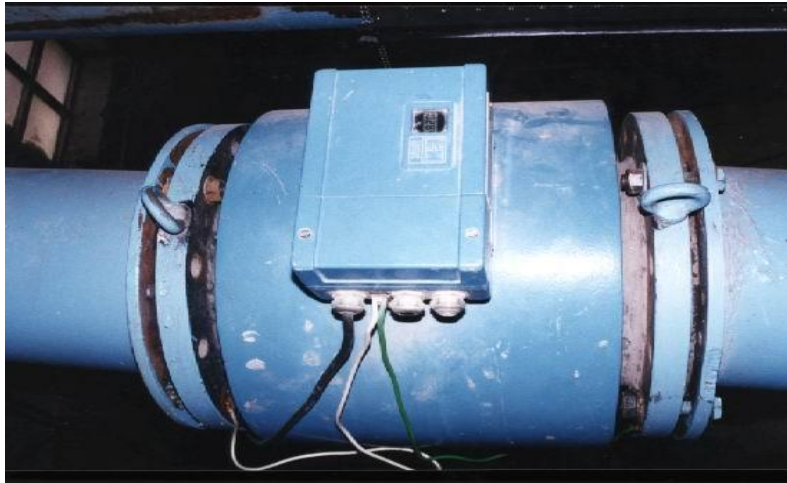


Photo 3-2: The electromagnetic flowmeter



Photo 3-3: The ultrasonic flowmeter

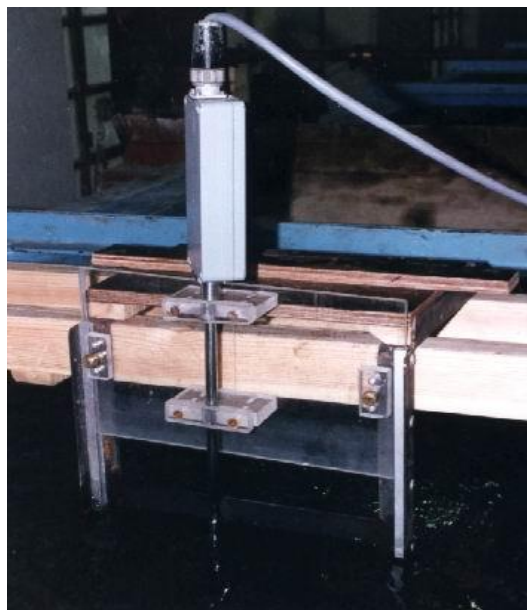


Photo 3-4: The electromagnetic currentmeter



Photo 3-5: point gauge



Photo 3-6: used digital camera

3.13 Model Test Program

In this chapter a detailed description of the test programme is presented. The undertaken measurements are given in this chapter as well. Also, the steps of executing a run are explained.

Different design shapes of stilling basins were tested in order to investigate and study the sluiceway stilling basins in presence of the submerged hydraulic jump. The investigation included the characteristics of the submerged hydraulic jump, the flow conditions along the stilling basin, and the stability of bed protection downstream the apron as well. For each proposed design several runs were executed using six different flow conditions. Table 3.1 show the ranges of the different hydraulic variables tested, while Table 3.2 provides the actual conditions used in each run.

3.14 Geometric Variables

In this section the geometric variables were determined for each test series. Some of the geometric variables were fixed during all the test series and some were varied. The variables that were fixed during the test series were the radius of curvature of the radial gate, the top length of the sill under the gate, the upstream water depth, and the length of the stilling basin. On the other hand, the variables that were varied from one test series to another were the location and the height of the end sill, end step, the elevation of the apron and the downstream water depth and consequently the differential heads. Moreover, the back slope of the sill under

the gate was changed from one test series to another. Table 3.1 shows the summary of the geometric variables that were used in this study.



Photo 3-7: Data Acquisition systems and the data logger

Table 3-6: Geometric variables of the tested stilling basin

Geometric Variables	Symbo l	Series Name				
		A	B	C	D	E
Stilling Basin						
Stilling basin length	(L_b)	2.50				
Stilling basin width	(B)					
At gate location	($B1$)	0.81				
Downstream of pier	($B2$)	1.00				
Radial Gate						
Radius of curvature	(R)	0.57				
Gate width	(w)	0.810				
Height of gate axis	(S)					
Sill under Gate						
Top length	(b)	0.55	0.55	0.55	0.55	0.55
Sill height	(e)	0.25	0.25	0.25	horizontal	0.15
Back slop angle	($-$)	paraboli	linear	2-parab.	horizontal	linear
Upstream face		Rounded for all test series				

3.15 Hydraulic Variables

The hydraulic variables were designed in such a way to cover a wide range of barrages along the Nile River such as New Esna Barrage, New Naga Hammadi Barrage, Assuit Barrage, Delta Barrage, Zifta and Idfina Barrages. The main hydraulic variables were; the discharge, differential head and the downstream water depth. Table 3.2 summarized the ranges of these hydraulic variables.

Based on the prototype hydraulic conditions of the different barrages on the Nile River, the hydraulic conditions for all test series were prepared. Table (3.3) shows the test programme for all test series that tested

in this study. In this table the discharge and the water levels for each test were defined according to the prototype condition for Assiut barrage.

Table 3-7: The Hydraulic Variables

Hydraulic Variables	Ranges
Discharge	5-25 m ³ /s/m
Differential Head	3-8.0 m
Downstream Depth	6.5-12.5 m

Table 3-8: The test programme applied for all test series

Test No.	Q (total, Proto.) (m ³ /sec)	Q/Gate (Proto.) (m ³ /sec)	Q(model) l/sec	U.S.W.L (m)+asl	D.S.W.L (m)+asl
1	600	75	37.1	50.80	44.74
2	1000	125	61.9	50.80	45.63
3	1600	200	99.0	50.80	46.71
4	2000	250	123.7	50.80	47.30
5	2400	300	148.4	50.80	47.81
6	3000	375	185.6	50.80	48.44

3.16 Test Series Description

In this section a detailed description for each proposed design of sluiceway stilling basin will be explained. The study was carried out through two stages. The first stage was focused on the investigation of sloping apron downstream the gate. This stage consists of three designs for the stilling basins which namely series A, B, and C as shown in Figures 3.1, 3.2 and 3.3. the second stage consists of two designs for the stilling basin which namely series D and E as shown in Figures 3.4 and 3.5. The second stage was focused on the investigation of different drop between sill under gate and the apron.

1st Stage: Study Slope between Sill under Gate and the Apron.

1- Study the Parabolic Slope $x^2 = (47/21)*y$

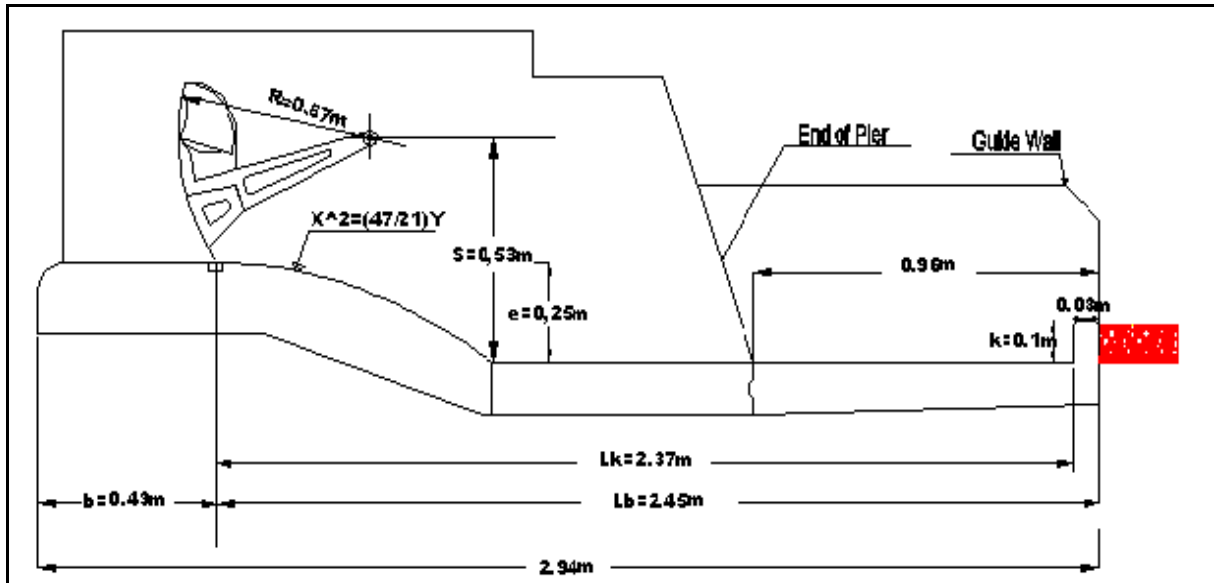


Figure 3- 6: Sluiceway stilling basin with parabolic slope, test series A

2- Study the Linear Slope $y=5x$

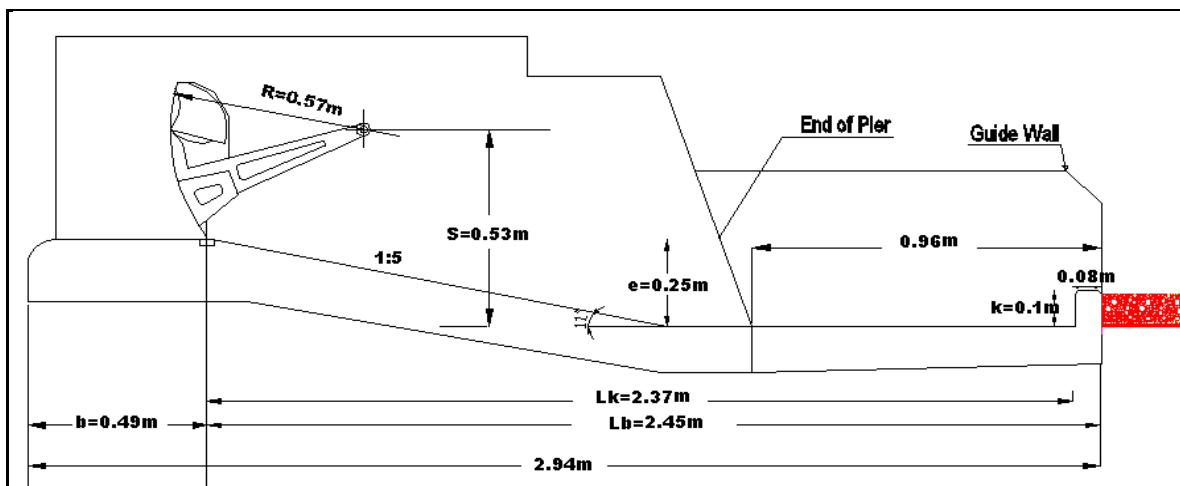


Figure 3-7: Sluiceway stilling basin with linear slope, test series B

3- Study the Double Parabolic Slope $X^2= (23.5/21)*Y$.

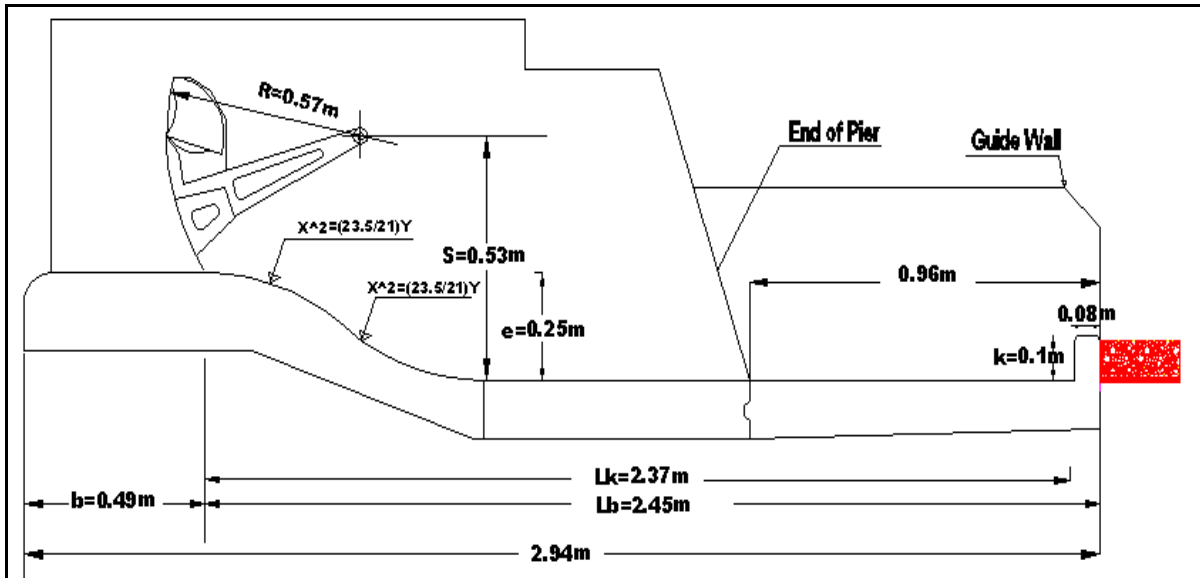


Figure 3-8: Sluiceway stilling basin with double parabolic slope, test series C

2nd stage: Study Drop between Sill under Gate and the Apron

1-Drop between Sill under Gate and the Apron ($e = 0.0$ m).

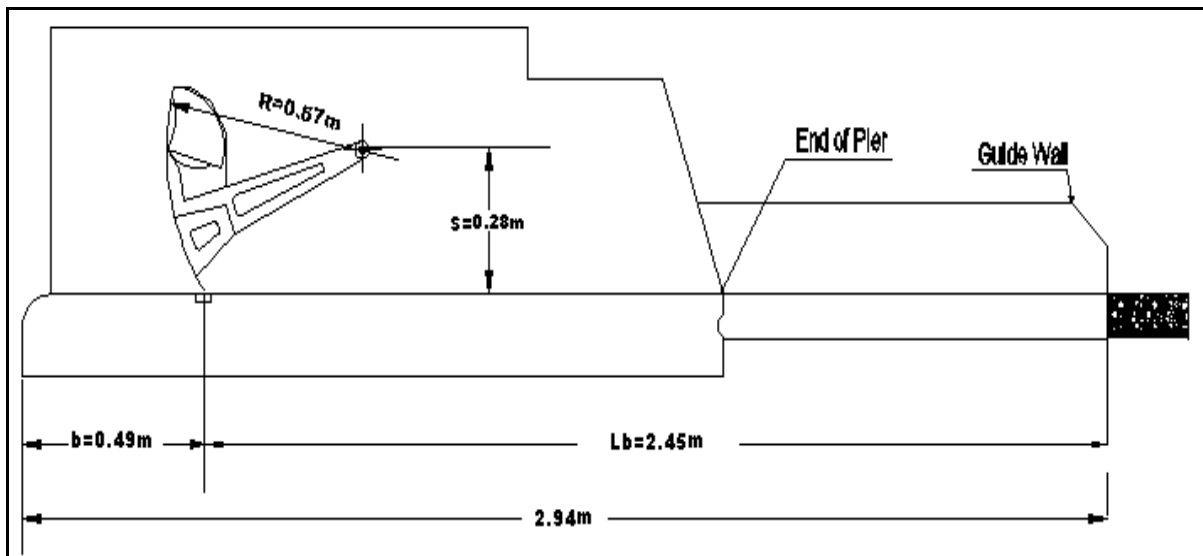


Figure 3-9: Sluiceway stilling basin with horizontal apron, test series D

2-Horizontal Apron ($e=0.15$ m).

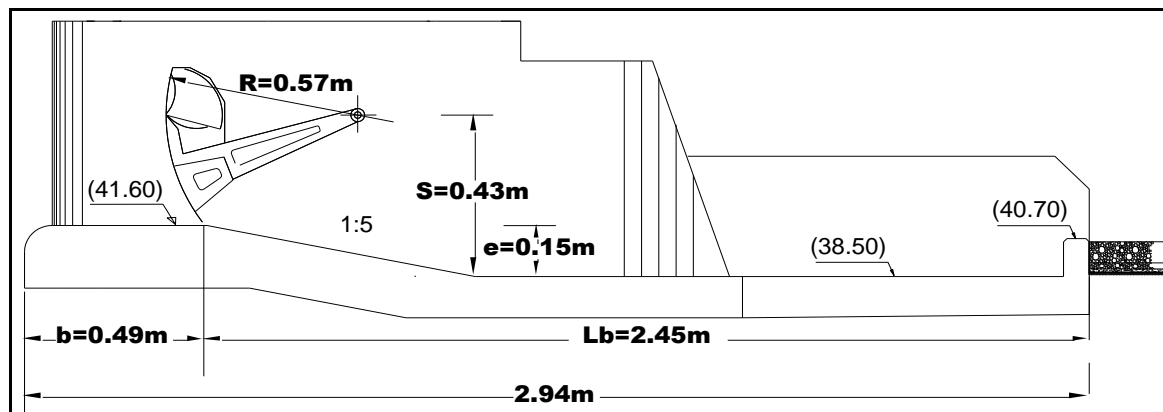


Figure 3-10: Sluiceway stilling basin with linear slope and raised apron

3.17 Test Procedures

The following systematic steps were applied during the existing study for all test series. Each Test series (design) was tested under six different flow conditions. The following procedures were used to conduct these tests.

1. The level of the bed protection downstream the apron was adjusted at the same level as the end sill.
2. The underground was filled with clear water.
3. The flow was adjusted by the control valve and measured by an electromagnetic flowmeter or ultrasonic flowmeter.
4. The upstream and downstream water depths were adjusted to the required test condition.
5. After reaching the stability condition the measurements were recorded.
6. The bed protection downstream the apron was reshaped and the new test starts to be adjusted.
7. The steps no. 3 to 6 were repeated.

3.18 The Undertaken Measurements

During each test series the following measurements were carried out:

- The flow velocity was measured at ten cross sections distributed along the centerline of the simulated bay.
- The scour of the protected bed downstream the apron.
- The characteristics of the flow under gate and the submerged hydraulic jump.
- The length of the reverse flow L_{rf} .

3.19 Velocity Measurements

The flow velocity measurements were measured using an electromagnetic current-meter type EMS, manufactured by Delft Hydraulics, Holland. The current-meter was connected to a data logger, which receives the data directly from the currentmeter. The data logger also was connected to the computer, which receives the data from the data logger and save it in a file. The data logger was set to record 25 readings during time of 10 seconds at each point depth of the cross section. The currentmeter measured the flow velocity in two directions; in the flow direction, and perpendicular to the main flow.

The flow velocity was measured at ten cross sections. The distance between each two cross section was equal to 0.50m except the cross section No. 2. Six cross sections were located on the apron area, and three sections

were located on the rip rap area, downstream the apron. There was one cross section located upstream the gate. Figure 3.6 shows the location of the velocity profiles. The velocity values were measured at five depth points along the water depth at relative distances from the water surface of 0.2, 0.4, 0.6 and 0.8 and 3.0 cm above the bed.

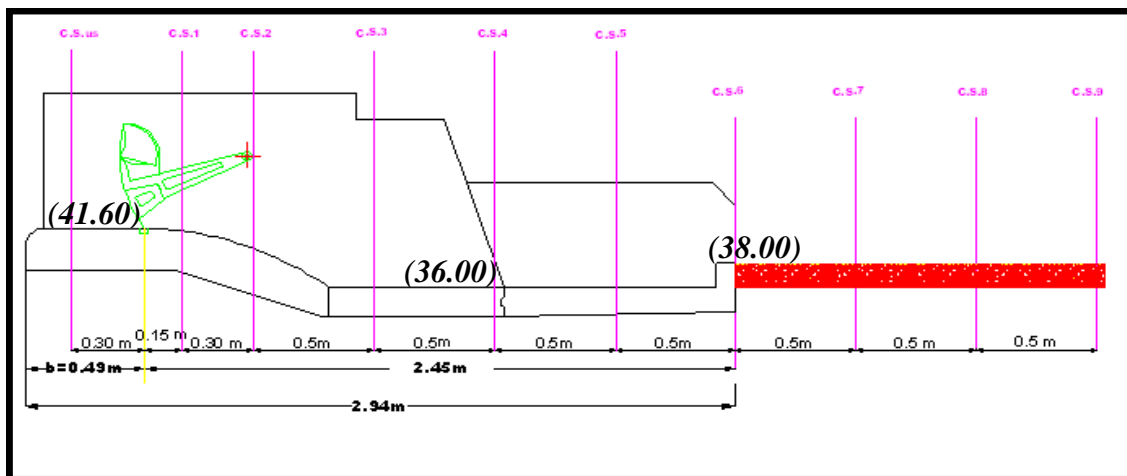


Figure 3-11: locations of the velocity measurements

3.20 Scour Profile Determination

The movement of the bed material just downstream the apron was measured after each test run. The depth and length of the scouring hole was measured. The scour profile was measured using a point gauge with accuracy $\pm 0.1\text{mm}$. The scoured bed was measured each five centimeters along the centerline of the simulated bay of spillway Figure 3.7 shows the scouring profile downstream the apron.

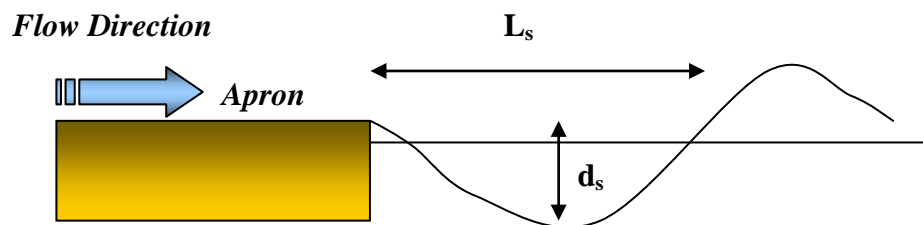


Figure 3-12: Typical scour profile downstream apron

3.21 Characteristics of the Flow under gate and Hydraulic Jump

During each test series, the hydraulic jump parameters were measured for instances the conjugate depth (y_1), the back up water depth just downstream the gate (y_3) and the length of the jump (L_{sj}). The length of the jump was measured using the currentmeter, which was installed (five to six cm) under the water surface. It was used to trace the zero surface flow velocity, and the distance from that point to the gate was measured. This distance represents the length of the submerged jump. Moreover, the gate opening (a), the upstream water depth (H_0), and the tailwater depth (y_t) were measured. The upstream water depth was measured above the sill under the gate, and the tail water depth was measured at the end of the apron. Figure 3.8 provides a definition sketch of the variables measured.

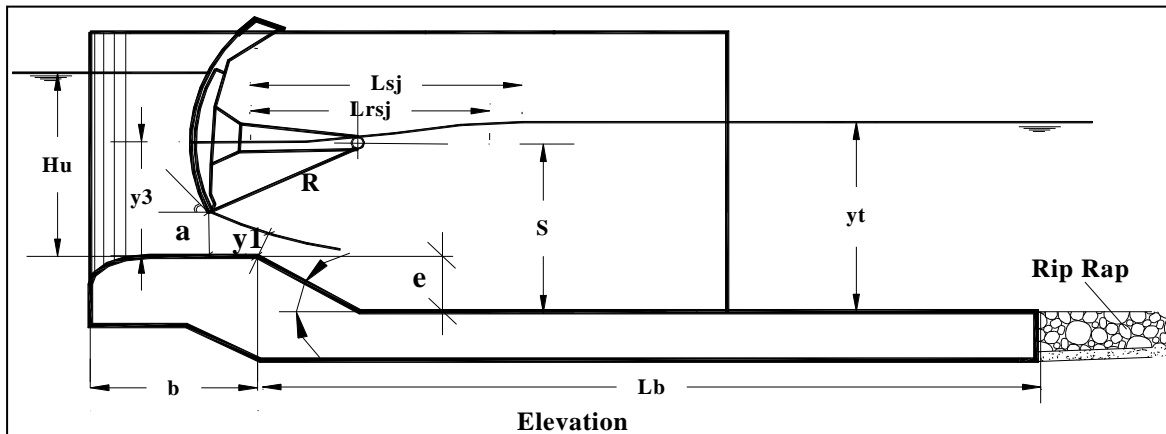


Figure 3-13: The measured flow and the submerged hydraulic jump parameters

3.22 Measuring the Length of the Reverse Flow L_{rf}

During the test series where an end sill was used, a reverse flow was observed downstream the end sill and extended to some downstream distance. Figure 3.10 provides a sketch showing the zone of reverse flow. These distances were measured during each test run. The length of the reverse flow zone was determined using the currentmeter, which was installed five centimeters above the bed.

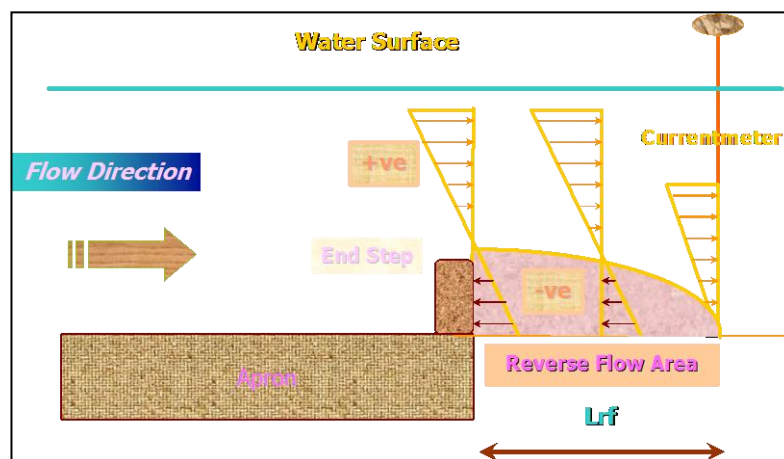


Figure 3-14: Length of the reverse flow

3.23 Results

For each tested sluiceway stilling basin different measurements were carried out. The results of these measurements were found in the Annexes attached with this report. Sample of the measurements are presented in this chapter. The result which presented in this chapter covers the following measurements:

- The velocity distribution along the centerline of the simulated bay downstream the gate.
- The nearbed velocity along the centerline of the simulated bay downstream the gate.
- The scour downstream the apron.
- The characteristics of the submerged hydraulic jump.

3.23.1 The velocity distribution

The velocity distributions were measured at the predefined cross section along the centerline of the simulated stilling basin. Figures 3-15 to 3-22 presented the results of the velocity distribution for test No. 4 and 5 for the test series A, B, C, and D.

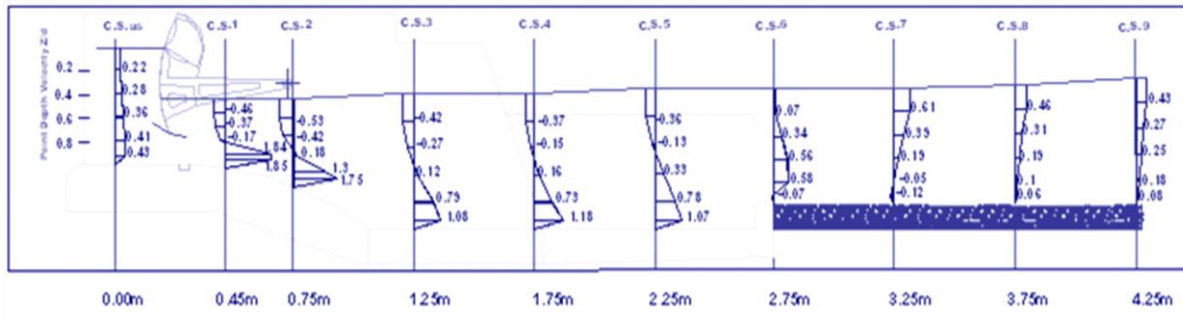


Figure 3-15: Velocity distribution downstream the gate, test No. 4, series A

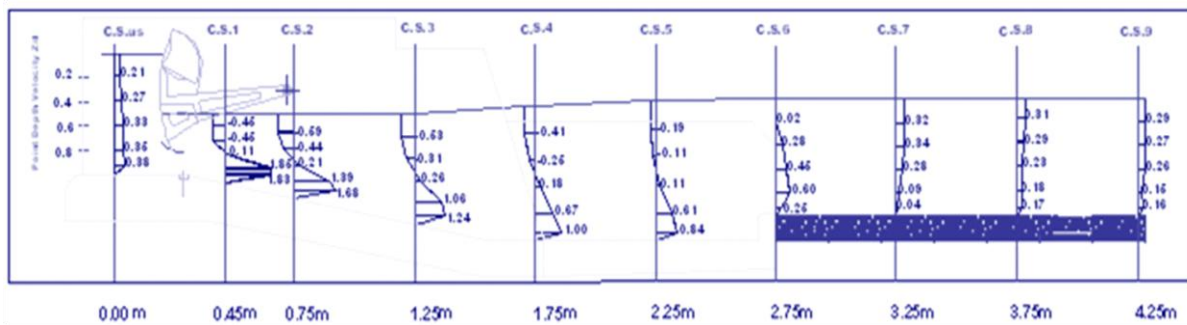


Figure 3-16: Velocity distribution downstream the gate, test No. 4, series B

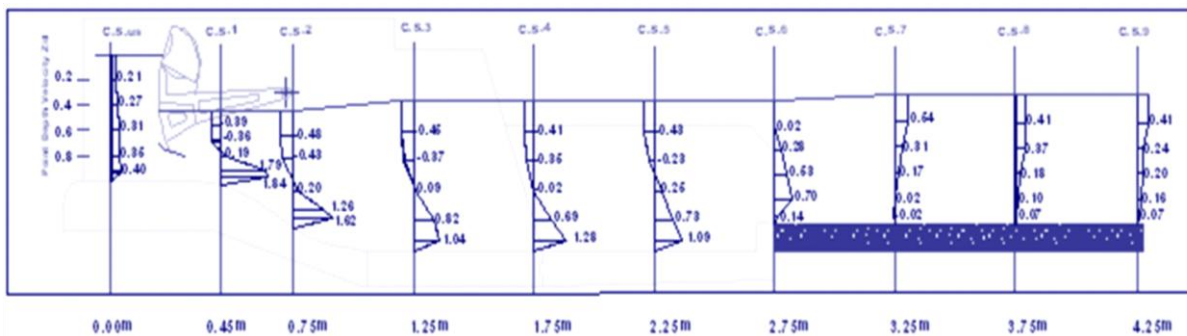


Figure 3-17: Velocity distribution downstream the gate, test No. 4, series C

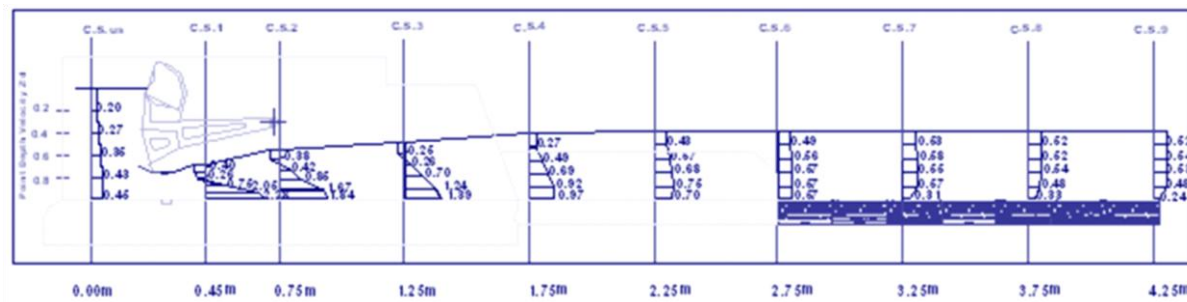


Figure 3-18: Velocity distribution downstream the gate, test No. 4, series D

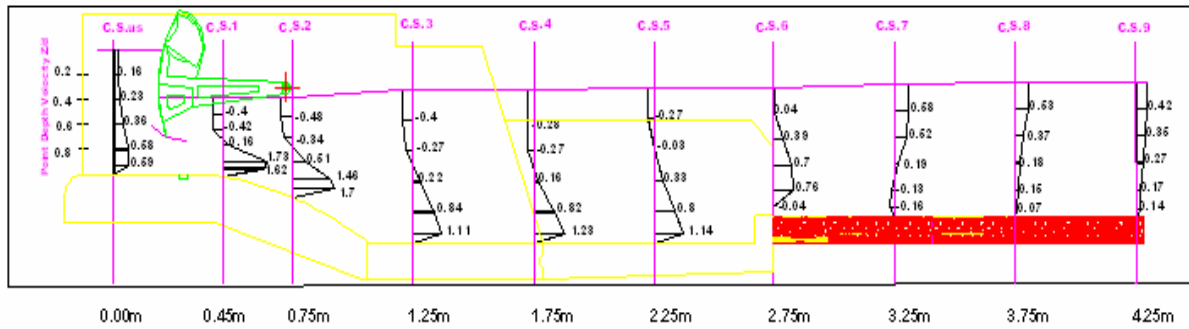


Figure 3-19: Velocity distribution downstream the gate, test No. 5, series A

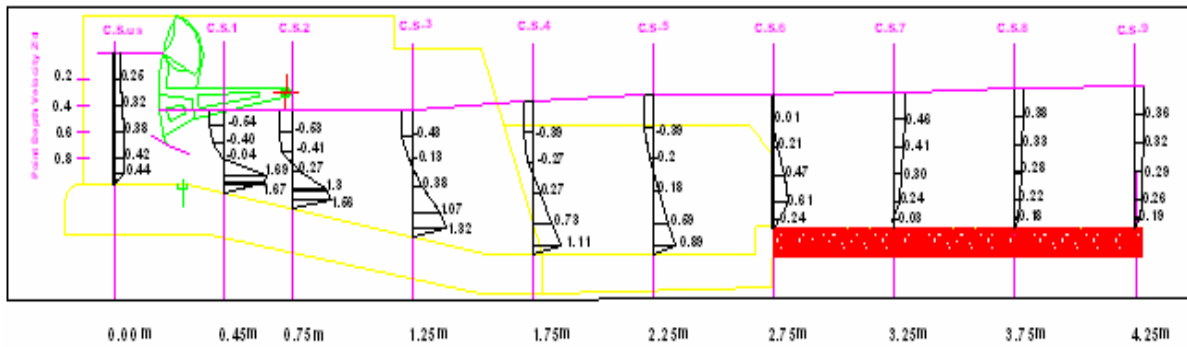


Figure 3-20: Velocity distribution downstream the gate, test No. 5, series B

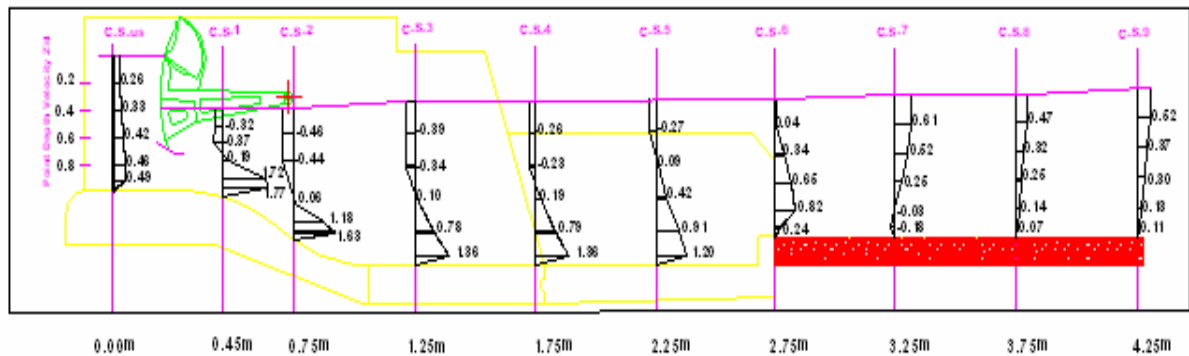


Figure 3-21: Velocity distribution downstream the gate, test No. 5, series C

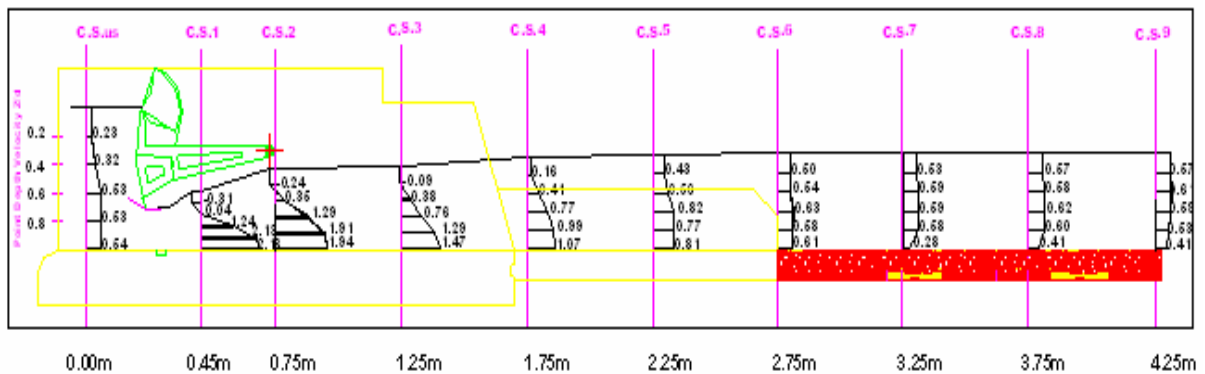


Figure 3-22: Velocity distribution downstream the gate, test No. 5, series D

3.23.2 The near bed velocity

The near bed velocity was measured at each cross section. The near bed velocity was measured at 3 cm above the bed. Samples of the near bed velocity were presented in this section. Figure 3-23 shows the near bed velocity for the test series A.

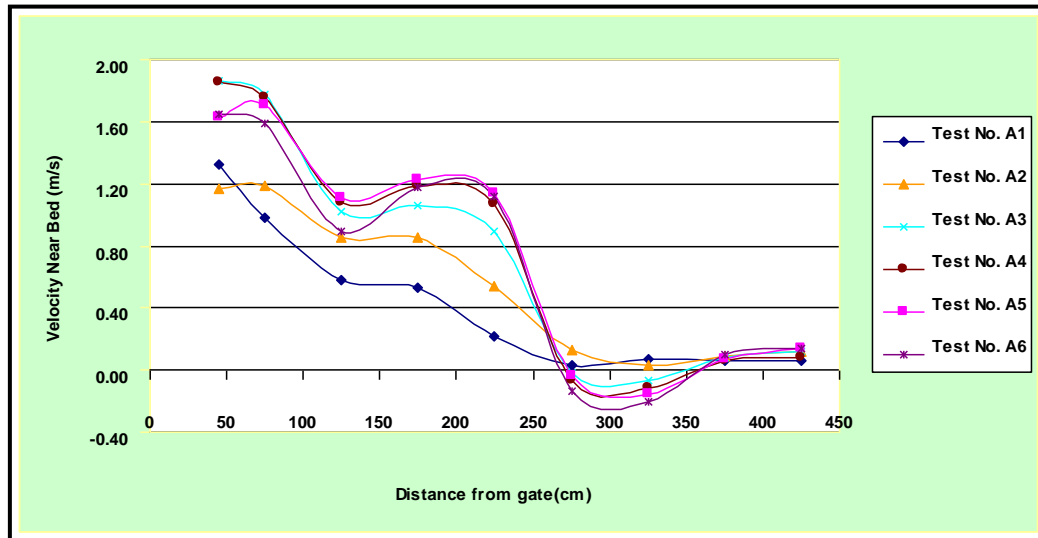


Figure 3-23: the near bed velocity distribution downstream the gate, series A

3.23.3 Scour downstream the apron

The scour downstream the apron was recorded for each test run of the tested stilling basin. Figure 3-24 presented the scour that takes place downstream the apron after test run No. 4, test series A. the remaining results of the scour downstream the apron are found in the Annex (C).

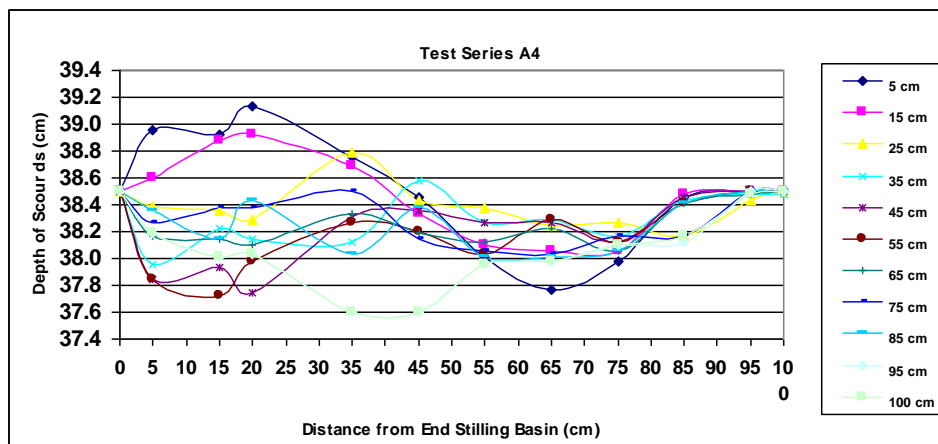


Figure 3-24: the scour profiles downstream the apron, test No. 4, series A

3.23.4 The characteristics of the submerged hydraulic jump

for each test runs following measurements were recorded, the gate opening (a), the back up water depth (y_3), the initial water depth of the jump (y_1), the length of jump (L_{sj}), the length of reverse flow (L_{rf}). Table 3-9 presented the results of results of test series A. the remaining results for the other test series are found in the Annex (D).

Table 3-9: Results of the Submerged Hydraulic Jump Parameters

Test No.	Q(model) l/sec	y₃ (cm)	y₁ (m)	Gate Opening (cm)	y_t (cm)	L_s (cm)	Scour Depth (cm)	LS_J (cm)	L_{rf} (cm)
A1	37.1	15	0.02	2.80	40.20	0	0.00	239	0
A2	61.9	18	0.027	4.70	44.42	67	3.8	239	20
A3	99.0	23	0.055	8.50	49.59	81	5.2	240	72
A4	123.7	25.5	0.075	11.90	52.39	96	4.3	240	75
A5	148.4	28	0.13	15.20	54.79	106	5.2	241	77
A6	185.6	31.4	0.17	20.60	57.80	112	6.4	241	80

4

NUMERICAL MODEL SIMULATIONS OF STILLING BASIN

4.1 Introduction

The numerical models are an alternative tool to predict the hydraulic performance of the stilling basin. The key issue pertaining to these models is the reliability of their results to ensure a proper structure functionality and serviceability throughout the project lifetime. Nobody can deny that there is a great booming of advanced technology leading to development of supercomputers. With such supercomputers, the need to adopt numerical models in the design process of the stilling basin becomes deceive. The hydraulic performance of the stilling basin inherits a complex turbulence structure with rapidly varied flow represented by the hydraulic jump generation.

At the beginning of this research project, it was a great interest to find the suitable numerical model that can produce the reliable results. Some models with different numerical scheme, finite difference or volume of fluid, as stated below can produce relatively good results. Amongst these models, commercial numerical models (FLUENT, FLOW3D, and DELFT3D) as well as the non-commercial source codes that are not available, are studied.

This chapter describes the researcher's attempts to simulate numerically the hydraulic performance – specifically the hydraulic jump – of the stilling basin.

Hirt and Nichols (1981) developed a simple but powerful, method that is based on the concept of a frictional volume of fluid (VOF). This method is shown to be more flexible and efficient than other methods for treating complicated free boundary configurations. It is particularly useful because it uses a minimum of stored information, treats intersecting free boundaries automatically – efficient for rapidly varied flow – and can be readily expended to three-dimensional calculations. Hirt and Nichols defined a function F , whose value is unity at any point occupied by fluid and zero otherwise. The average value of F in a cell would then represent the frictional volume of the cell occupied by fluid. In particular, a unit value of F would correspond to a cell full of fluid, while a zero value would indicate that the cell contained no fluid. Cell with F values between zero and one must then contain a free surface. Thus, the fractional volume (VOF) method provides the same coarse interface information available to the marker particle method. Yet the VOF method requires only one storage word for each mesh cell, which consistent with the storage requirements for all other dependent variables.

Ma el al. (2001) adopted the technique of Hirt and Nichols (1981) and numerically studied the turbulence characteristics of two-dimensional submerged hydraulic jumps by means of the standard $k-\epsilon$ turbulence model. In the calculations, the VOF method is employed to deal with the moving, highly variable free surface. The jumps calculated have Froude numbers ranging from 3.2 to 8.2 and submergence factors ranging from 0.24 to 0.85. The calculated results, including surface profiles, time averaged velocities, hydrodynamic pressures as well as turbulent quantities, are compared with available experimental measurements. The achieved results provide insights into not only the macroscopic structure but also the turbulent structure of submerged hydraulic jumps. However, They noted that the inclusion of air entraining, the effect of streamline curvature and more accurate free surface conditions for turbulence quantities and the implementation of a suitable low Reynolds number turbulence model for the boundary layer flow would improve the numerical calculation of hydraulic jumps significantly.

The problem of transitional flow from supercritical flow to subcritical flow or vice versa is characterized by steep gradients in either water surface or bed topography or both. Numerically, such steep gradients entail the necessity of applying full vertical momentum equation rather than adopting Boussinesq approximation. Consequently, algorithms developed for coastal regions and estuaries are not suitable for transitional flow modeling (Elzeir, 1996, and Busnelli, 2001).

Busnelli (2001) stated that a different class of numerical schemes was applied to solve discontinuous flows. The methods of Godunov (Hirsch, 1990; Vreugdenhil, 1994; Toro, 1997; Wesseling, 2001) are in general explicit and based upon non-staggered grids. One disadvantage of the Godunov type schemes resides in the treatment of non-homogeneous term of shallow water equations. Moreover, the explicit solution to the shallow water equations is restricted by the Courant-Friedrichs-Lewy (CFL) stability condition.

Casulli and Stelling (1998) and Casulli (1999) developed a one-dimensional model to solve the Reynolds-averaged Navier-Stokes equations for transitional flows. They split the momentum equations such that the free surface elevation and the hydrodynamic pressure are determined in two steps. First, the hydrodynamic pressure is neglected and free surface levels are determined. In the second step, the velocities are computed by considering the hydrodynamic pressure terms. In this way, the free surface levels and the hydrodynamic pressure are obtained independently. Later, Busnelli (2001) extended the model to 2DV and 3D. Stansby and Zhou (1998) proposed a similar approach but in their method, the hydrodynamic pressure was explicitly included in the first step and in the second step, the hydrodynamic pressure was corrected to fulfill the local continuity equation.

Busnelli (2001) reported that her 2DV model could fairly predict the position of the hydraulic jump downstream a sluice gate and the length of the surface roller. However, the model failed to predict the reverse flow in the region of the hydraulic jump roller. Busnelli (2001) attributed the deviation to using the standard $k-\epsilon$ model. It was suggested that an anisotropic turbulence closure model would be adequate to represent the supercritical flow and the transition to the subcritical flow along the length of the surface roller.

Patankar and Spalding (1972) introduced the concept of parabolic flow which satisfies the following conditions:

- (a) The existence a predominant direction of flow (i.e. there is no reverse flow in that direction).
- (b) The occurrence of diffusion of momentum, heat, mass, etc. is negligible in that direction;
- (c) The downstream pressure field has little influence on the upstream flow conditions.

Patankar and Spalding (1972) developed a 2-D model to calculate heat, mass, and momentum transfer in parabolic flow. The model has the following features. The longitudinal and cross-stream pressure gradients are uncoupled which made the equation to be parabolic. The method is non-iterative. The usage of upstream convection fluxes, the explicit corrections of pressure and velocity, and the double sweep-TDMA (Tri-Diagonal Matrix Algorithm) solution for the finite difference equations. From a personal communication, it was perceived that Koji Shiono (Loughborough University) constructed a model using the method of Patankar and Spalding (1972) and applied three types of closure model, namely; the standard $k-\epsilon$ model, Algebraic Stress Model (ASM) and a non-linear $k-\epsilon$ model. The model was successfully tested in reproducing secondary circulation in compound channels.

A complete survey was made to find a commercial or an open source code which are capable of investigating the flow field in the stilling basin. Flow3D, Fluent and Delft3D with their new development can be utilized, although they are quite expensive. As for Flow3D, the developers claimed that the model is capability to simulate flow with discontinuity; however, it cannot be used in the current research due to the lack of scientific validation and the reluctance of the developers to provide any sort of scientific manual to the program as well as the deficiency of financial support. On the other hand, Delft3D which is available at HRI with the new development – including the non-hydrostatic assumption- that can be utilized and examined in the next Project stages.

4.2 General

A stilling basin provides a means to absorb or dissipate the energy from the spillway discharge and protects the spillway area from erosion and undermining. Many laboratory studies have been made for stilling basins. Nevertheless, it is often necessary to conduct hydraulic modeling studies on individual structures to be certain that these stilling basins will perform as anticipated. Determining the amount of energy absorption and estimating the velocity values and its fluctuations, especially near the bed, is essential for downstream bed protection stability analysis. Any excessive scouring in the river bed downstream the stilling basin can eventually result in the failure of the hydraulic structure.

4.3 Problem definition and analysis

Stilling basins are considered one of the important hydraulic structures to protect the bed against erosion downstream the outlets. Without a proper design for stilling basins it is expected a severe erosion and lowering in the bed level. Bed lowering can move in both an upstream direction (as a 'headcut' or 'nick point') and/or downstream, influencing the channel stability over an extensive length of the river or stream system.

Riverbed lowering can:

- Initiate extensive bank erosion because the height of the banks relative to the bed is effectively increased, leaving them more susceptible to collapse.
- Undermine riverbanks, resulting in overall channel enlargement with all the associated adverse impacts of bank erosion on economic and environmental values.
- Cause lowering of river water level. This may deny water to pumps for irrigation and/or domestic supplies. It may also decrease habitat for in stream fauna such as fish and platypus.
- Cause lowering of groundwater level in the adjacent floodplain. This may deny water to bore wells and adversely affect the aquifer.
- Cause downstream siltation which can destroy aquatic habitats and have adverse impacts on water quality, water availability, flooding, navigation and recreational pursuits.
- Result in damage to infrastructure including bridges, crossings and pumps.

4.4 Objectives

This study aims to investigate the hydraulic performance and the flow conditions in a stilling basin and examining if and how accurately the flow in the stilling basin could be computationally modeled. Delft 3D software was used to simulate the sluiceway behaviour of the New Naga Hammadi Barrage on the Nile River. 1D, 2DV (2D Vertical) and 3D numerical models have been used to study the sluiceway in two operational cases fully open gate and partially open gate.

The results of these models have been compared with the results of the hydraulic flume model which was built at the Hydraulics Research Institute (HRI), also theoretical analysis using formulas and empirical charts was applied to check the numerical model results.

4.5 Physical & Numerical models

Physical models provide an opportunity to observe the flow characteristics and to make measurements in limited locations. Velocity measurements in the stilling basin of the physical models are not obtainable due to excessive turbulence in addition to the high operational cost required to run the physical models. Therefore three dimensional mathematical models are developed to simulate such conditions. Such models provide another tool to describe, define and evaluate the flow characteristics within the stilling basin. Several models have been developed in that field like CFD (computational fluid dynamics) and Delft 3D. Numerical models can also be used to evaluate stilling basin modifications (deflectors, Baffle block removal, etc.).

Physical modeling is an unalterable tool to guarantee economic and ecological design of complex hydraulic structures. Besides this “traditional” method, numerical modeling has become more and more important in the last few years. Powerful computers and improved mathematical algorithms supported this trend. Emphasis must be drawn to the fact that today numerical models are not able to compensate physical models. To simulate a three-dimensional flow field with computers under real state boundary conditions is impossible or better: unaffordable. It is for sure that engineers will go on using physical models, but with the support of numerical modeling to improve developing time, guarantee economic design and optimize the ecological value of the hydraulic structure. However, due to the complexity of the physical phenomenon related to energy dissipation and to the obvious three dimensional motion with high degree of turbulence, the use of mathematical models are subjected to further analyses.

By using both the physical and numerical model a synergetic effect could be observed. The positive influences of numerical in combination with physical modeling are definitely an innovative way for engineers to develop hydraulic structures.

4.6 The Case Study

The New Naga Hammadi Barrage, opened on 12th January 2008, has been used as a case study. The New Naga Hammadi Barrage (NNHB) consists of a sluiceway, a low head power plant, and a navigation lock. The sluiceway is equipped with 7 radial gates of 17 m width and 13.5 m height each, see figures 1 and 2. The Hydraulics Research Institute (HRI) conducted hydraulic model investigations of the sluiceway in a 2-D flume model. The 2D-detail model of one discharge opening of the sluiceway is used to test the discharge capacity and hydraulic performance of the sluiceway.

For the new barrage normal operation (partially open gates) the upstream water level will be maintained at 65.90 m asl up to river discharges of 5700 m³/s. During flood flow conditions, above 5700 m³/s, the gates will be fully open and the upstream water level establishes according to the head loss under subcritical flow conditions.

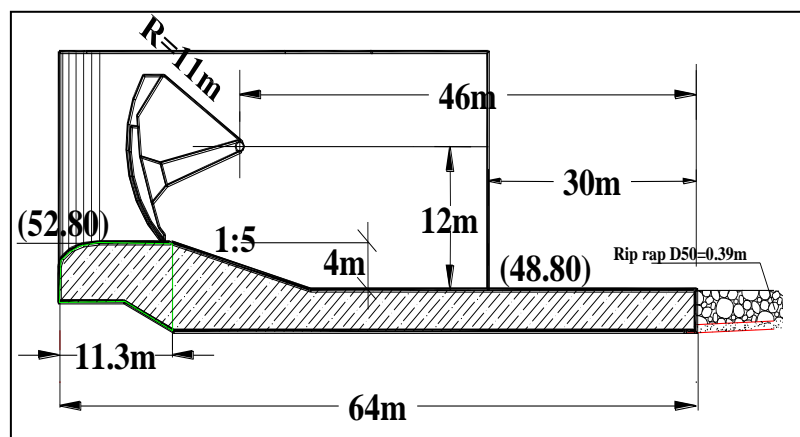


Figure 4-1: Longitudinal Section of the New Naga Hammadi Spillway Stilling Basin (HRI 1998)



Figure 4-2: Location of New Naga Hammadi Barrage

4.7 The Numerical Model (Delft 3D) Setup and Operation

Delft Hydraulics has developed a fully integrated computer software suite for a 3D multi-disciplinary approach for coastal, river and estuarine areas. The model can simulate flows, sediment transports, waves, water quality, morphological developments and ecology and it is composed of several modules, grouped around a mutual interface, while being capable to interact with one another. Delft 3D Version 3.54.28.00 was used to setup 1D (One Dimensional Model) and 2DV (Two Dimensional Vertical Model) for two sill levels (52.80 & 53.45) and Delft 3D Version 3.55.05.779 was used to setup 3D (Three Dimensional Model) for sill level (52.80). DELFT3D software package was used for

For setting up the three models (1D, 2DV and 3D) different modules have been used: RGFRID for generating of computational or numerical grid and QUICKIN for introducing bathymetry of the model.

The general model for Naga Hammadi stilling basin, includes one sluiceway bay 17 m width with a concrete gated sill and concrete apron to cover a length of about 64 m. The upstream and downstream approach floors are protected with riprap. The mathematical model simulates a reach with total length of about 450 m, including two channel extensions; around 100 m before the slope 15:1 in the upstream side and 50 m after the slope 15.2:1 in the downstream side to assure that flow at the upstream and downstream boundary conditions is steady and uniform.

The grid cells have been generated using the grid generator program QUICKIN because the model in this study is symmetric, but in cases of unsymmetrical models RGFRID should be used.

By selecting different flow layers in both horizontal and vertical directions the degree of the results accuracy obtained is influenced. Selecting a large number of horizontal or vertical layers will result in a more accurate calculation of the velocity profile but the time needed for one run increases substantially from one alternative to another. Therefore, a study of the grid sensitivity was performed to select the most efficient alternative.

The input file for the hydrodynamic simulation program contains all the necessary data required for defining a model, called scenario, and running the simulation program. The data of the bathymetry and the numerical grid, also information on boundary conditions, discharges and grid related quantities such as monitoring points, discharges etc. are stored in separate, so-called attribute files. In the input file only a reference is made to these files instead of including all data in the input file itself. The big advantage of using attribute files is that the data can be used in many scenarios but is stored only once on the system disks.

After number of trials it was found that in most of all simulated models the flow becomes steady after ± 30 minutes so the total simulation time was taken 1 hour to guarantee that the steadiness conditions are achieved. The selection for simulation time step is based on numerical scheme stability criterion i.e., the Courant number C_r , which is dependent on the grid size of the model and on the flow depths. It was found that most suitable value for the time step is 0.001 minutes or 0.06 seconds in most of the models, this value provides an accurate and stable numerical computation in both the hydrodynamic and other simulation processes.

In models which the local scour downstream the basin has been studied, the process Sediments (non-cohesive) was selected; to enable the process of erosion and sedimentation.

Initial conditions specify the initial values the computation will start with and they were taken as a uniform value in the whole models areas and equal to the downstream boundary conditions (downstream water levels) to avoid the discrepancy between the initial condition and the boundary conditions which can result in short wave disturbances that propagate into the model area and the simulation might even become unstable.

There are two boundary conditions:

$$\frac{\partial Q}{\partial t} = 0 \rightarrow Q = \text{constant (upstream boundary)}$$

$$\frac{\partial h}{\partial t} = 0 \rightarrow h = \text{constant (downstream boundary)}$$

Manning Coefficient (n) was assumed as an average value = 0.011 (as a common value for concrete roughness) but in cases of studying local scour downstream the basin a roughness map was implemented and in that case Manning Coefficient (n) for the upstream and downstream areas of the models which are covered by the riprap, was calculated from Muller (1943) equation. Flooding scheme was applied for all the models because it is implemented for problems that include rapidly varying flows like in cases of hydraulic jumps and bores (Stelling and Duijnmeijer, 2003). Table 1 indicates summary for the important computational parameters.

Table 4-1: Summary for the important computational parameters

No.	Computational Parameters	Value
1	Length of computational cells in the longitudinal direction	450 m
2	Width of computational cells in the transverse direction	17 m
3	Computational time step	0.001 minutes
4	Number of layers	10
5	Roughness coefficient (n)	0.011
6	Sediment size (D_{50})	20 μm
7	Sediment transport formula	Van Rijn's
8	Turbulent model	k- ϵ
9	Type of velocity profile	Logarithmic
10	Morphological time scale factor	100

Several observation points (12 observation points) are specified in the model in order to monitor the computational results. These observation points are used to monitor the time-dependent behaviour of the velocities and water levels along the longitudinal section. Observation points are located at cell centre of the sluiceway, i.e. at water level points. It should be noted that CS1 & CS2 were selected in regions of steady and uniform flow conditions near the boundaries to represent the two gauge points in the physical model (at 150 m upstream the sill and 200 m downstream the sill), see figure 3.

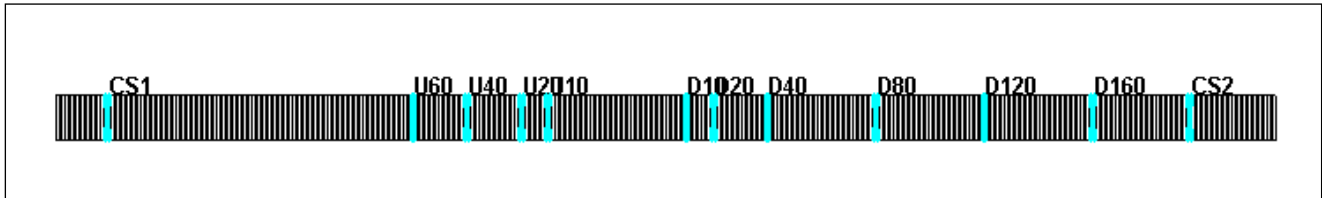


Figure 4-3: The observation points along the horizontal grid

4.8 Results and Analysis

4.8.1 Fully Open Gates and Uncontrolled Upstream Water Level

Case of Flood Simulation “Fully Open Gate” - Subcritical Flow Conditions

The numerical model was used to test the case of fully open gate, which will occur in the case of high flood operation or in case of hydropower maintenance. This test series (A1 to A8) was performed for the range of discharges 950 to 7000 m³/s for two sill levels (52.80 m asl and 53.45 m asl), the following fields of study have been studied in case of fully open gate.

- Discharge capacity.
- Upstream water level and water drop over the sill.
- Head losses between u/s & d/s stations (gauges).
- Flow velocities 1 m above the river bed at distances of 10, 20, 40 and 60 m in the upstream side and measured from the u/s face of the sill moreover, velocities at distances of 10, 20, 40, 80, 120 and 160 m downstream from the start of the horizontal apron.
- Vertical velocity distribution at u/s and d/s point gauge stations (CS1 & CS2) at 0.2, 0.6 and 0.8 water depth or/and @ 1m above bed level.

Table 4-2: The Flume Data

Test	Q	Q (per vent)	U.S.W.L	V ₁	Sill W.L.	D.S.W.L	V ₂	Δh	Initial Cond ^l .	U.S. B.C.	D.S. B.C.*
No.	m ³ /s	(m ³ /s/vent)	m asl	m/s	m asl	m asl	m/s	m	W.L. (m)	Q (m ³ /s)	W.L. (m)
A1	950	135.7	59.43	1.32	59.42	59.43	0.99	0.01	-9.57	135.7	-9.57
A2	1700	242.9	60.8	1.87	60.77	60.8	1.39	0.03	-8.20	242.9	-8.20
A3	2000	285.7	61.26	2.04	61.23	61.26	1.55	0.03	-7.74	285.7	-7.74
A4	3000	428.6	62.15	2.57	62.07	62.10	2.3	0.08	-6.90	428.6	-6.90
A5	5300	757.1	65.00	3.65	64.88	65.00	3	0.12	-4.00	757.1	-4.00
A6	5700	814.3	65.37	3.8	65.23	65.37	3.1	0.14	-3.63	814.3	-3.63
A7	6300	900.0	65.93	4.01	65.77	65.89	3.31	0.16	-3.11	900.0	-3.11
A8	7000	1000.0	66.46	4.36	66.26	66.46	3.48	0.20	-2.54	1000.0	-2.54

* Below the Reference Level (69.00)

Where;

V_1 & V_2 are the upstream and downstream average velocities

Δh is the water drop over the sill = (USWL – Sill water level)

4.8.2 Discharge Capacity (Rating Curve)

The discharge values per one vent and the downstream water levels were used as upstream and downstream boundary conditions respectively to setup the models. D' Aubuisson equation has been used to check if and how accurately the 1D Model results (USWL, DSWL and upstream approach velocities) could represent the flow capacity. 1D Model was used in this check because the velocity in d' Aubuisson equation is a depth averaged velocity. Rating curves for low-head dams under submerged uncontrolled flow conditions can be computed by the d' Aubuisson equation (United States Army Corps of Engineers, Chapter 5). The model and computation results are shown in figure 4.

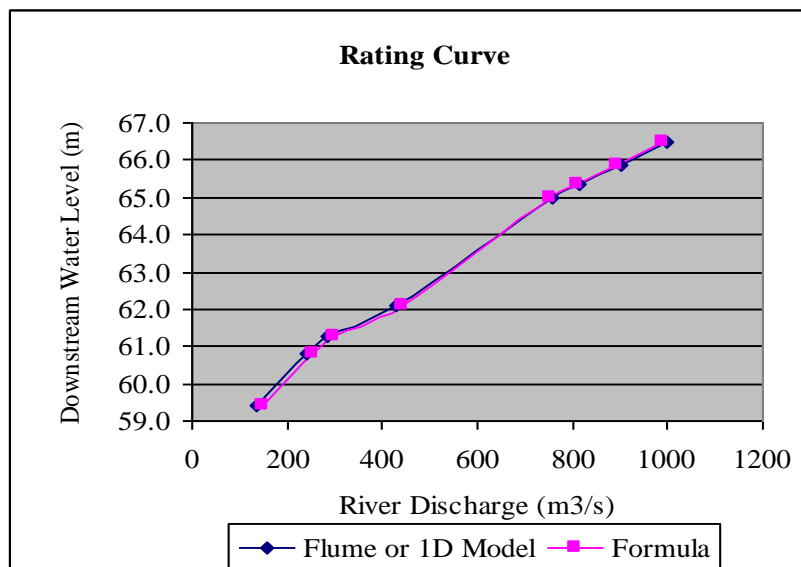


Figure 4-4: Rating curves using 1D Model and d' Aubuisson Formula

From figure 4 a very good agreement is shown between the rating curve of the 1D Model and the calculated one from the formula which indicates that the numerical model is very efficient in representing the flow capacity.

4.8.3 Water Levels

Eight tests were conducted for different values of discharges to measure the water levels, a summary for the physical model results are presented in table 3.

Table 4-3: Water levels from the flume Data in case of fully open gate and sill level (52.80)

Test No.	Q (m ³ /s)	Q (per vent) (m ³ /s/vent)	U.S.W.L (m asl)	U.S.W.L* (m)	Sill W.L. (m asl)	Sill W.L.* (m)	D.S.W.L (m asl)	Δh (m)
A1	950	135.7	59.43	-9.57	59.42	-9.58	59.43	0.01
A2	1700	242.9	60.8	-8.2	60.77	-8.23	60.8	0.03
A3	2000	285.7	61.26	-7.74	61.23	-7.77	61.26	0.03

A4	3000	428.6	62.15	-6.85	62.07	-6.93	62.10	0.08
A5	5300	757.1	65	-4	64.88	-4.12	65.00	0.12
A6	5700	814.3	65.37	-3.63	65.23	-3.77	65.37	0.14
A7	6300	900.0	65.93	-3.07	65.77	-3.23	65.89	0.16
A8	7000	1000.0	66.46	-2.54	66.26	-2.74	66.46	0.2

* Remark: the data in this column (in table 4) represents the upstream water level with respect to the Reference Level (69.00)

It should be noted that the upstream and downstream water levels were measured at the upstream and downstream gauge stations.

Upstream Water Level

Up to river discharges of 5700 m³/s the upstream water level is to be maintained at the Normal Operation Water Level of (65.90) m asl by the control of the radial gates. For flood discharges above 5700 m³/s, the gates will be fully open and the upstream water level establishes according to the head loss under subcritical flow conditions.

Mathematical models 1D, 2DV (Z-Grid) and 3D (Z-Grid) were used in case of sill level (52.80) to check the upstream water levels for different discharges and the results were compared with the flume data, check figure 5.

In case of sill level (52.80) it was noticed that the 3D (Z-Grid) results are very similar to 2DV (Z-Grid) or in other words the baffle blocks in case of the 3D model has no significant influence on the water levels so it was decided to use only 1D, 2DV (Z-Grid) in case of sill level (53.45) as presented in table 4.

It was decided also not to use 2DV Sigma Grid in case of sill level (53.45) because it was noticed that it gives similar results as 2DV Z-Grid, particularly in case of measuring water level above flat bed level as it will be discussed later.

Table 4-4: Upstream water levels

Test No.	Q (m ³ /s)	Sill level (52.80)				Sill level (53.45)		
		U.S.W.L. (m)				U.S.W.L. (m)		
		Flume	1D Model	2DV Z-Grid	3D Z-Grid	Flume	1D Model	2DV Z-Grid
A1	950	59.43	59.45	59.47	59.46	59.43	59.46	59.47
A2	1700	60.80	60.86	60.86	60.85	60.8	60.87	60.91
A3	2000	61.26	61.34	61.33	61.33	61.26	61.34	61.41
A4	3000	62.15	62.24	62.21	62.22	62.15	62.24	62.29
A6	5700	65.37	65.61	65.59	65.60	65.37	65.62	65.69
A7	6300	65.93	66.15	66.13	66.13	65.93	66.16	66.24
A8	7000	66.46	66.75	66.71	66.70	66.46	66.76	66.85

In table 4 the last two highlighted rows represent the case of flood events when the discharge becomes higher than 5700 m³/s. The capacity of the sluiceway for full gate opening and without upstream water level rise over the designed water level (65.90) is 6300 m³/s.

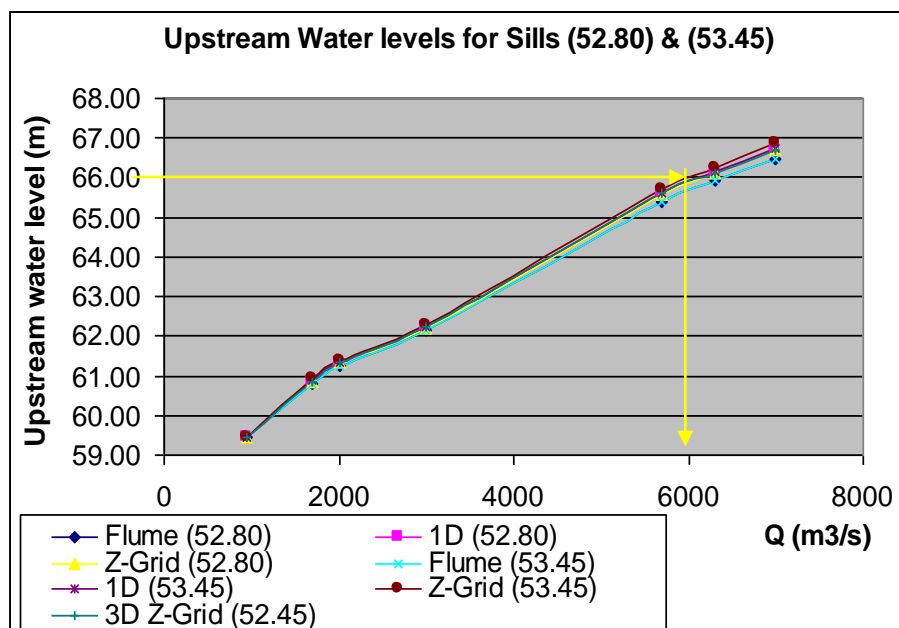
**Figure 4-5:** Upstream water levels

Figure 4-5 and table 4-4 show a very good agreement between the flume data and the different models, nevertheless it should be noted that the change in the sill levels or the baffle blocks existence has no significant influence on the upstream water levels, this is due to the relatively small crest height with respect to the water depth.

Water Drop over the Sill

Water drop over the sill happens due to the convergence of the flow in the vertical direction and increasing of the velocity head which leads to decreasing in the water depth above the sill. This drop could be easily calculated from the model as the difference between the upstream water levels and the lowest water level above the sill. The final results of the water drop over the sill are presented in table 4-5; also figure 4-6 shows the water levels at the upstream gauge station and the water level over the sill (52.80)

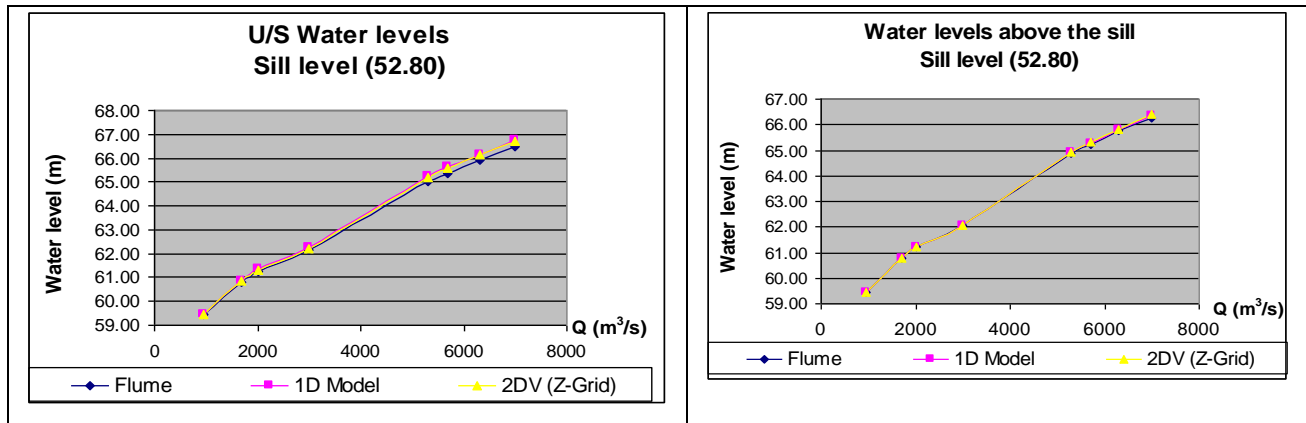


Figure 4-6: water levels upstream the sill and water levels over the sill (52.80)

In case of sill level (52.80) different models were used; 1D, 2DV Z-Grid, 2DV Sigma Grid and 3D Z-Grid but in case of sill level (53.45) two models only were used 1D and Z-Grid as it was noticed that 3D Z-Grid model gives similar results as 2DV Z-Grid for the same reason which was mentioned before, also it was found that Sigma Grid is not sensitive with respect to the bed variations, as it will be discussed later, so it was decided not to use it also in the second sill level.

Table 4-5: Water drop over sills

Test No.	Q m ³ /s	Δh (m) for sill (52.80)					Δh (m) 53.45	
		Flume	1D Model	2DV (Z-grid)	2DV (Sigma)	3D (Z-Grid)	1D Model	2DV (Z-Grid)
A1	950	0.01	0.03	0.05	0.01	0.04	0.06	0.06
A2	1700	0.03	0.08	0.08	0.02	0.08	0.12	0.16
A3	2000	0.03	0.11	0.09	0.02	0.09	0.14	0.21
A4	3000	0.08	0.19	0.15	0.04	0.16	0.26	0.28
A6	5700	0.14	0.32	0.27	0.04	0.25	0.42	0.44
A7	6300	0.16	0.35	0.29	0.05	0.27	0.46	0.47
A8	7000	0.2	0.39	0.31	0.05	0.28	0.52	0.58

Remark: there is no flume data in case of sill (53.45) because water levels above the sill are not mentioned in the physical model report.

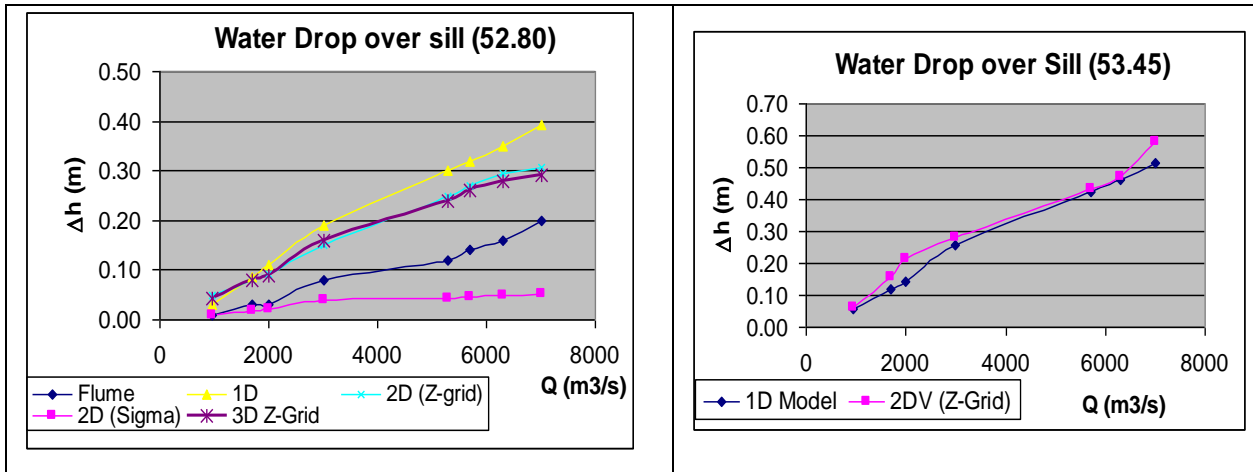


Figure 4-7: Water drop over sills (52.80) and (53.45)

Figure 4-7 shows the water drop over sills (52.80) and (53.45), in the first figure (from the left) 2D and 3D Z-Grid models have a similar trend as in the flume and the largest deviation equal to 13 cm only which is considered very small with respect to the total water depth, whilst for the Sigma Grid it is noted that it is not sensitive with respect to bed variations particularly with high discharges (higher than 2000 m³/s) as it applies the shallow water equations without taking the vertical acceleration and the non hydrostatic pressure into considerations.

Water drop levels over sills (52.80) and (53.45) are combined in Figure 8, it is noted that the water drop increases in the higher sill level due to the increase in the flow contraction which leads to an increase in the velocity head and increase in the water drop.

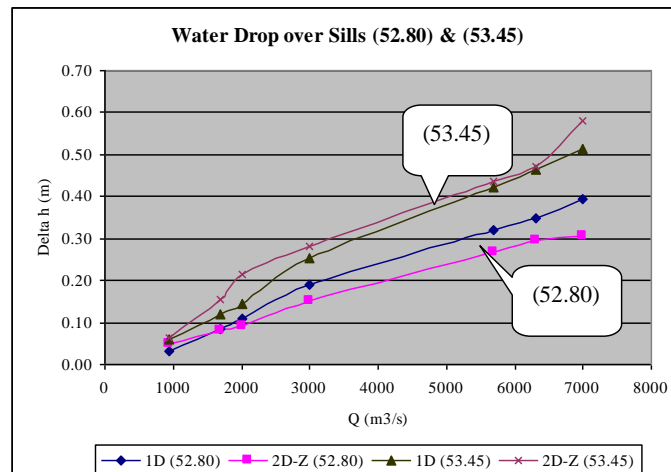


Figure 4-8: Water drop over sills (52.80) & (53.45)

Head Losses between Sections CS1 and CS2

Head losses were calculated between upstream U/S and Downstream D/S point gauges at cross section CS-1 and CS-2 for river discharges ranging from 950 to 7000 m³/s. The head loss was calculated by application of Bernoulli's equation:

$$H_1 + \frac{V_1^2}{2g} = H_2 + \frac{V_2^2}{2g} + h_L \quad (4-1)$$

Where:

H_1 : Upstream water level in m asl.

H_2 : Downstream water level in m asl.

V_1 : Upstream velocity *at one meter above the bed* in the CS-1 in m/s.

V_2 : Downstream velocity *at one meter above the bed* in the CS-2 in m/s.

h_L : Head loss between sections CS-1 and CS-2 in m.

It was noticed that the upstream and downstream water levels are almost equal with the different discharges so the head loss was calculated as the difference between the velocity heads only.

$$h_L \approx \frac{V_1^2}{2g} - \frac{V_2^2}{2g} \quad (4-2)$$

the total head losses are presented in table 6, see the charts in Figures 9 and 10.

Table 4-6: Total Head loss between sections CS1 and CS2

Q (m ³ /s)	h _L (52.80)					h _L (53.45)		
	Flume	1D	2D (Z-grid)	2D (Sigma)	3D (Z-Grid)	Flume	1D	2D (Z-grid)
950	0.04	0.05	0.05	0.04	0.05	0.04	0.05	0.06
1700	0.08	0.10	0.09	0.07	0.09	0.09	0.10	0.09
2000	0.09	0.11	0.11	0.08	0.11	0.11	0.11	0.13
3000	0.12	0.20	0.19	0.13	0.19	0.12	0.20	0.24
5700	0.25	0.30	0.31	0.14	0.31	0.21	0.29	0.38
6300	0.26	0.32	0.33	0.15	0.33	0.26	0.32	0.42
7000	0.35	0.35	0.36	0.25	0.37	0.37	0.35	0.52

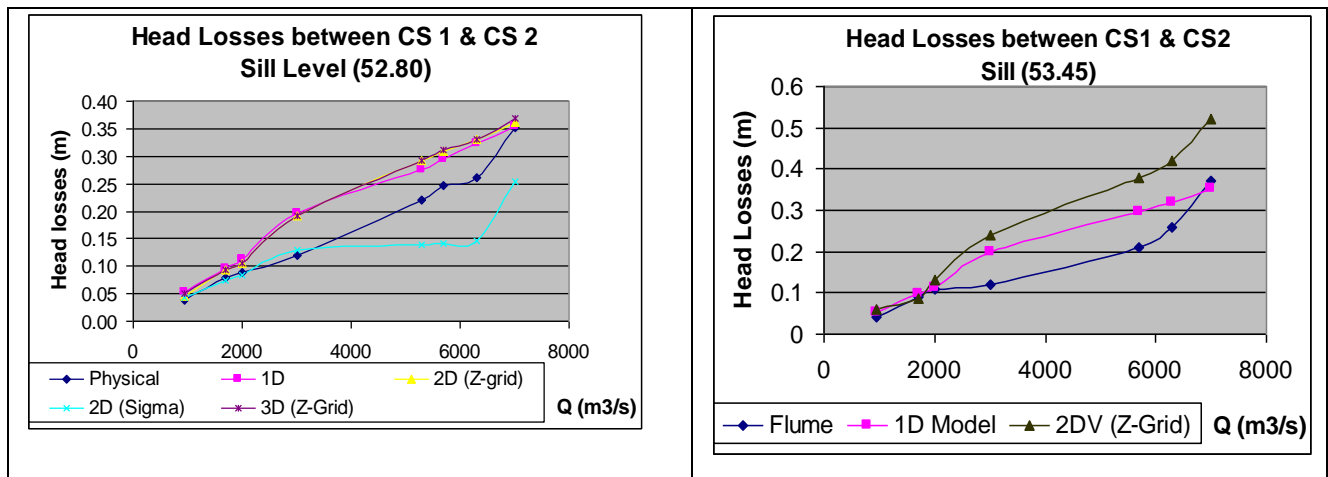


Figure 4-9: Total Head loss for sill levels (52.80) & (53.45)

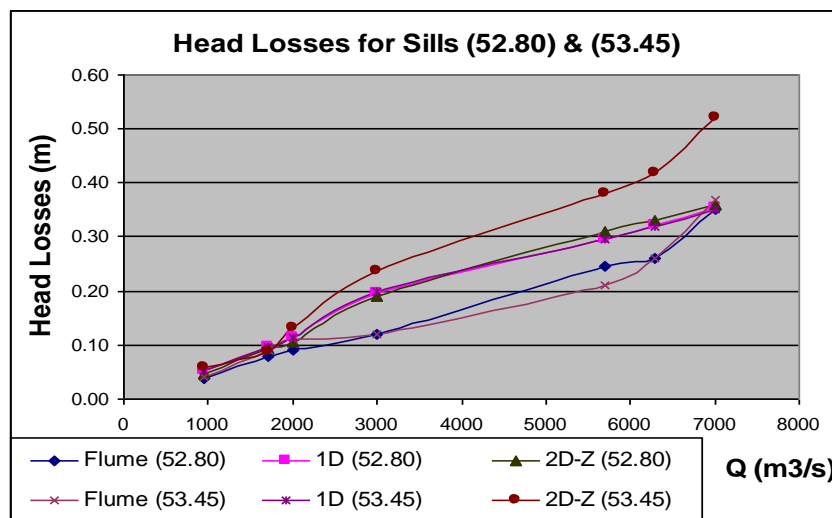


Figure 4-10: total head losses for different models

From figures 9, 10 it is noted the followings:

1. Head losses are increasing with the discharge nevertheless the total head losses are small in absolute values in all the cases due to the relatively small crest height above the river bed. The maximum measured head losses between cross sections CS1 and CS2 are 0.35 m and 0.37 m for the two tested sill elevations, as shown in figure 13 and table 7.
2. The influence of the crest level change from 52.80 to 53.45 m a.s.l. on the head losses is not significant.
3. 1D and 2DV (Z-Grid) have good correlations with the flume data whilst Sigma grid is not sensitive particularly with high discharges (higher than 200 m³/s).

Velocities near the bed at CS1 and CS2

The velocities were measured at one meter above the river bed along the centreline of the sluiceway bay at the point gauges upstream CS1 and downstream CS2, near to the open boundaries where the bed is flat and the flow is steady and uniform. The results are presented in table 4-7 and figures 4-11 and 4-12 for sill levels (52.80) and (53.45).

Table 4-7: Velocities at u/s and d/s gauge stations at one meter above the bed

Q	Sill Level (52.80)						Sill Level (53.45)					
	Flume		1 D Model		2 DV (Z-grid)		Flume		1 D Model		2 DV (Z-grid)	
	V ₁	V ₂	V ₁	V ₂	V ₁	V ₂	V ₁	V ₂	V ₁	V ₂	V ₁	V ₂
m ³ /s	m/s	m/s	m/s	m/s	m/s	m/s	m/s	m/s	m/s	m/s	m/s	m/s
950	1.32	0.99	1.48	1.08	1.37	0.98	1.31	0.92	1.48	1.07	1.48	1.02
1700	1.87	1.39	2.13	1.62	1.97	1.43	1.85	1.31	2.13	1.62	2.01	1.52
2000	2.04	1.55	2.35	1.82	2.18	1.64	2.11	1.56	2.35	1.82	2.32	1.67
3000	2.57	2.30	3.18	2.50	2.91	2.17	2.6	2.12	3.18	2.50	3.16	2.31
5700	3.80	3.10	4.32	3.58	4.01	3.16	3.63	3.00	4.31	3.58	4.26	3.28
6300	4.01	3.31	4.57	3.81	4.12	3.24	3.91	3.2	4.56	3.81	4.51	3.48
7000	4.36	3.48	4.85	4.07	4.40	3.50	4.31	3.37	4.84	4.07	4.73	3.48

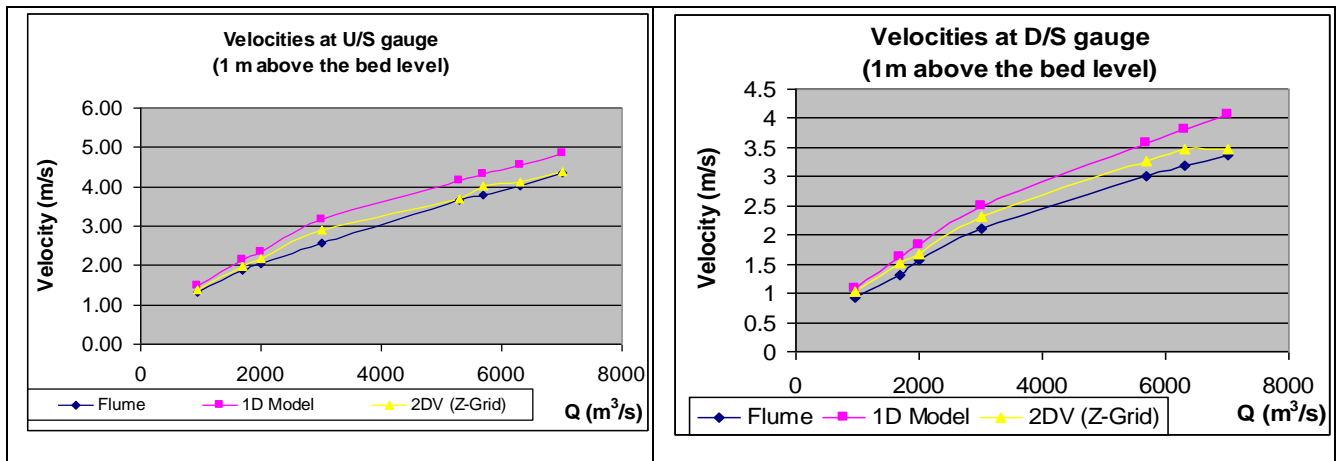


Figure 4-11: Velocities at u/s and d/s gauge stations, sill level (52.80)

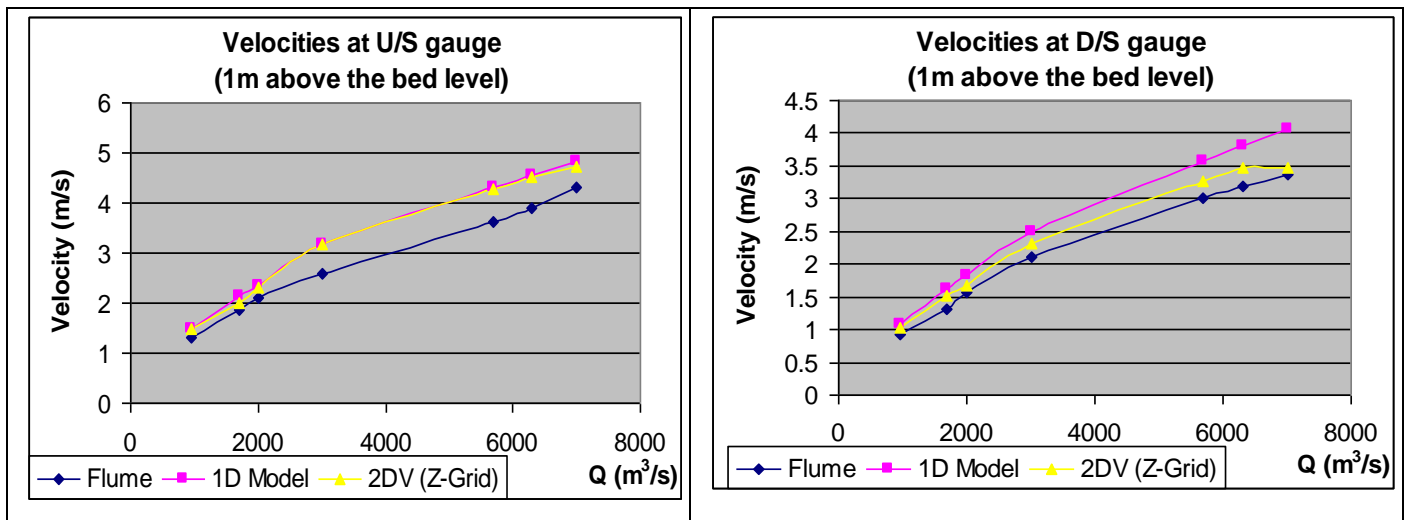


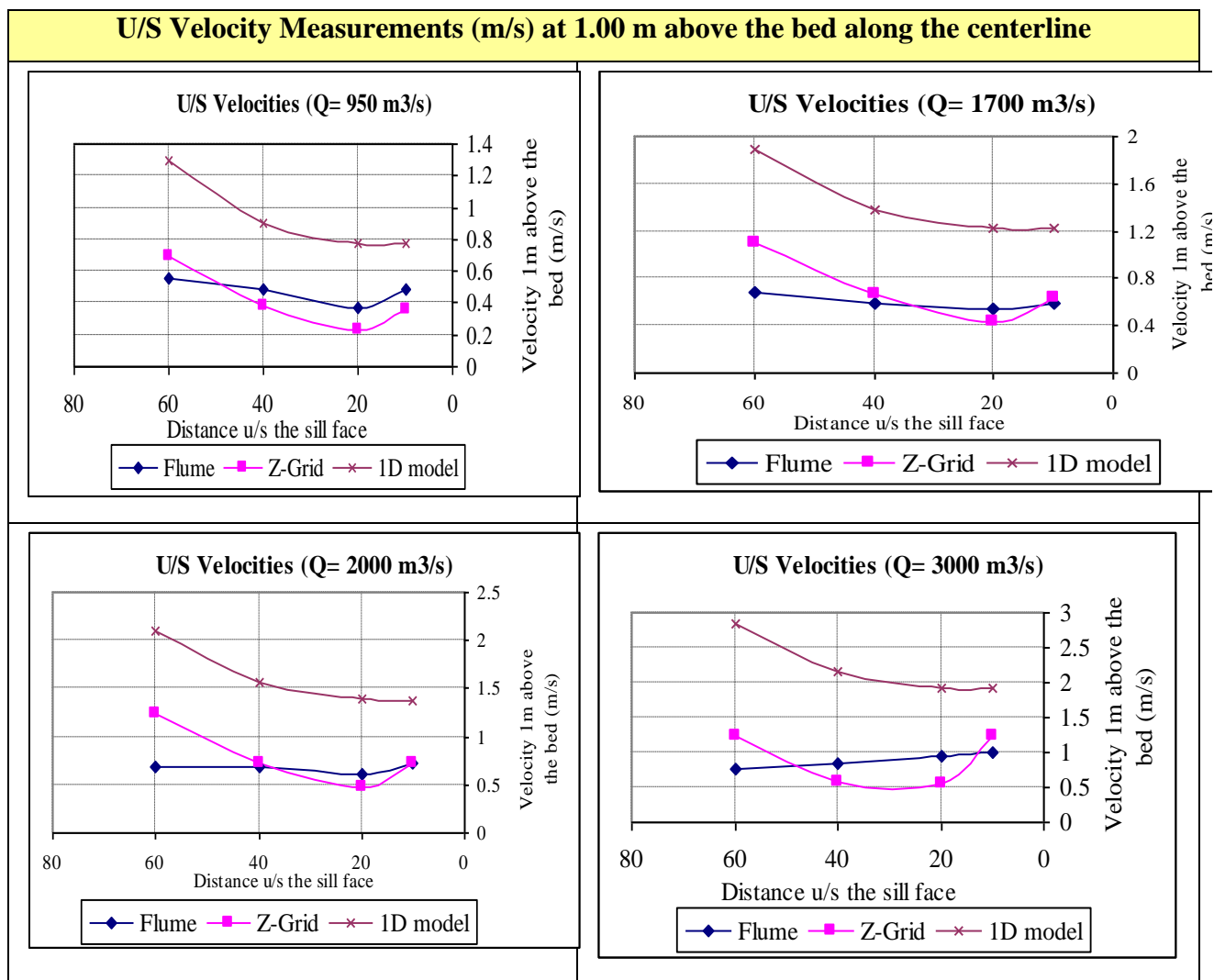
Figure 4-12: Velocities at u/s and d/s gauge stations, sill level (53.45)

As shown in the above figures 2DV Z-Grid gives accurate results with respect to the flume data. 1D model has a good agreement also with the flume data nevertheless it gives slight higher values because it gives depth averaged velocities.

Velocities near the variable bed along the longitudinal section

The flow velocity was measured at one meter above the river bed along the centreline of the sluiceway bay at distances 10, 20, 40, and 60 m upstream from the face of the sill and 10, 20, 40, 80, 120, and 160 m downstream from the beginning of the horizontal apron using 2DV models. Results for the velocity measurements are presented in charts versus the distance see tables 8 and 9.

Table 4-8: Upstream Velocity Measurements above variable bed for Fully Open Gate



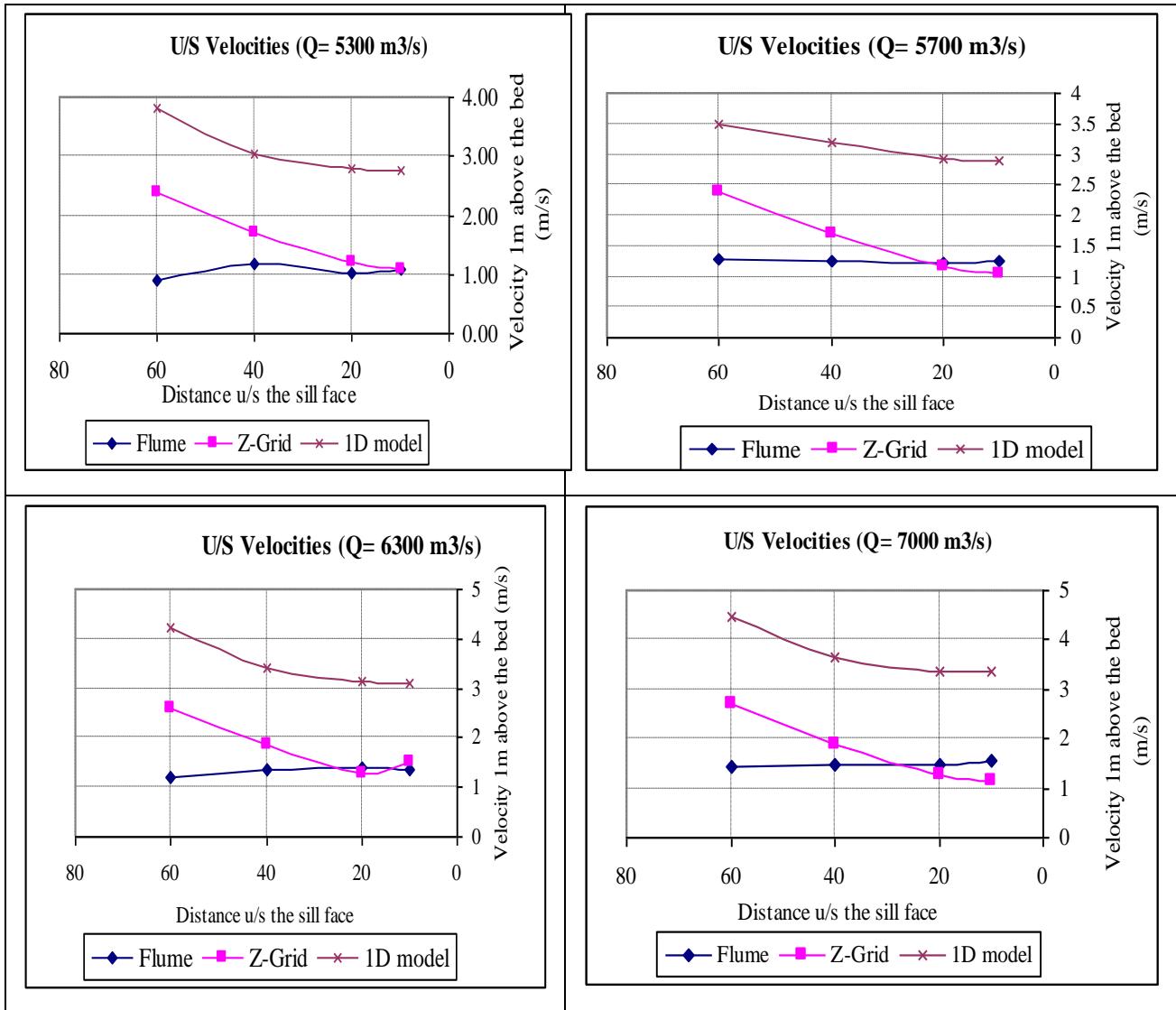
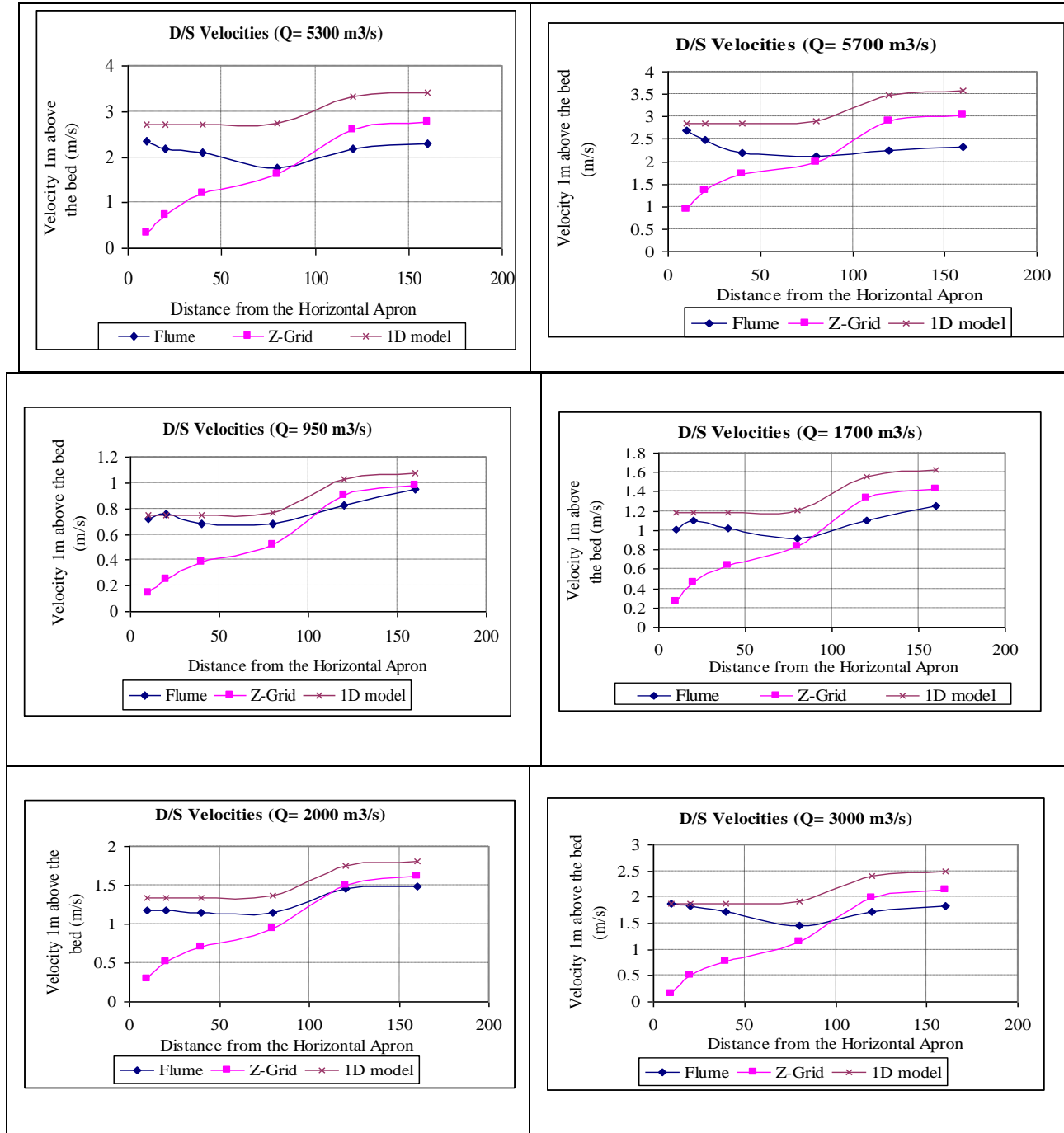
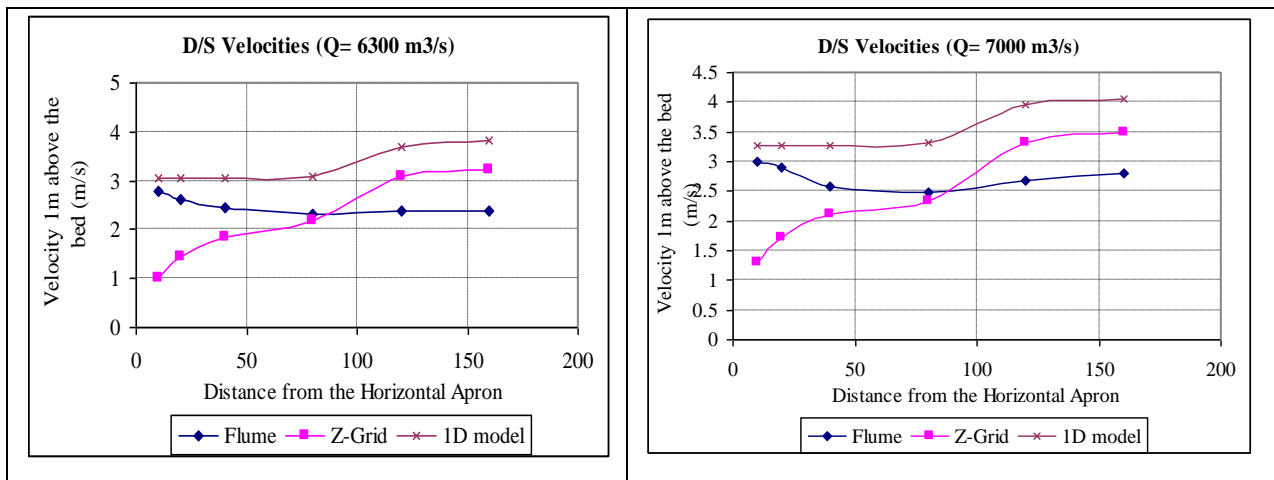


Table 4-9: Downstream Velocity Measurements above variable bed for Fully Open Gate

D/S Velocity Measurements (m/s) at 1.00 m above the bed along the centreline





4.9 Partially Open Gate

2nd Stage : Normal Operation “Partially Open Gate” - Supercritical Flow Conditions

The sluiceway and the stilling basin has been simulated using Delft 3D for the case of partially open gates. Through tests (B1 to B7) several discharges values ranging from 600 to 5700 m³/s have been used in order to study the flow characteristics and to calibrate the sluiceway radial gate to obtain on the gate opening for the different discharge values.

The main objectives

Checking the ability of Delft 3D on simulating a controlled flow by a partially open gates and to study the submerged hydraulic jump through it.

The fields of the study

- Studying the capability of Delft 3D on simulating the submerged hydraulic jump.
- Studying the velocities and Froude No. at the vena contracta.
- Checking the head losses.
- The relative energy losses.
- Calibration for the sluiceway radial gate opening (using floating structure & Barrier options).
- Studying the velocities profiles (along the water depth) and in the longitudinal direction.
- Studying the submerged hydraulic jump length.
- Checking some results theoretically (using equations & empirical charts).

The Hydraulic Jump Characteristics

Table 4-10: Measured and calculated parameters

Test No.	Q m ³ /s	U.S.W.L m asl	D.S.W.L** m asl	y ₁ * m	F _r **	y ₂ ** m	y _t ** m	y _t >y ₂
B ₁	600	65.9	58.61	0.32	8.89	3.87	6.61	Submerged
B ₂	1000	65.9	59.54	0.57	6.17	4.70	7.54	Submerged
B ₃	1700	65.9	60.80	1.15	3.70	5.47	8.80	Submerged
B ₄	2600	65.9	62.10	2.31	1.99	5.44	10.10	Submerged
B ₅	4000	65.9	63.73	4.41	1.16	5.35	11.73	Submerged
B ₆	5000	65.9	64.73	7.56	0.65	4.09	12.73	Submerged
B ₇	5700	65.9	65.37	10.71	0.44	3.15	13.37	Submerged

* : Measured from the flume.

** : Calculated using formulas.

D.S.W.L : downstream water level = $(0.1166*Q^{0.5132})+55.5$ {the rating curve equation}

y₁: Thickness of the vena contracta in m.

F_r : Froude number at the vena contracta.

y₂ : Conjugate water depth = $0.5 y_1 * ((1+8F_r^2)^{0.5}-1)$

y_t : Tailwater (normal) water depth in the downstream = DSWL – Bed level (52.00).

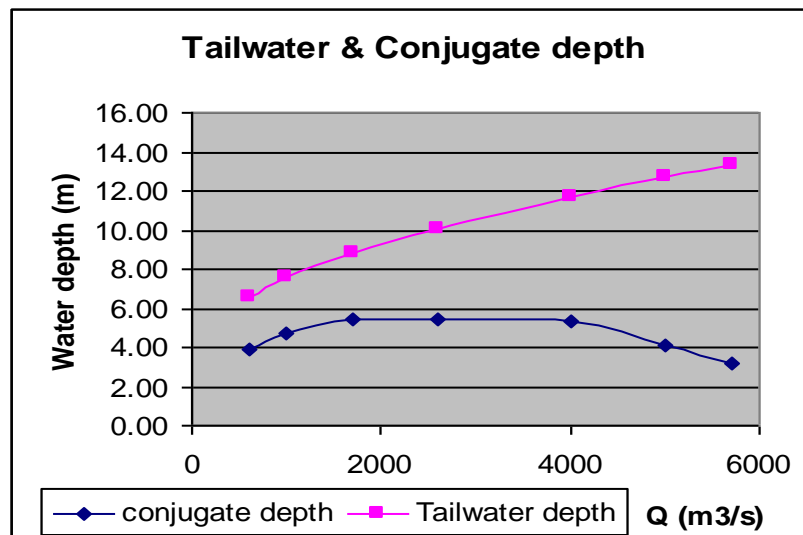


Figure 4-13: Tailwater and conjugate depth

From table 4-10 and figure 4-13 it is obvious that the tailwater depth is higher than the conjugate water depth in all discharges so that the hydraulic jump is submerged. Consequently, for the submerged jump formed for high discharges only little energy dissipation can be expected.

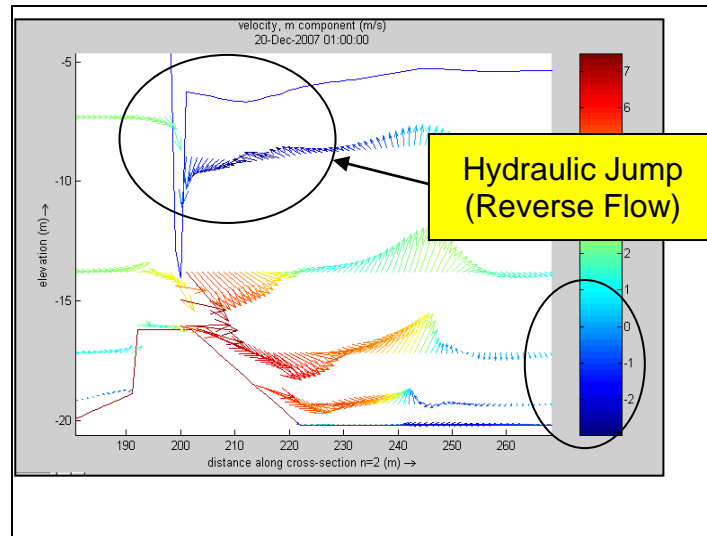


Figure 4-14: The hydraulic jumps according to Z Grid ($Q = 4000 \text{ m}^3/\text{s}$)

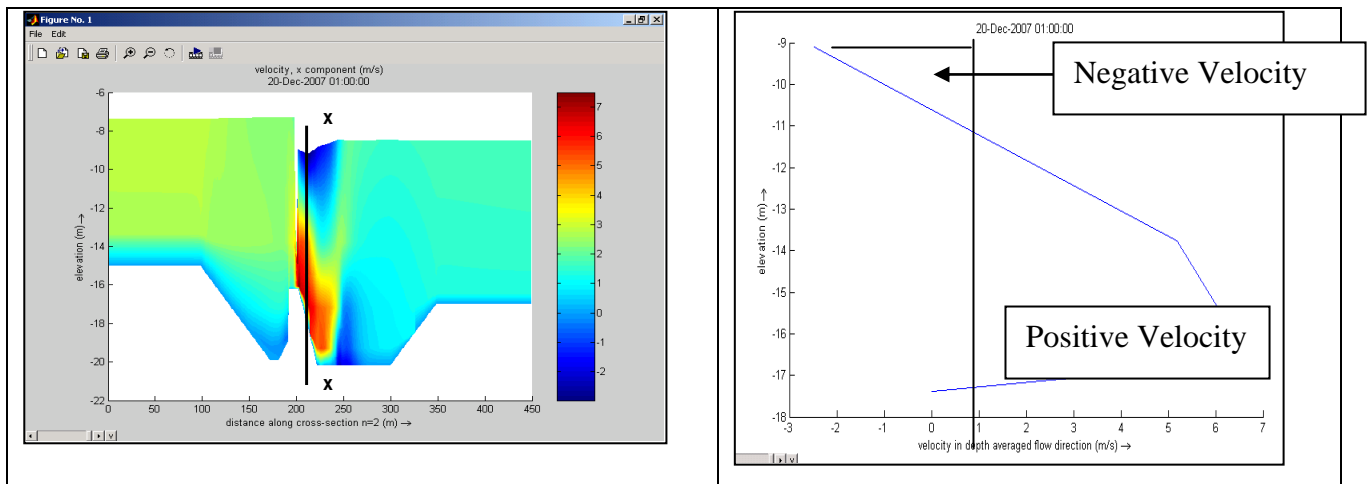


Figure 4-15: The velocity distribution at section X-X (Z-Grid)

From figures 14 & 15 the flow recirculation is presented in Z models through the negative velocities and the flow directions after the gate, it is a good evident that Delft 3D is able to present the submerged hydraulic jump.

Froude Number at the Vena-Contracta

Table 4-11: Froude Number at the Vena-Contracta

Flume				Delft 3D (1D Model)				
Q	y ₁	V _c **	F _r **	y ₁ *	V _c *	F _r **	V _c **	F _r **
m ³ /s	m	m/s	Calculated	m	m/s	Model	Calculated	Calculated
600	0.32	15.76	8.89	0.41	7.35	3.66	15.37	8.57
1000	0.57	14.64	6.17	0.76	6.76	2.48	13.86	5.68
1700	1.15	12.42	3.70	1.54	6.24	1.60	11.59	3.33
2600	2.31	9.46	1.99	2.70	6.00	1.17	10.12	2.20
4000	4.41	7.62	1.16	4.87	5.75	0.83	8.63	1.40
5000	7.56	5.56	0.65	6.74	5.54	0.68	7.79	1.07
5700	10.71	4.47	0.44	8.05	5.32	0.60	7.44	0.94

V_c* : velocity at the vena contracta section (average from the 1D Model).

V_c** : calculated = Q / (17*7* y₁)

Common characteristics of the hydraulic jump applied to the Naga Hammadi sluiceway are plotted in figure 20. The steady jump with an energy dissipation of 45 to 70% is limited to low discharges ranging from 600 to 1400 m³/s. The mean range of the discharge 1400 to 4500 m³/s, characterised by oscillating (F_r = 2.5 to 4.5), weak (F_r = 1.7 to 2.5), and undular jump formation (F_r = 1 to 1.7), causes small energy dissipation.

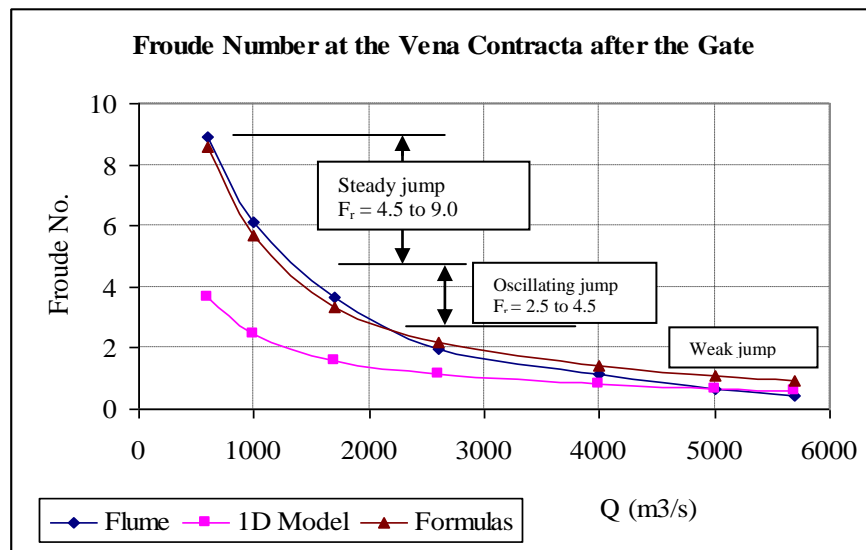


Figure 4-16: Froude Number at the Vena-Contracta

Analyzing the stability of the apron these characteristics have to be taken into consideration. With regard to the hydraulic phenomena for low Froude numbers as of the present case, the U.S. Bureau of Reclamation gives the following description:

- The oscillating jump, frequently encountered in the design of canal structures, diversion dams, and even outlet works, is difficult to handle. Baffle blocks or appurtenances are one of the main sources of difficulty.
- The weak jump requires no baffles or special considerations. The only requirement is to provide a proper length of the apron.

To get more accurate values for Froude No. from Delft 3D (1D Model) it is recommended to use the gate opening from the model in calculating the velocities at the vena-contracta, hence Froude number could be calculated. These steps could be summarized in the following points:

1. Assume the average coefficient of contraction = 0.8 (it was found from the flume data).
2. $y_1 = 0.8 * GO$.
2. $V_C = Q / (y_1 * 17m * 7)$
3. $F_r = V_C / (9.81 * y_1)^{0.5}$

Remark: The coefficient of contraction for sluice gates is a function of the ratio of the gate opening to the approach piezometric head, called the gate-opening ratio. The coefficient of contraction for tainter (radial) gates is taken to be a function of the angle that the upstream face of the gate lip makes with the horizontal plane (Toch, 1955).

Head Losses in case of partially open gate:

Table 4-12: Head Losses in partially open gate

Flume			1 Dimensional Model				2 Dimensional Model (Z-grid)			
Test	Q	Q	V ₁	V ₂	D.S.W.L	h _L	V ₁	V ₂	D.S.W.L	h _L
No.	m ³ /s	(m ³ /s/vent)	m/s	m/s	m asl	m	m/s	m/s	m asl	m
B ₁	600	85.7	0.43	0.8	58.61	7.27				
B ₂	1000	142.9	0.705	1.13	59.54	6.32				
B ₃	1700	242.9	1.2	1.643	60.8	5.04				
B ₄	2600	371.4	1.833	2.185	62.09	3.74				
B ₅	4000	571.4	2.825	2.89	63.73	2.15	1.60	1.4	63.73	2.20
B ₆	5000	714.3	3.52	3.326	64.73	1.24	2.5	3.4	64.73	0.90
B ₇	5700	814.3	4.02	3.61	65.37	0.69	4.03	3.9	65.37	0.57

In case of partially open gate 2DV model using Z-Grid and the floating structure option (to represent the gate effect) it could not realize the Upstream water level (65.90) with any gate opening for all discharges less than 400 m³/s even after closing the gate completely.

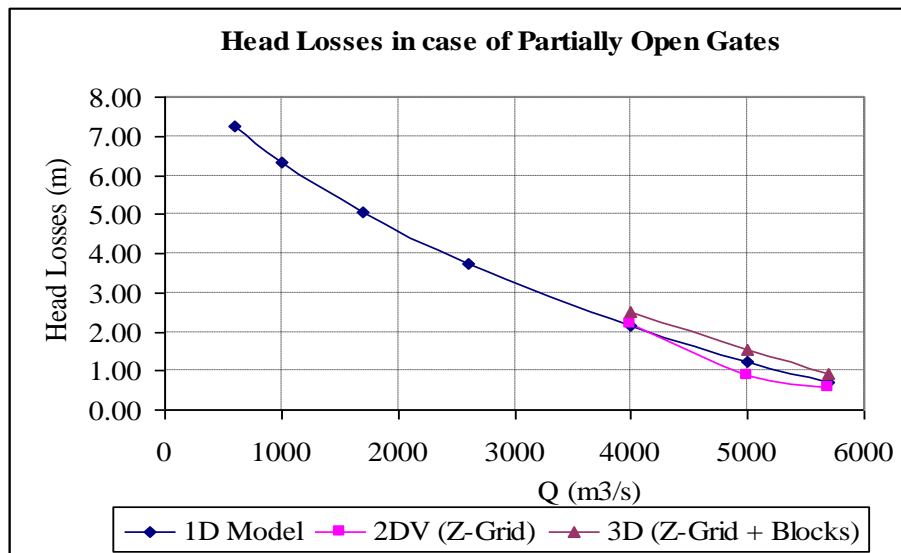


Figure 4-17: Head Losses in partially open gate

From figure 4-17 it is obvious that there is a slight increase in the head losses in case of 3D Model (Z-Grid) with a baffled apron.

The head losses in cases of fully and partially open gates are combined in table 13 and figure 18 to compare the results.

Table 4-13: Head losses in partially and fully open gates

Fully opened			Partially opened	
Q	h _L (m)		Q	h _L (m)
m ³ /s	Flume	1D Model	m ³ /s	1D Model
950	0.04	0.05	600	7.27
1700	0.08	0.10	1000	6.32
2000	0.09	0.11	1700	5.04
3000	0.12	0.20	2600	3.74
5700	0.25	0.30	4000	2.15
6300	0.26	0.32	5000	1.24
7000	0.35	0.35	5700	0.69

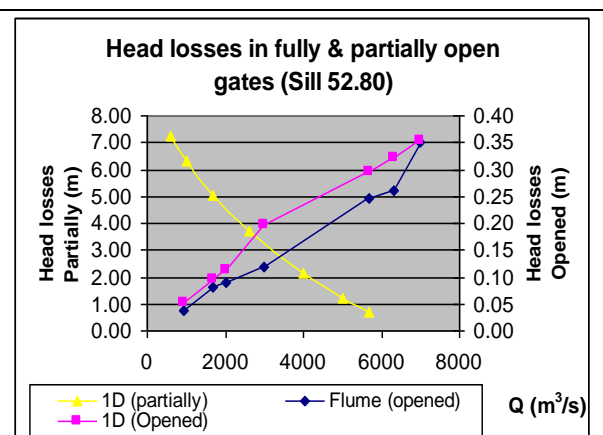


Figure 1: Head losses in partially and fully open gates (Sill 52.80)

From the previous table and figure it is obvious that the head losses in case of partially open gates are much higher than in case of fully open gates due to the existence of the hydraulic jump. Moreover the losses are inversely proportional with the discharge in case of partially open gates as the hydraulic jumps become stronger with lower discharges as discussed in the previous section.

Energy Losses (Partially Opened)

The following equation could be used to calculate the relative energy losses (E_L/E_1)

$$\frac{E_L}{E_1} = \frac{\left(\psi - \frac{(1+S)}{2}\phi\right) + 0.5F_{r1}^2\left(1 - \frac{4}{(1+S)^2\phi^2}\right)}{\psi + 0.5F_{r1}^2} \quad (4-3)$$

Where

E_L = Energy loss in the submerged jump.

E_1 = Energy loss at the beginning of the submerged jump.

S_j = Submergence ratio = $(Y_n - Y_1)/Y_2$

$\phi = [(1+8F_{r1}^2)^{0.5} - 1]$

From table 4-14 and figure 4-19 it is obvious that the energy losses which have been calculated from the 1D Model have a very good agreement with the energy losses which have been calculated from the flume data.

The steady jump with energy dissipation between 40 and 70 % is limited to small gate openings, e.g. low discharges from 600 to 1700 m³/s.

Table 4-14: Energy losses in partially open gates

Test No.	Q	Q (per vent)	E_L/E_1 (Flume)	E_L/E_2 (1D Model)
	m ³ /s	(m ³ /s/vent)	%	%
B ₁	600	85.7	65.50	64.31
B ₂	1000	142.9	56.47	53.51
B ₃	1700	242.9	40.03	36.22
B ₄	2600	371.4	19.91	22.85
B ₅	4000	571.4	7.66	10.96
B ₆	5000	714.3	1.47	6.10
B ₇	5700	814.3	0.15	4.18

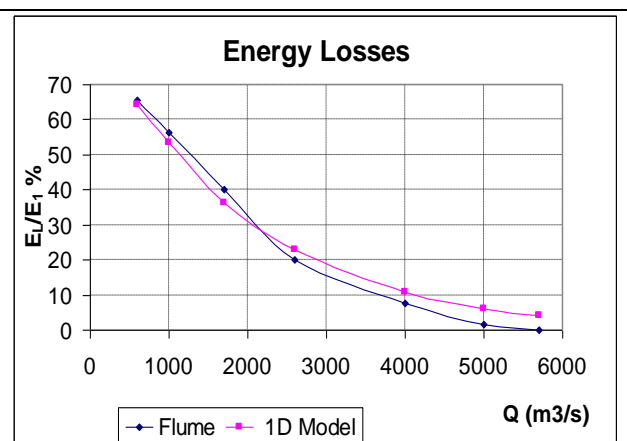


Figure 4-2: Energy losses in partially open gates

Gate Openings

The function of the radial sluice gate is to regulate the flow of the river according to the required water levels. For all the different water flow values during the normal operation case ($Q < 5700$ m³/s), the upstream water level should be kept at level (65.90 m asl). In order to obtain on the corresponding gate openings which achieve this condition with different discharges using Delft 3D the downstream water level for each flow value was set as the downstream boundary condition and the discharges as upstream boundary conditions and several gate openings have been tested until the upstream water level reached the required level (65.90), these trials have been summarized in *Excel* work sheets. Table 15 and figure 20 show the values of the gate opening obtained by Delft 3D in comparison with those measured by the hydraulic flume model. Two different methods were applied to check the results of the numerical model using formulas and an empirical chart, these results are also presented in the same table 15.

Since there is no radial gate option in Delft 3D, a pressure on the water surface was applied using floating structure to represent the gate effect. In case of 1D Model this procedure gave good results but in cases of 2D Vertical models it did not, particularly with low discharges as the upstream water level (65.90) could not be realized at all. Another new tool, still under test, Barriers was applied on some few cases to represent the gate openings and it gave quite good results but not very accurate, particularly for the upstream water levels.

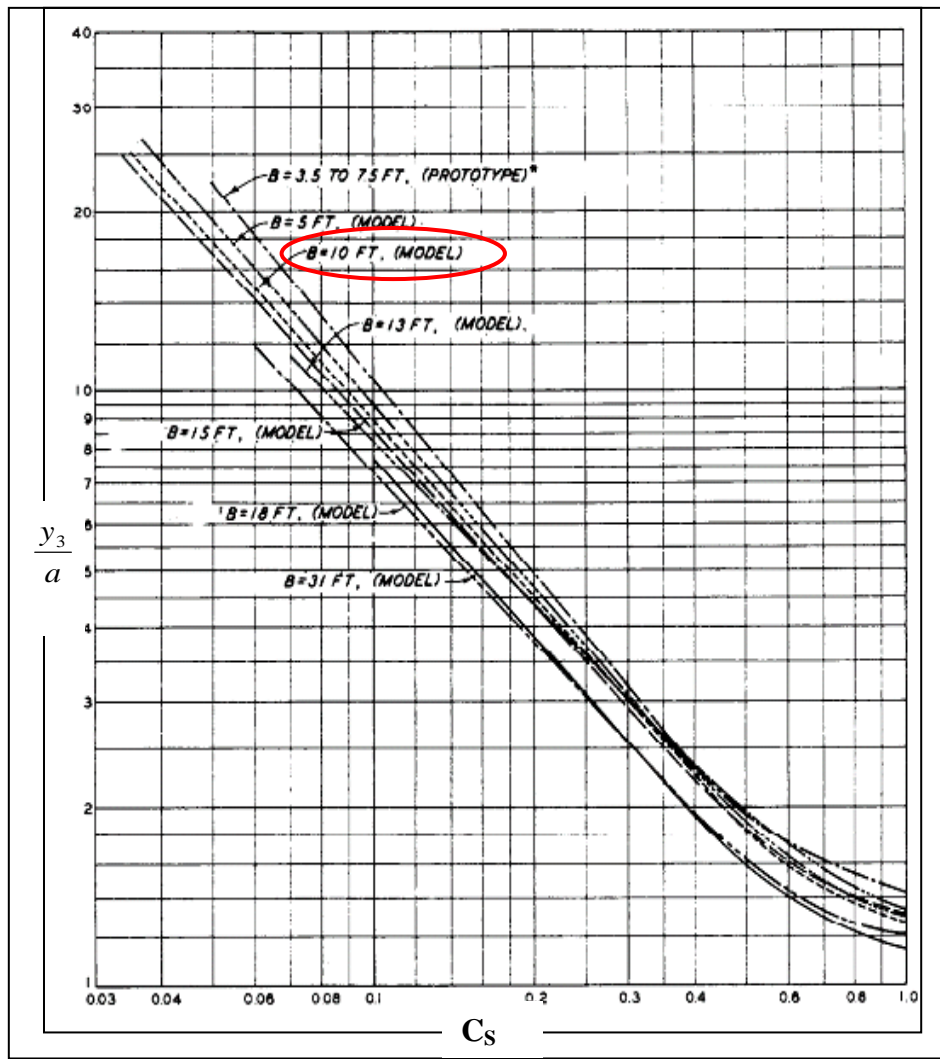


Figure 4-18: Discharge Coefficients for submerged hydraulic jump (US Army)

Table 4- 15: Gate openings from the 1D model and theoretical analysis

Test	Physical Model (Flume)				1 Dimensional Model				Equation	US Army
	Q	Q (per vent)	GO	V _c (Model)	GO	The difference	% error	V _c	GO	GO
No.	m ³ /s	(m ³ /s/vent)	m	m/s	m	m	%	m/s	m	m
B ₁	600	85.70	0.4	15.76	0.41	-0.01	-2.50	7.35	0.66	0.39
B ₂	1000	142.9	0.74	14.48	0.76	-0.02	-2.70	6.76	1.17	0.71

B ₃	1700	242.9	1.72	12.36	1.541	0.18	10.41	6.24	2.07	1.33
B ₄	2600	371.4	3.03	9.45	2.70	0.33	10.89	6.00	3.50	2.58
B ₅	4000	571.4	5.88	7.62	4.873	1.01	17.13	5.75	6.15	5.88
B ₆	5000	714.3	8.82	5.55	6.736	2.08	23.63	5.54	8.80	7.02
B ₇	5700	814.3	10.54	4.47	8.34	2.20	20.87	5.32	12.41	8.38

A new profile and a new option (Barrier)

A separate study on the hydraulic jump characteristics and the velocity distribution in case of partially open gate was done by comparing the results coming from a new scale (physical) model, which has the same dimensions of the previous mentioned scale model except the sill slope was increased to 30° (instead of 5:1), with the numerical model results after simulating the new dimensions on Delft 3D.

Figure 20 shows a schematization for the physical model dimensions and figure 21 shows the bathymetry of the new studied sluiceway using Delft 3D.

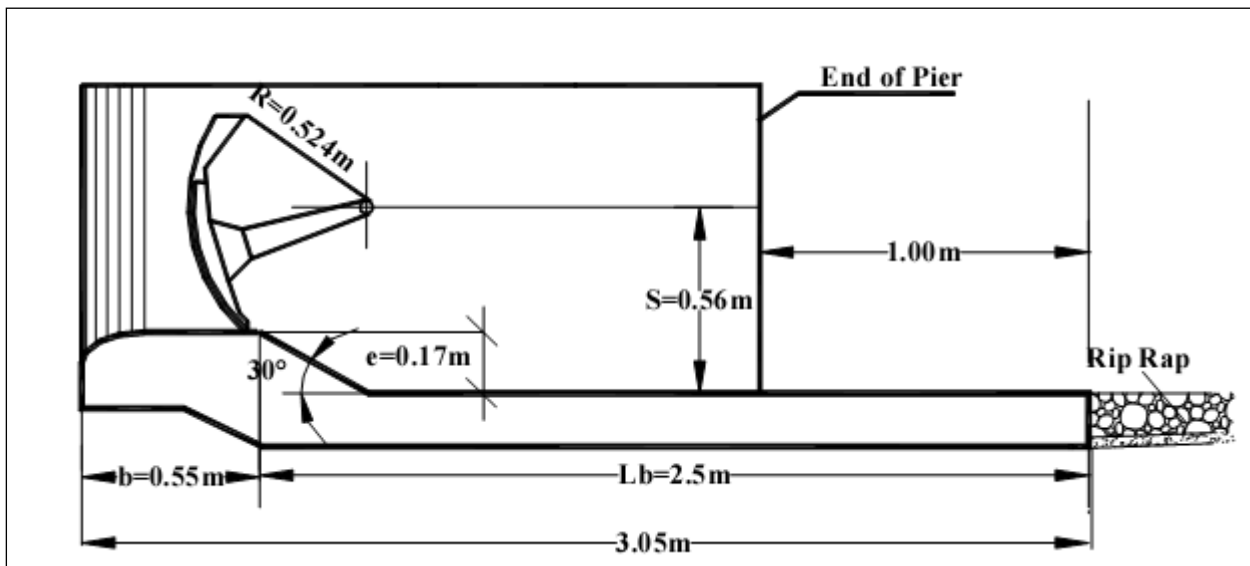


Figure 4-19: The new studied profile (Abdel Azim, 2005)

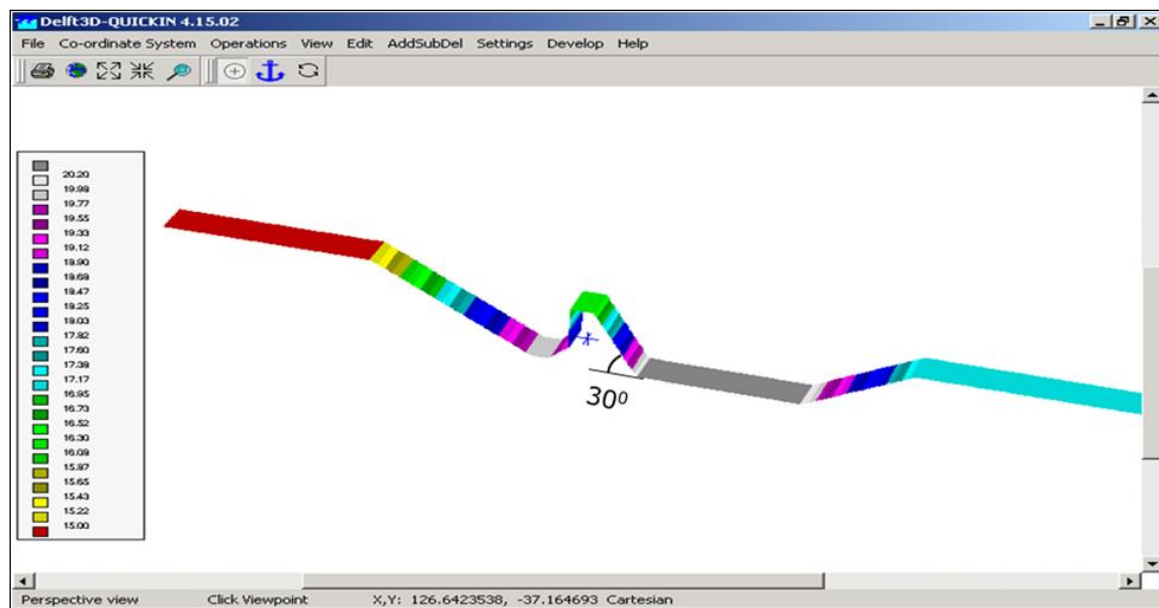


Figure 4-20: The new bathymetry

To ensure more accurate results a roughness map was generated on Delft 3D, see figure 4-22. For the concrete areas Manning's Coefficient (n) was taken = 0.014 while the upstream and downstream riprap areas Manning's Coefficient (n) was calculated by applying Muller (1943) equation first

$$K_s = \frac{26}{d_{90}^{1/6}} = 28.08, (d_{90} = 0.63 \text{ m for the riprap}) \text{ then } n = \frac{1}{K_s} = 0.035$$

Where

K_s is Manning-Strickler Coefficient

d is the particle size diameter in m

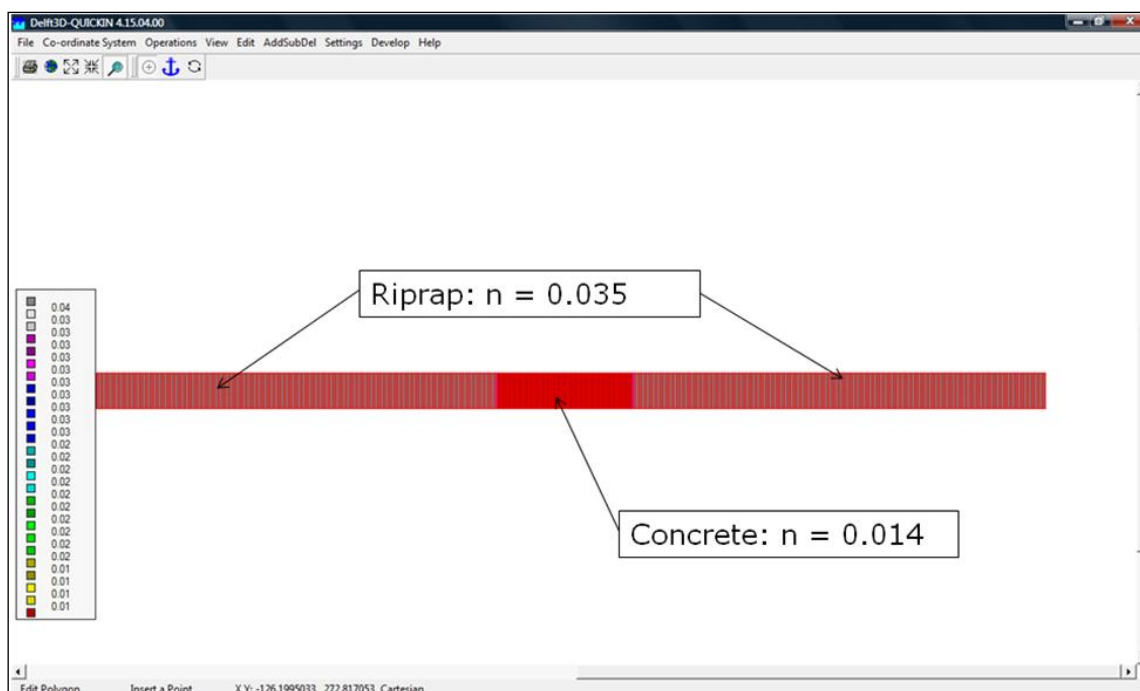


Figure 4-21: The roughness map

4.10 Test Procedure

For this new design six flow conditions were used, and each flow condition has six tailwater depths i.e. 36 conditions in all. For each run, which has constant discharge and head, the corresponding gate opening and submerged hydraulic jump length were recorded. The following table summarizes the new flume results.

Table 4-16: some of the new obtained flume results

The Flume Results						
Test No.	Q (litre/ s)	G.O. (cm)	Hu (m)	Yt (m)	Delta h (m)	Lsj (cm)
1	40	2.7	0.63	0.47	0.33	197
2	40	3	0.63	0.51	0.29	210
3	40	3.3	0.63	0.55	0.25	235
4	40	3.6	0.63	0.58	0.22	250
5	40	3.9	0.63	0.61	0.19	259
6	40	4.2	0.63	0.64	0.16	262
7	70	4.6	0.63	0.47	0.33	227
8	70	4.9	0.63	0.51	0.29	244
9	70	5.2	0.63	0.55	0.25	251
10	70	5.6	0.63	0.58	0.22	256
11	70	6.1	0.63	0.61	0.19	262

The Flume Results						
Test No.	Q (litre/ s)	G.O. (cm)	Hu (m)	Yt (m)	Delta h (m)	Lsj (cm)
12	70	6.6	0.63	0.64	0.16	269
13	100	6.1	0.63	0.47	0.33	240
14	100	6.6	0.63	0.51	0.29	245
15	100	7.3	0.63	0.55	0.25	250
16	100	7.7	0.63	0.58	0.22	256
17	100	8.5	0.63	0.61	0.19	260
18	100	9.3	0.63	0.64	0.16	270
19	130	8.7	0.63	0.47	0.33	255
20	130	9.6	0.63	0.51	0.29	266
21	130	10.2	0.63	0.55	0.25	296
22	130	10.8	0.63	0.58	0.22	310
23	130	11.8	0.63	0.61	0.19	330
24	130	12.9	0.63	0.64	0.16	335
25	160	10.6	0.63	0.47	0.33	261
26	160	11.4	0.63	0.51	0.29	275
27	160	12.3	0.63	0.55	0.25	287
28	160	14.6	0.63	0.58	0.22	305
29	160	15.6	0.63	0.61	0.19	316
30	160	17.2	0.63	0.64	0.16	334
31	190	11.8	0.63	0.47	0.33	256
32	190	12.8	0.63	0.51	0.29	271
33	190	13.6	0.63	0.55	0.25	276
34	190	15.1	0.63	0.58	0.22	281
35	190	16.6	0.63	0.61	0.19	293
36	190	18.4	0.63	0.64	0.16	315

It was necessary to convert the obtained flume results into prototype results to compare them with the results coming from Delft 3D which was used to simulate the prototype (the true) dimensions.

The conversion factors were deduced and calculated from Froude number and the length scale ratio (L_r). The inertia and gravity forces are dominant, so that the model is based on Froude similarity with the prototype.

$$Fr_r = \frac{v_r}{\sqrt{g_r L_r}} = 1$$

Where

Fr_r = Froude number scale ratio.

v_r = velocity scale ratio.

L_r = Length scale ratio (it is taken =21).

g_r = gravitational scale ratio.

($g_r=1$ because the gravity acceleration is the same in the model and the prototype).

From the last equation: $v_r = L_r^{0.5}$

With the geometric scale 1:21, the other relevant scales result as:

Velocity scale $v_r = L_r^{0.5} = 21^{0.5} = 4.58$

Discharge scale ratio $Q_r = A_r V_r = L_r^2 L_r^{0.5} = L_r^{2.5} = 2021$

The following table presents the prototype results calculated from the obtained flume results mentioned in the previous table.

Table 4-17: The Prototype Results

The Prototype Results								
Q (m ³ /s)	Q total	G.O. (m)	H _u (m)	Y _t (m)	Delta h (m)	DSBC*	G.O. (m)	L _{sj} (m)
80.84	565.86	0.57	13.23	9.87	6.93	-7.13	-15.63	41.37
80.84	565.86	0.63	13.23	10.71	6.09	-6.29	-15.57	44.10
80.84	565.86	0.69	13.23	11.55	5.25	-5.45	-15.51	49.35
80.84	565.86	0.76	13.23	12.18	4.62	-4.82	-15.44	52.50
80.84	565.86	0.82	13.23	12.81	3.99	-4.19	-15.38	54.39
80.84	565.86	0.88	13.23	13.44	3.36	-3.56	-15.32	55.02
141.46	990.25	0.97	13.23	9.87	6.93	-7.13	-15.23	47.67
141.46	990.25	1.03	13.23	10.71	6.09	-6.29	-15.17	51.24
141.46	990.25	1.09	13.23	11.55	5.25	-5.45	-15.11	52.71
141.46	990.25	1.18	13.23	12.18	4.62	-4.82	-15.02	53.76
141.46	990.25	1.28	13.23	12.81	3.99	-4.19	-14.92	55.02
141.46	990.25	1.39	13.23	13.44	3.36	-3.56	-14.81	56.49
202.09	1414.64	1.28	13.23	9.87	6.93	-7.13	-14.92	50.40
202.09	1414.64	1.39	13.23	10.71	6.09	-6.29	-14.81	51.45
202.09	1414.64	1.53	13.23	11.55	5.25	-5.45	-14.67	52.50
202.09	1414.64	1.62	13.23	12.18	4.62	-4.82	-14.58	53.76
202.09	1414.64	1.79	13.23	12.81	3.99	-4.19	-14.42	54.60
202.09	1414.64	1.95	13.23	13.44	3.36	-3.56	-14.25	56.70
262.72	1839.03	1.83	13.23	9.87	6.93	-7.13	-14.37	53.55
262.72	1839.03	2.02	13.23	10.71	6.09	-6.29	-14.18	55.86
262.72	1839.03	2.14	13.23	11.55	5.25	-5.45	-14.06	62.16
262.72	1839.03	2.27	13.23	12.18	4.62	-4.82	-13.93	65.10
262.72	1839.03	2.48	13.23	12.81	3.99	-4.19	-13.72	69.30

The Prototype Results								
Q (m ³ /s)	Q total	G.O. (m)	H _u (m)	Y _t (m)	Delta h (m)	DSBC*	G.O. (m)	L _{sj} (m)
262.72	1839.03	2.71	13.23	13.44	3.36	-3.56	-13.49	70.35
323.35	2263.43	2.23	13.23	9.87	6.93	-7.13	-13.97	54.81
323.35	2263.43	2.39	13.23	10.71	6.09	-6.29	-13.81	57.75
323.35	2263.43	2.58	13.23	11.55	5.25	-5.45	-13.62	60.27
323.35	2263.43	3.07	13.23	12.18	4.62	-4.82	-13.13	64.05
323.35	2263.43	3.28	13.23	12.81	3.99	-4.19	-12.92	66.36
323.35	2263.43	3.61	13.23	13.44	3.36	-3.56	-12.59	70.14
383.97	2687.82	2.48	13.23	9.87	6.93	-7.13	-13.72	53.76
383.97	2687.82	2.69	13.23	10.71	6.09	-6.29	-13.51	56.91
383.97	2687.82	2.86	13.23	11.55	5.25	-5.45	-13.34	57.96
383.97	2687.82	3.17	13.23	12.18	4.62	-4.82	-13.03	59.01
383.97	2687.82	3.49	13.23	12.81	3.99	-4.19	-12.71	61.53
383.97	2687.82	3.86	13.23	13.44	3.36	-3.56	-12.34	66.15

Due to the limited time for this study it was decided to use the first run from each group only to be applied on the numerical model and to be used in the analysis, in that case six discharges were used as upstream boundary conditions and constant head difference (= 6.93 m) was used as a downstream boundary condition for all the discharges.

Figure 4-23 shows the gate openings versus the different discharges while the head difference is constant, this chart could be used to study the different operational scenarios like in case of passing more discharge from one gate if other gates are closed where both upstream and downstream water levels do not change.

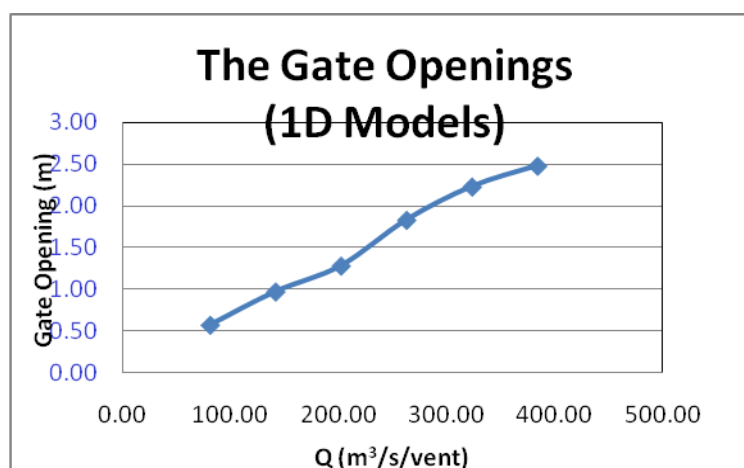


Figure 4-22: Gate openings vs. the discharges for constant head (H = 6.93 m)

4.11 Gate openings calibration using the new option (Barrier)

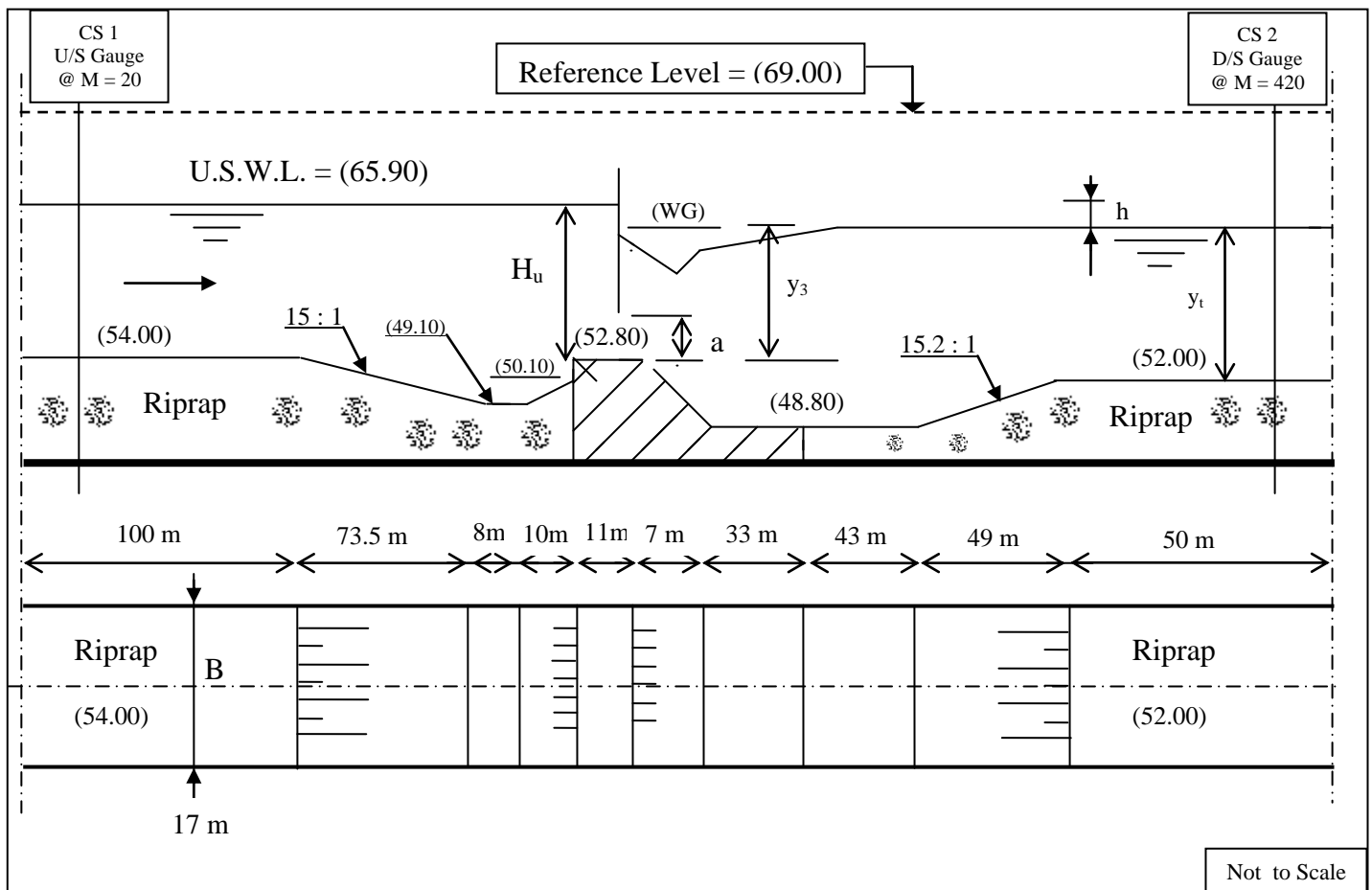


Figure 4-23: A definition sketch for partially open gate

The new option Barrier which has been implemented in Delft 3D recently was used to represent the gate openings. The losses coefficient due to the gate existence was used as a variable parameter to calibrate the gate openings using the new option Barrier. 1D and 2DV models were used in the calibration by changing the losses coefficients while the gate openings values are kept constant (for each corresponding discharge) and equal to the prototype data, number of trials have been done for each discharge until getting the upstream water level at (65.90). Table 18 presents all the trials which have been done using Delft 3D in case of 1D model and table 18 in case of 2D model.

Table 4-18: Gate Calibration in case of 1D Model

Gate Calibration 1D Model					
Q (m3/s)	G.O. (m)	G.O. (m)	LOSSES	Hu (m)	Hu (m)
383.97	2.48	-13.72	0.40	-3.40	12.80
383.97	2.48	-13.72	0.50	-2.50	13.70
383.97	2.48	-13.72	0.43	-3.14	13.06
383.97	2.48	-13.72	0.45	-2.96	13.24
323.35	2.23	-13.97	0.45	-3.55	12.65
323.35	2.23	-13.97	0.48	-3.30	12.90

Gate Calibration 1D Model					
Q (m3/s)	G.O. (m)	G.O. (m)	LOSSES	Hu (m)	Hu (m)
323.35	2.23	-13.97	0.50	-3.15	13.05
323.35	2.23	-13.97	0.54	-2.85	13.35
323.35	2.23	-13.97	0.52	-3.00	13.20
262.72	1.83	-14.37	0.58	-2.70	13.50
262.72	1.83	-14.37	0.55	-2.95	13.25
202.09	1.28	-14.92	0.58	-1.94	14.26
202.09	1.28	-14.92	0.54	-2.25	13.95
202.09	1.28	-14.92	0.50	-2.60	13.60
202.09	1.28	-14.92	0.47	-2.88	13.32
202.09	1.28	-14.92	0.45	-3.10	13.10
202.09	1.28	-14.92	0.46	-2.98	13.22
141.46	0.97	-15.23	0.55	-2.95	13.25
80.84	0.57	-15.63	0.56	-3.15	13.05
80.84	0.57	-15.63	0.58	-2.97	13.23

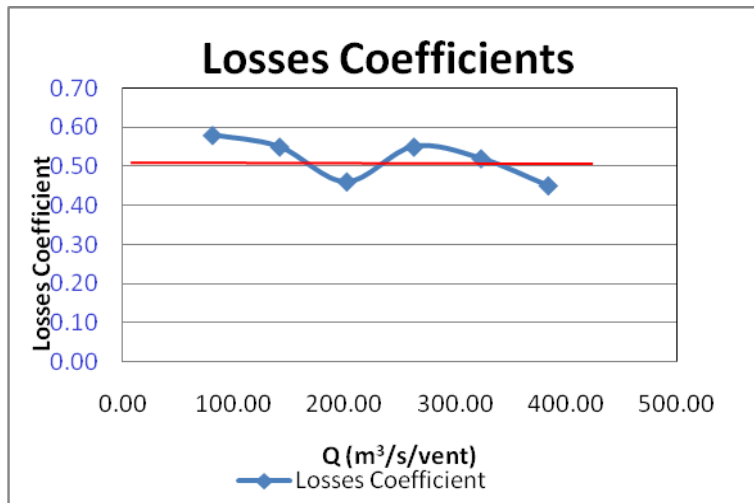


Figure 4-24: losses coefficients in case of 1D model

From the previous table and chart it was found that the average losses coefficient for the gate opening calibration in case of 1D models using Delft 3D = 0.5

Table 4-19: Gate Calibration in case of 2DV Model

Gate Calibration 2DV Model					
Q (m3/s)	G.O. (m)	G.O. (m)	LOSSES	Hu (m)	Hu (m)
141.46	0.97	-15.23	0.55	-0.85	15.35
141.46	0.97	-15.23	0.25	-2.96	13.24
202.09	1.28	-14.92	0.20	-0.75	15.45
202.09	1.28	-14.92	0.17	-1.50	14.70
202.09	1.28	-14.92	0.15	-1.15	15.05
202.09	1.28	-14.92	0.10	-1.57	14.63
202.09	1.28	-14.92			16.20
80.84	0.57	-15.63	0.20	-5.00	11.20
80.84	0.57	-15.63	0.25	-4.60	11.60
80.84	0.57	-15.63	0.40	-3.60	12.60
80.84	0.57	-15.63	0.46	-3.15	13.05
80.84	0.57	-15.63	0.51	-2.85	13.35
80.84	0.57	-15.63	0.50	-2.96	13.24
262.72	1.83	-14.37	0.23	-2.30	13.90
262.72	1.83	-14.37	0.21	-2.50	13.70
262.72	1.83	-14.37	0.19	-2.74	13.46
262.72	1.83	-14.37	0.17	-2.97	13.23
323.35	2.23	-13.97	0.19	-3.26	12.94
323.35	2.23	-13.97	0.21	-3.04	13.16
323.35	2.23	-13.97	0.22	-2.94	13.26
383.97	2.48	-13.72	0.25	-2.68	13.52
383.97	2.48	-13.72	0.22	-2.30	13.90
383.97	2.48	-13.72	0.15	-3.18	13.02
383.97	2.48	-13.72	0.19	-2.70	13.50
383.97	2.48	-13.72	0.17	-2.95	13.25

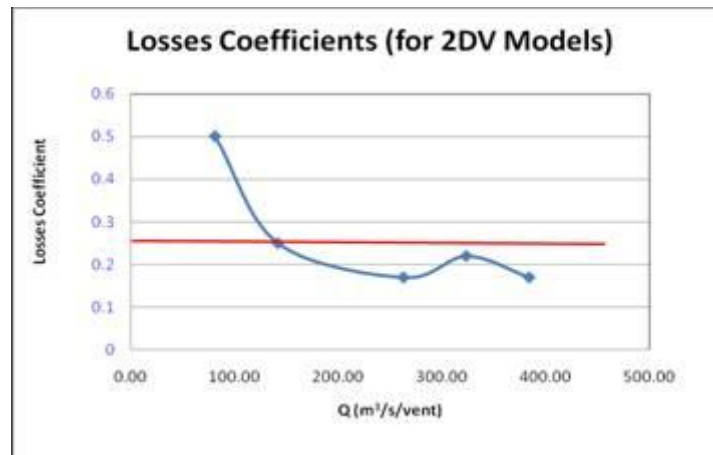


Figure 4-25: losses coefficients in case of 2DV models

From the previous table and chart it was found that the average losses coefficient for the gate opening calibration in case of 2DV models using Delft 3D = 0.25

4.12 Results and Analysis

Velocities Profiles

The flow velocity was measured at seven cross sections with equal distances apart.

The distance between each two cross section was equal to 0.50m. The first cross section was located at a distance of 1.0 m downstream the gate. Four cross sections were located on the apron area, and the other three sections were located on the rip rap area, downstream the apron. Figure 27 shows the location of the velocity profiles in the flume.

The velocity values were measured at four points along the water depth at relative distances from the bed of 0.2, 0.4, 0.6 and 0.8 of the total water depth, to represent the vertical velocity profile. An additional velocity measurement was conducted for each vertical at a fixed distance of 3.0 cm from the bed, to represent the near bed velocity values. These near-bed velocity values and their standard deviations were of great importance to assess the efficiency of energy dissipation, especially for the case of bed protection stability analysis.

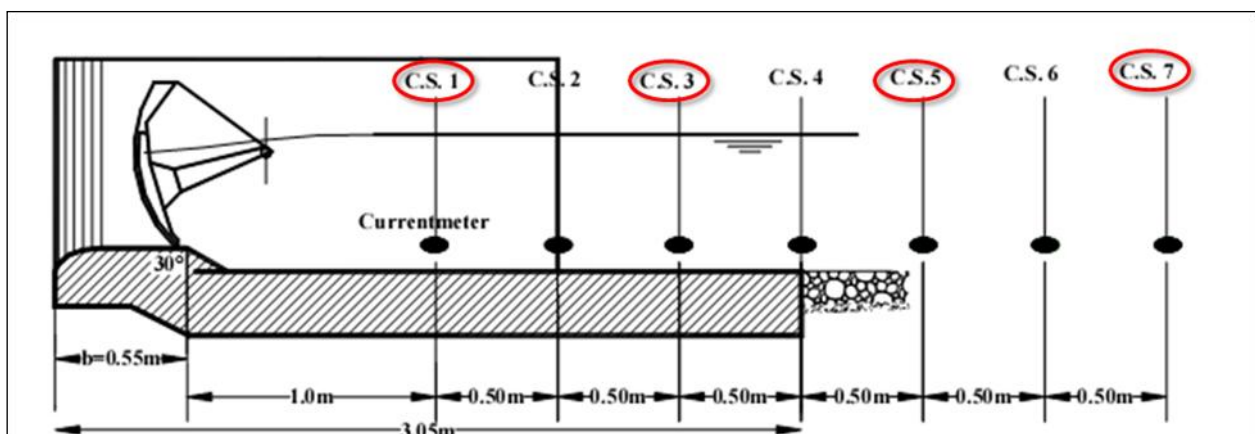


Figure 4-26: The different locations for the velocity measurements in the flume

Figures 4-28 and 4-29 provide a sample of the velocity profiles measured for test series A1 & A7. There are seven profiles were presented for each test; they are the profiles measured at the different locations downstream the gate. Also, five velocity values were shown on each profile; they are the near bed velocity 3

cm from Observation Points (in the flume) the bed and the four velocities at 0.2, 0.4, 0.6, and 0.8 relative depth. Table 19 presents a summary for the velocity values in the flume.

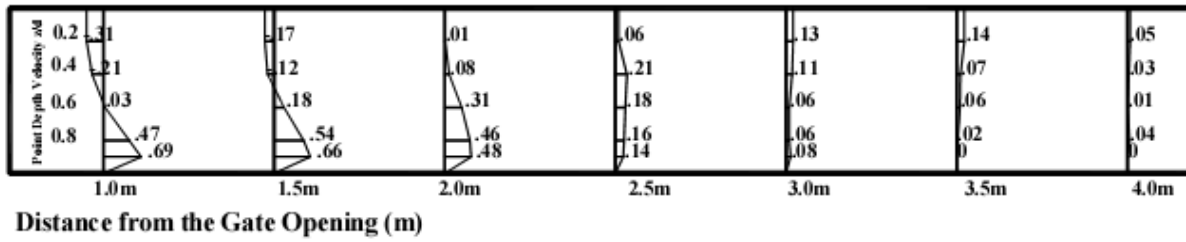


Figure 4-27: Velocity profiles for test group A1

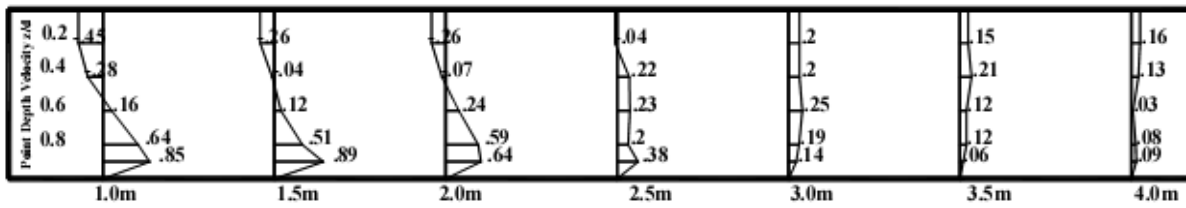


Figure 4-28: Velocity profiles for test group A7

Table 4-20: the velocity values in the flume

		Velocities Profiles in the Flume						
		Depth	Q= 40 l/s	Q= 70 l/s	Q= 100 l/s	Q= 130 l/s	Q= 160 l/s	Q= 190 l/s
Location 1 @ dist. 1 m (CS 1)	0.2d		-0.31	-0.45	-0.33	-0.43	-0.44	-0.36
	0.4d		-0.21	-0.28	-0.31	0.14	0.00	0.15
	0.6d		0.03	0.16	0.50	0.57	0.50	0.85
	0.8d		0.47	0.64	1.01	1.62	1.12	1.49
	3 cm		0.69	0.85	1.30	1.78	1.78	1.85
Location 2 @ dist. 2 m (CS 3)	0.2d		0.01	-0.26	0.06	-0.19	-0.17	0.01
	0.4d		0.08	-0.07	0.24	-0.03	0.16	0.22
	0.6d		0.31	0.24	0.42	0.46	0.59	0.64
	0.8d		0.46	0.59	0.81	0.81	1.04	0.91
	3 cm		0.48	0.64	0.89	0.93	1.14	1.30
Location 3 @ dist. 3 m (CS 5)	0.2d		0.13	0.20	0.25	0.27	0.33	0.30
	0.4d		0.11	0.20	0.33	0.33	0.45	0.43
	0.6d		0.06	0.25	0.42	0.48	0.52	0.52
	0.8d		0.06	0.19	0.27	0.47	0.48	0.51

		Velocities Profiles in the Flume					
		Depth	Q= 40 l/s	Q= 70 l/s	Q= 100 l/s	Q= 130 l/s	Q= 160 l/s
Location 4 @ dist. 4 m (CS 7)	3 cm	0.08	0.14	0.27	0.34	0.48	0.33
	0.2d	0.05	0.16	0.27	0.29	0.55	0.63
	0.4d	0.03	0.13	0.30	0.34	0.54	0.62
	0.6d	0.01	0.03	0.17	0.34	0.59	0.66
	0.8d	0.04	0.08	0.11	0.37	0.64	0.67
	3 cm	0.00	0.09	0.07	0.27	0.59	0.65

Table 4-21 presents a summary for the velocity values in the prototype after converting them from the flume results.

Table 4-21: the velocity values in the prototype

		Velocities Profiles (Prototype)					
		Depth (m)	Q = 80.84 m ³ /s	Q = 141.46 m ³ /s	Q = 202.09 m ³ /s	Q = 262.72 m ³ /s	Q = 323.35 m ³ /s
Location 1 @ dist. 21 m (CS 1)	0.2d	-1.42	-2.06	-1.51	-1.97	-2.02	-1.65
	0.4d	-0.96	-1.28	-1.42	0.64	0.00	0.69
	0.6d	0.14	0.73	2.29	2.61	2.29	3.90
	0.8d	2.15	2.93	4.63	7.42	5.13	6.83
	0.63	3.16	3.90	5.96	8.16	8.16	8.48
Location 2 @ dist. 42 m (CS 3)	0.2d	0.05	-1.19	0.27	-0.87	-0.78	0.05
	0.4d	0.37	-0.32	1.10	-0.14	0.73	1.01
	0.6d	1.42	1.10	1.92	2.11	2.70	2.93
	0.8d	2.11	2.70	3.71	3.71	4.77	4.17
	0.63	2.20	2.93	4.08	4.26	5.22	5.96
Location 3 @ dist. 63 m (CS 5)	0.2d	0.60	0.92	1.15	1.24	1.51	1.37
	0.4d	0.50	0.92	1.51	1.51	2.06	1.97
	0.6d	0.27	1.15	1.92	2.20	2.38	2.38
	0.8d	0.27	0.87	1.24	2.15	2.20	2.34
	0.63	0.37	0.64	1.24	1.56	2.20	1.51
Location 4 @ dist. 84 m	0.2d	0.23	0.73	1.24	1.33	2.52	2.89

		Velocities Profiles (Prototype)					
Depth (m)		Q = 80.84 m ³ /s	Q = 141.46 m ³ /s	Q = 202.09 m ³ /s	Q = 262.72 m ³ /s	Q = 323.35 m ³ /s	Q = 383.97 m ³ /s
	0.4d	0.14	0.60	1.37	1.56	2.47	2.84
	0.6d	0.05	0.14	0.78	1.56	2.70	3.02
	0.8d	0.18	0.37	0.50	1.70	2.93	3.07
	0.63	0.00	0.41	0.32	1.24	2.70	2.98

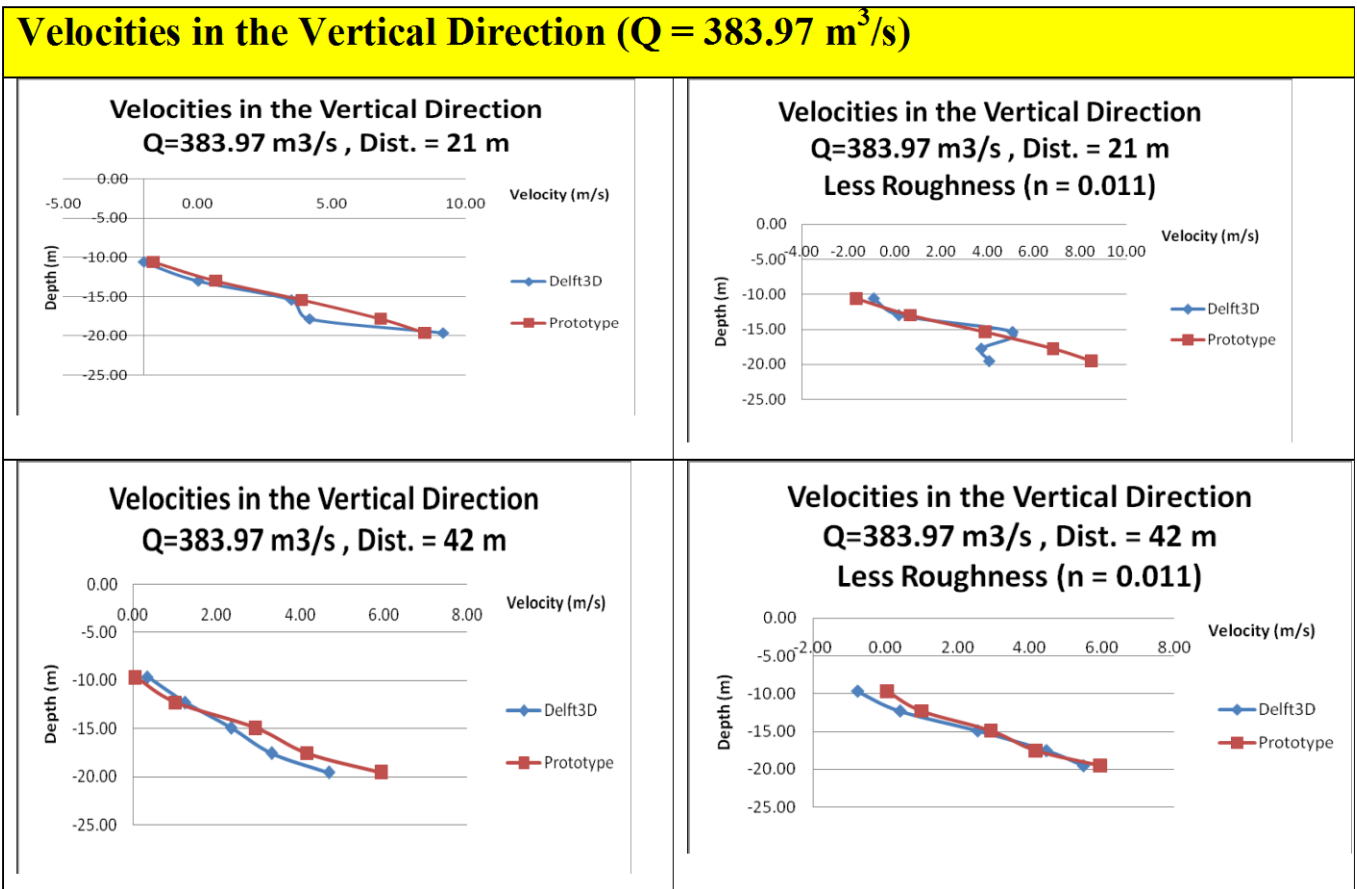
4.12.1 Sensitivity Analysis

The roughness coefficient and the turbulence mode were selected as variable parameters to study the sensitivity of Delft 3D and to study the effective parameters through which the rest of the study will be based on.

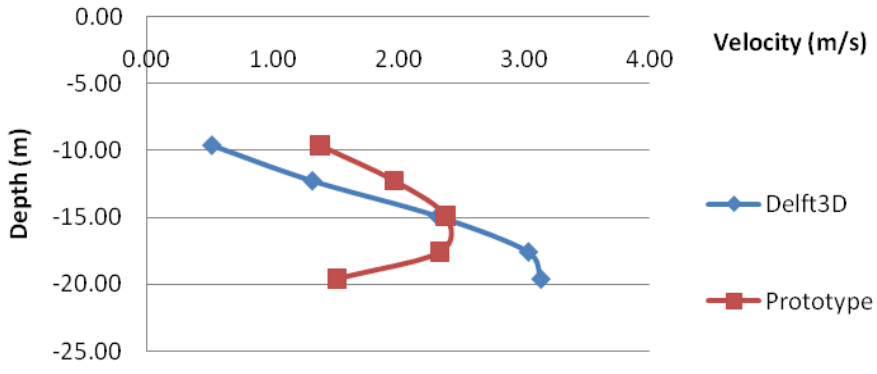
a) The Roughness Coefficient

It was noticed from the study of the velocity profiles at distances 63 and 84 meters that the values coming from Delft 3D are less than that ones from the prototype (the reference), so it was decided to reduce the roughness coefficient by taking a smaller value for Manning Coefficient ($n_{\text{new}} = 0.011$ instead of 0.035) for the riprap areas. The following figures represent a comparison between the results before and after changing the roughness coefficient for the case of maximum discharge only.

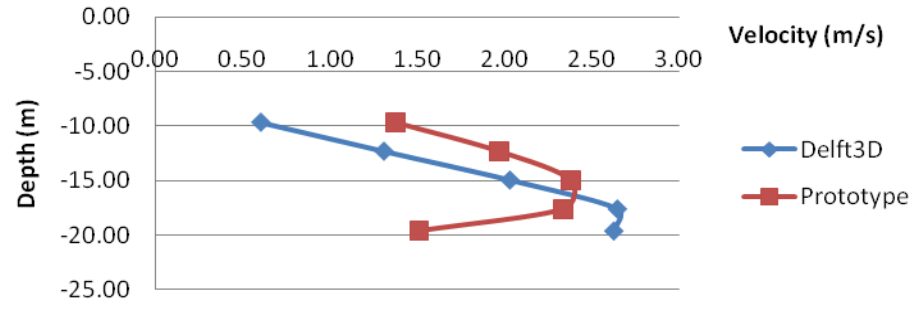
Table 4-22: Velocity profiles in the Vertical Direction (Q = 383.97 m³/s)



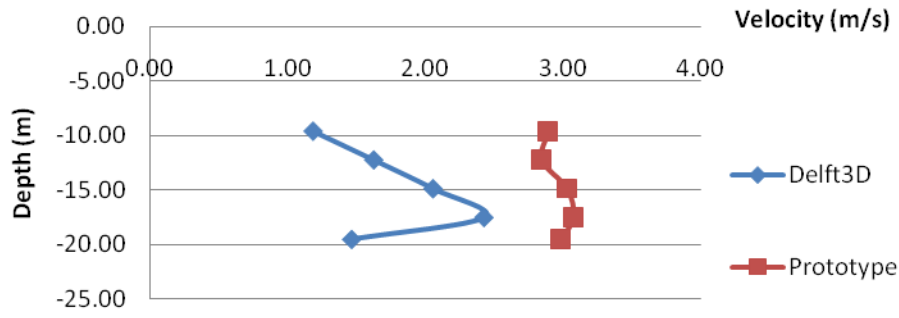
Velocities in the Vertical Direction
Q=383.97 m³/s , Dist. = 63 m



Velocities in the Vertical Direction
Q=383.97 m³/s , Dist. = 63 m
Less Roughness (n = 0.011)



Velocities in the Vertical Direction
Q=383.97 m³/s , Dist. = 84 m



Velocities in the Vertical Direction
Q=383.97 m³/s , Dist. = 84 m
Less Roughness (n = 0.011)

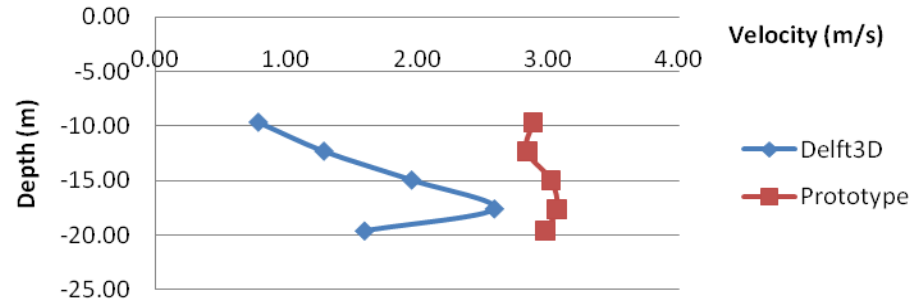
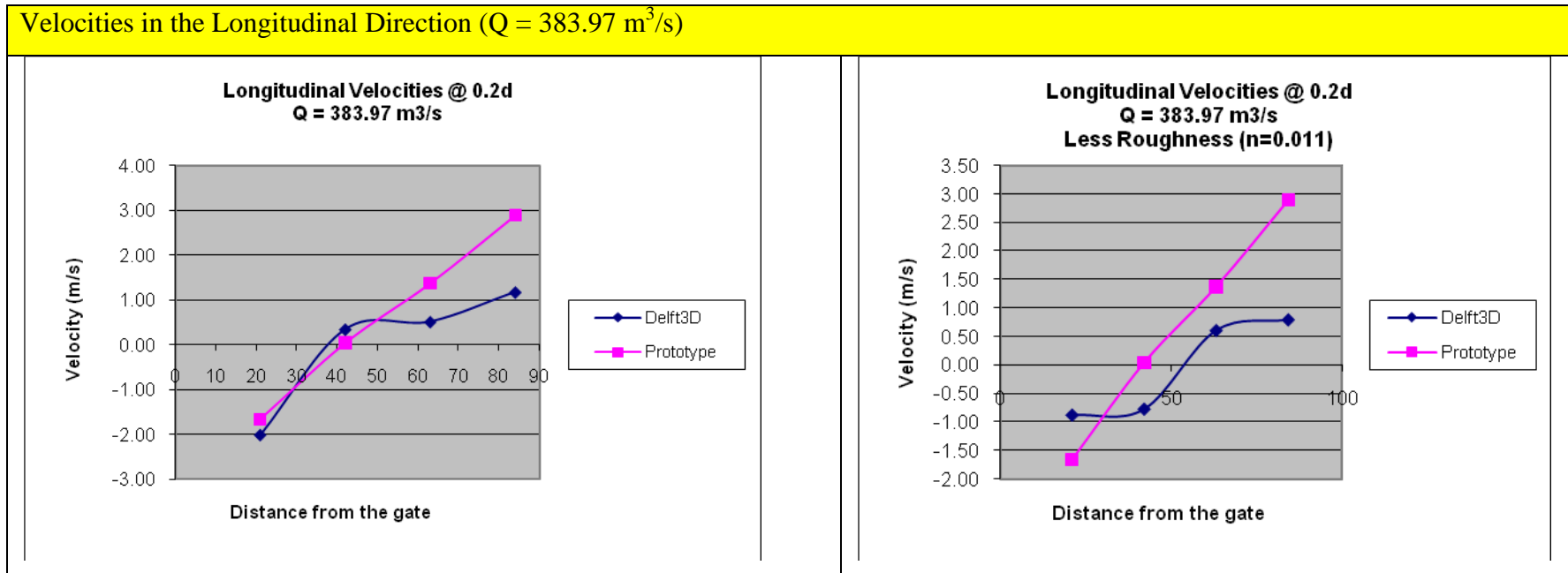
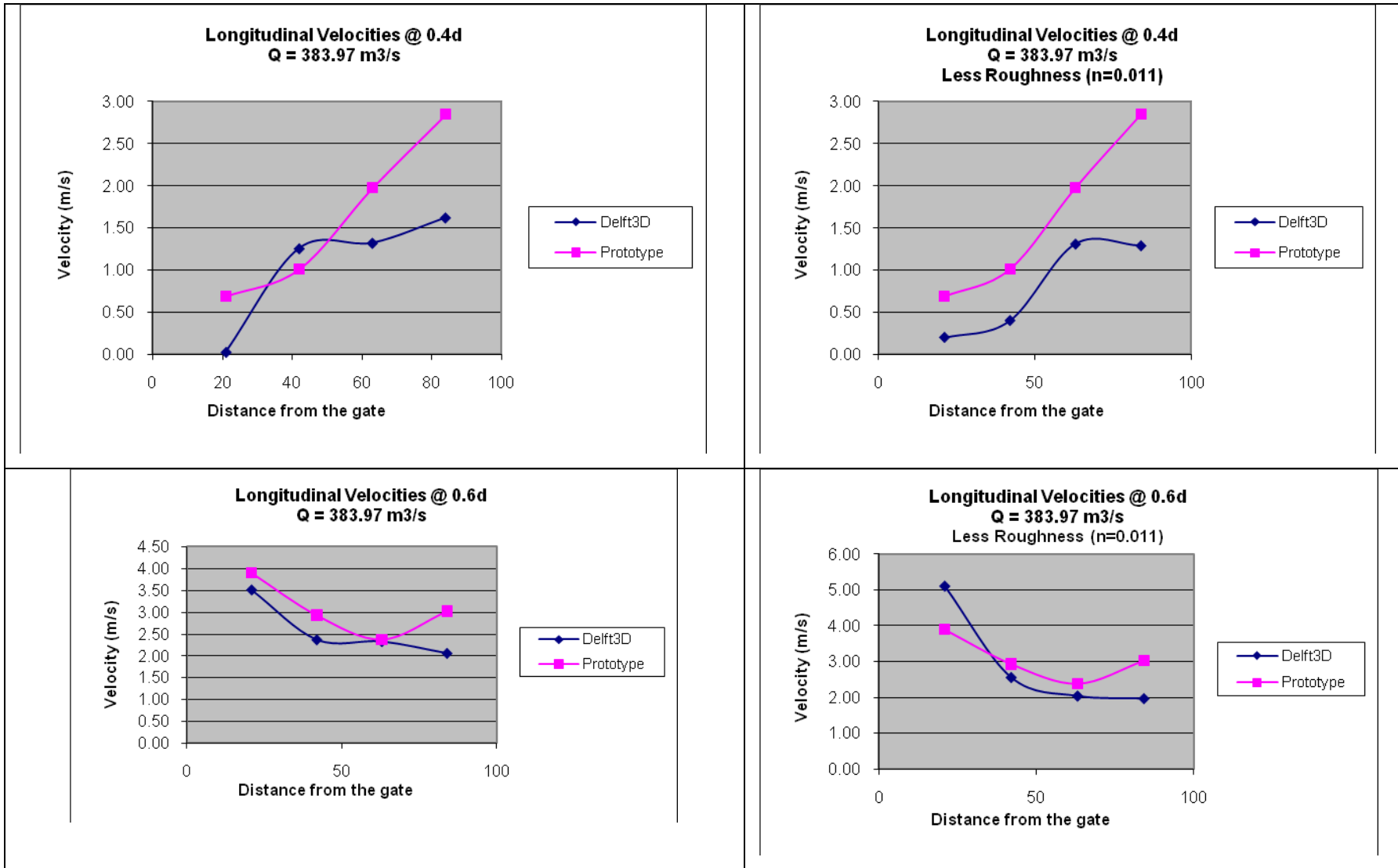
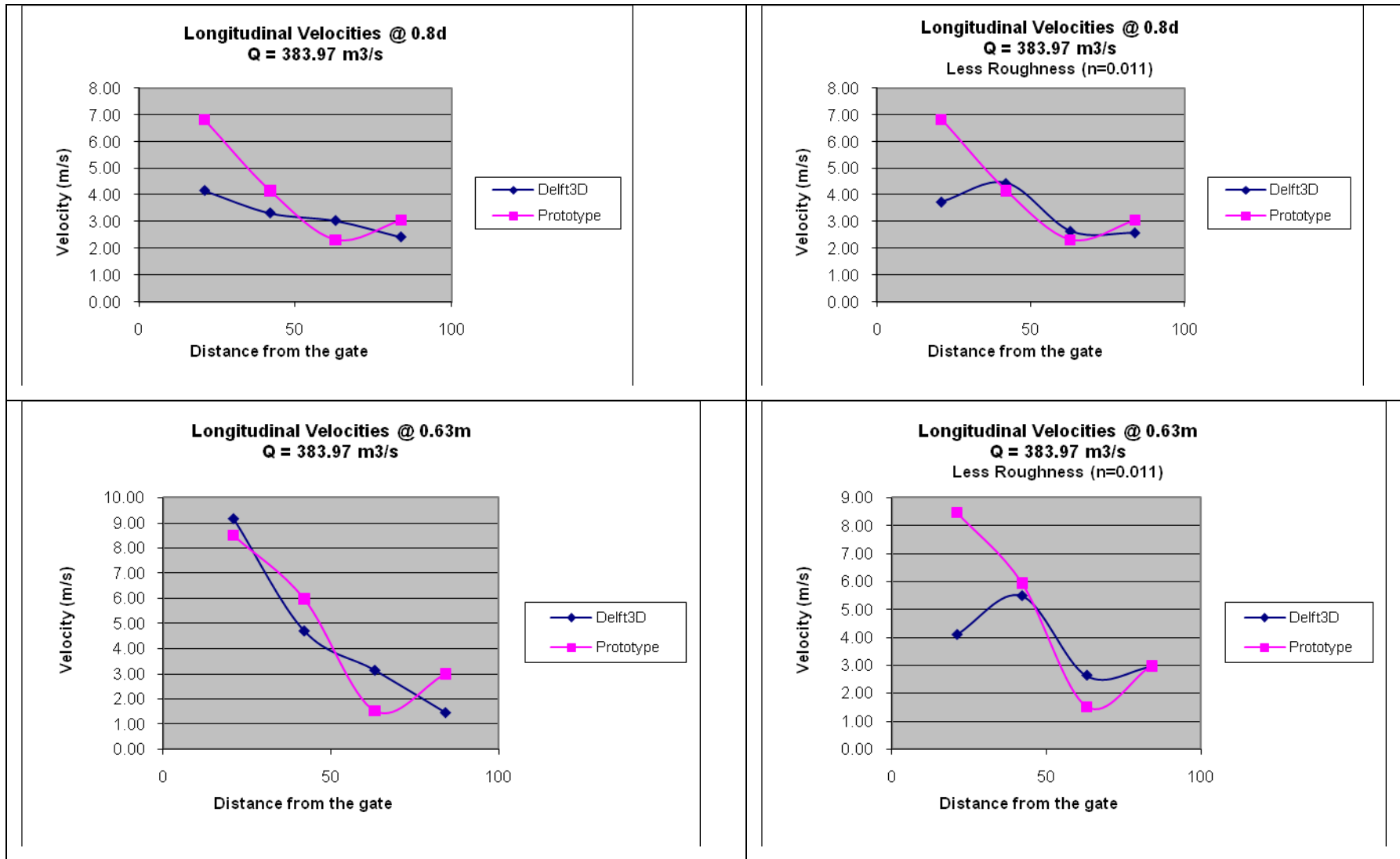


Table 4-23: Velocities in the longitudinal direction (Q = 383.97 m³/s)







From figures above it is noticed that the change in the roughness coefficient does not improve the results, so it could be said that Delft 3D is not sensitive with respect to the roughness coefficient.

b) The Turbulence Model

The second parameter which has been used in the sensitivity analysis is the turbulence model. It was decided to change the turbulence model from K- ϵ (by default) to K-L model.

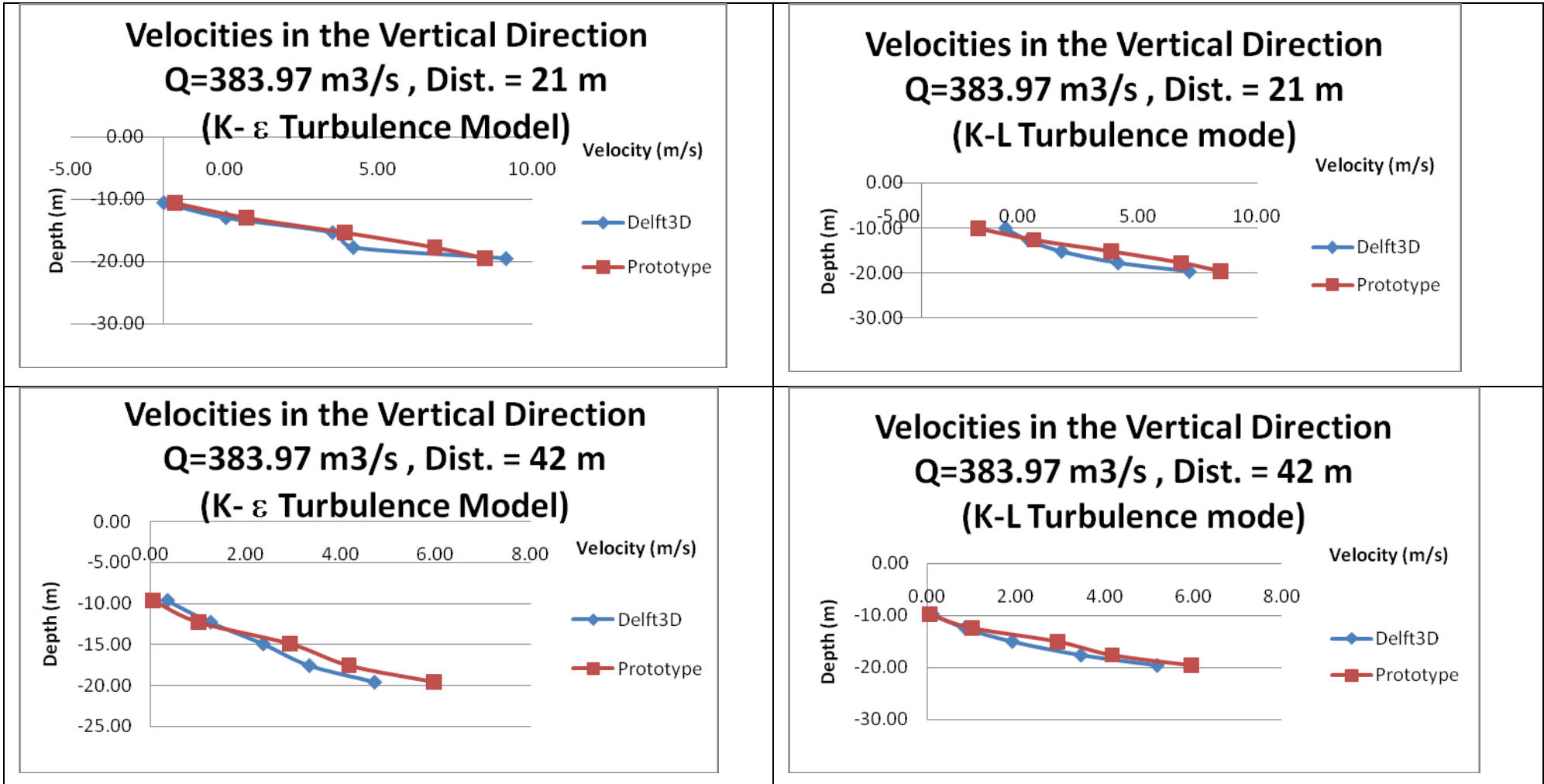
The differences between the two turbulence models:

k-L model: The coefficients are determined by a transport equation for the turbulent kinetic energy (k) and mixing length (L).

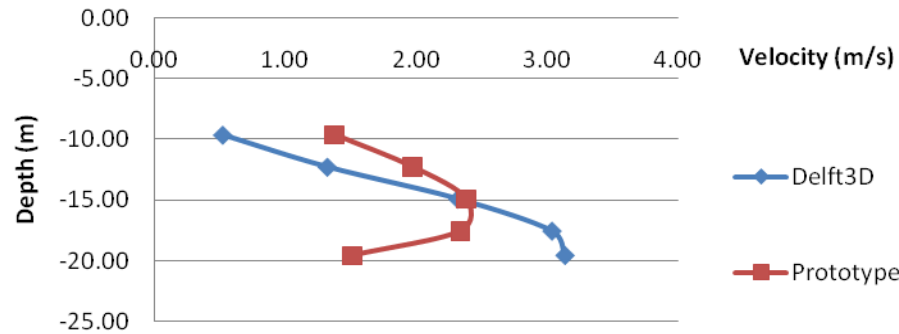
k- ϵ model: The coefficients are determined by transport equations for both the turbulent kinetic energy (k) and the turbulent kinetic energy dissipation (ϵ).

The following figures represent the results of using the two different models in case of maximum discharge.

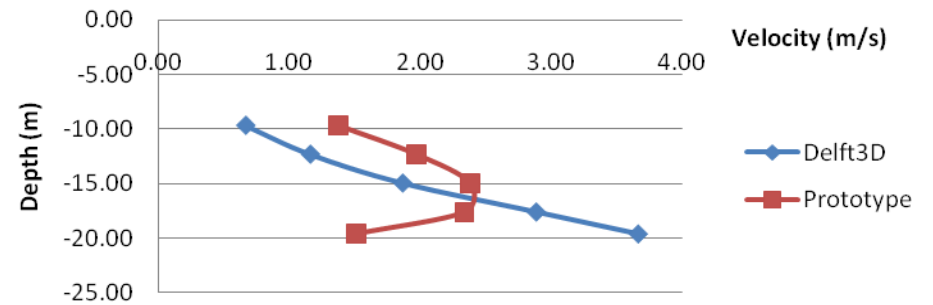
Table 4-24: Velocity profiles in the Vertical Direction downstream the sill (for Q = 383.97 m³/s only)



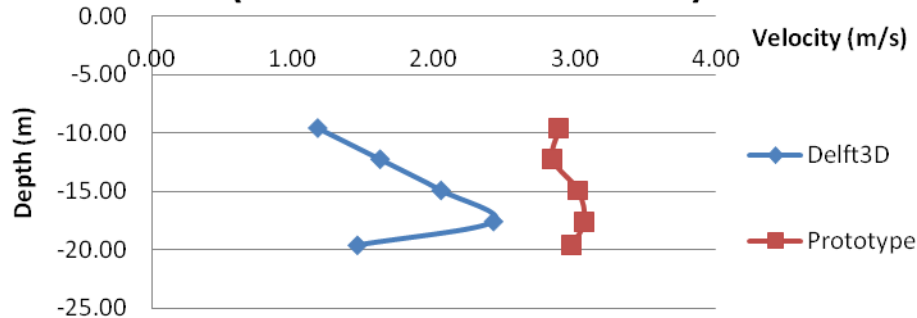
Velocities in the Vertical Direction
Q=383.97 m³/s , Dist. = 63 m
(K- ε Turbulence Model)



Velocities in the Vertical Direction
Q=383.97 m³/s , Dist. = 63 m
(K-L Turbulence mode)



Velocities in the Vertical Direction
Q=383.97 m³/s , Dist. = 84 m
(K- ε Turbulence Model)



Velocities in the Vertical Direction
Q=383.97 m³/s , Dist. = 84 m
(K-L Turbulence mode)

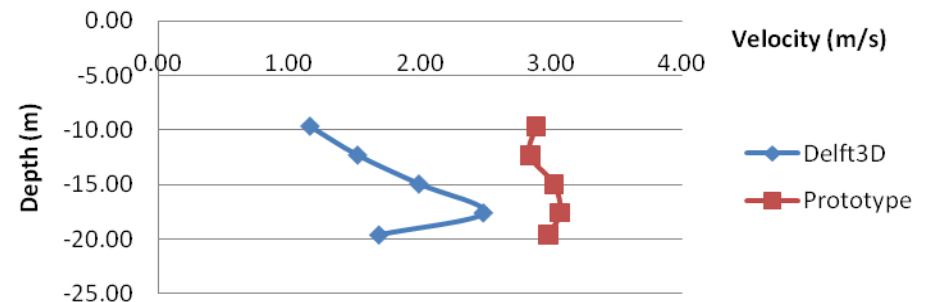
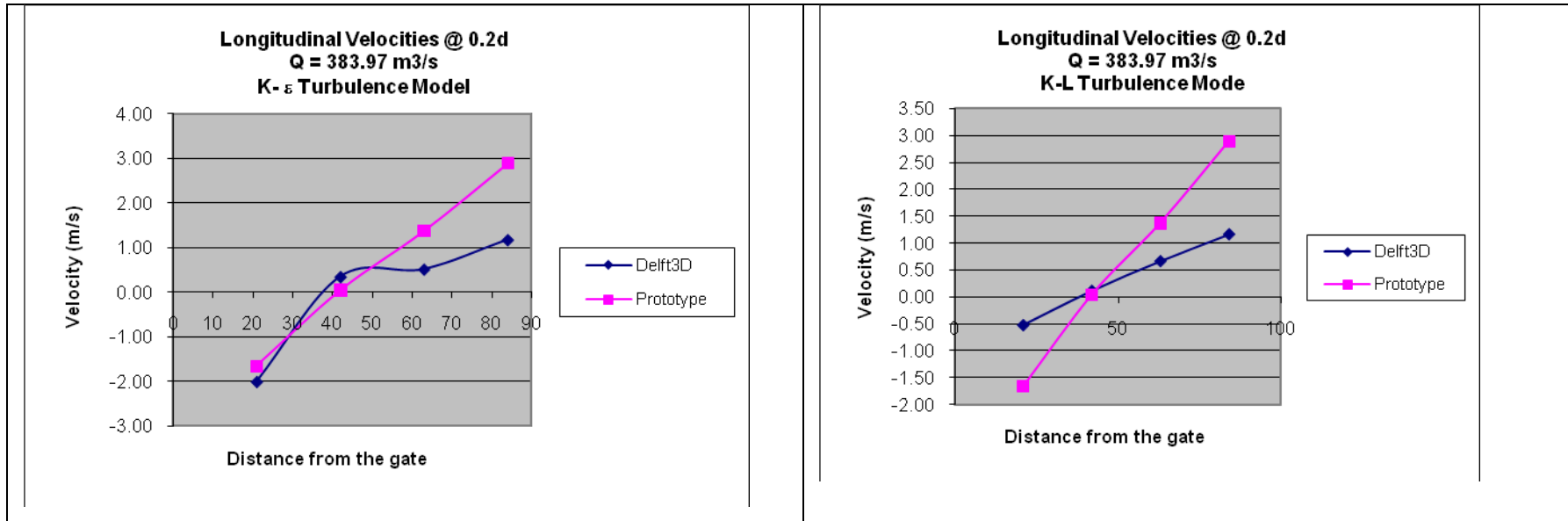
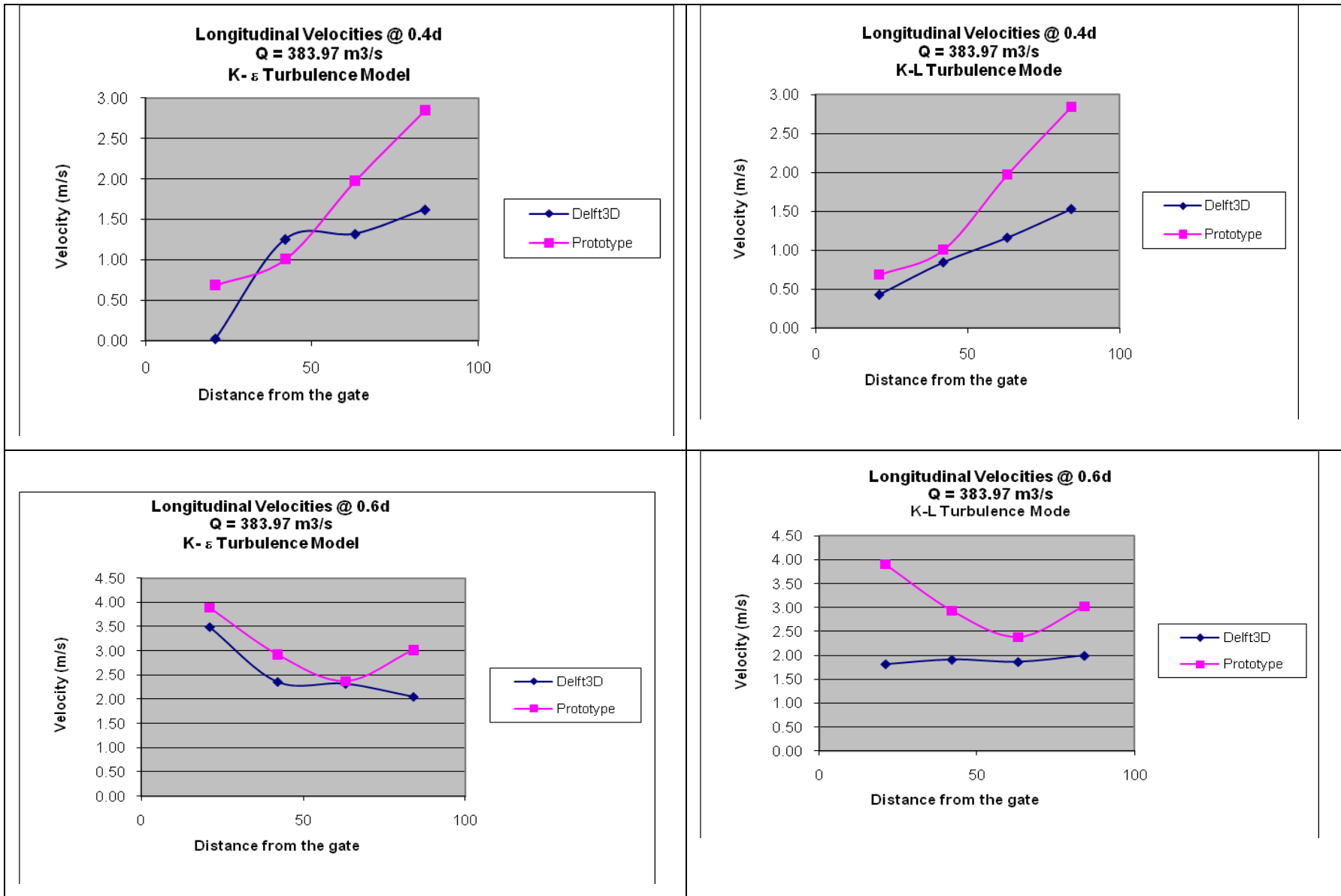
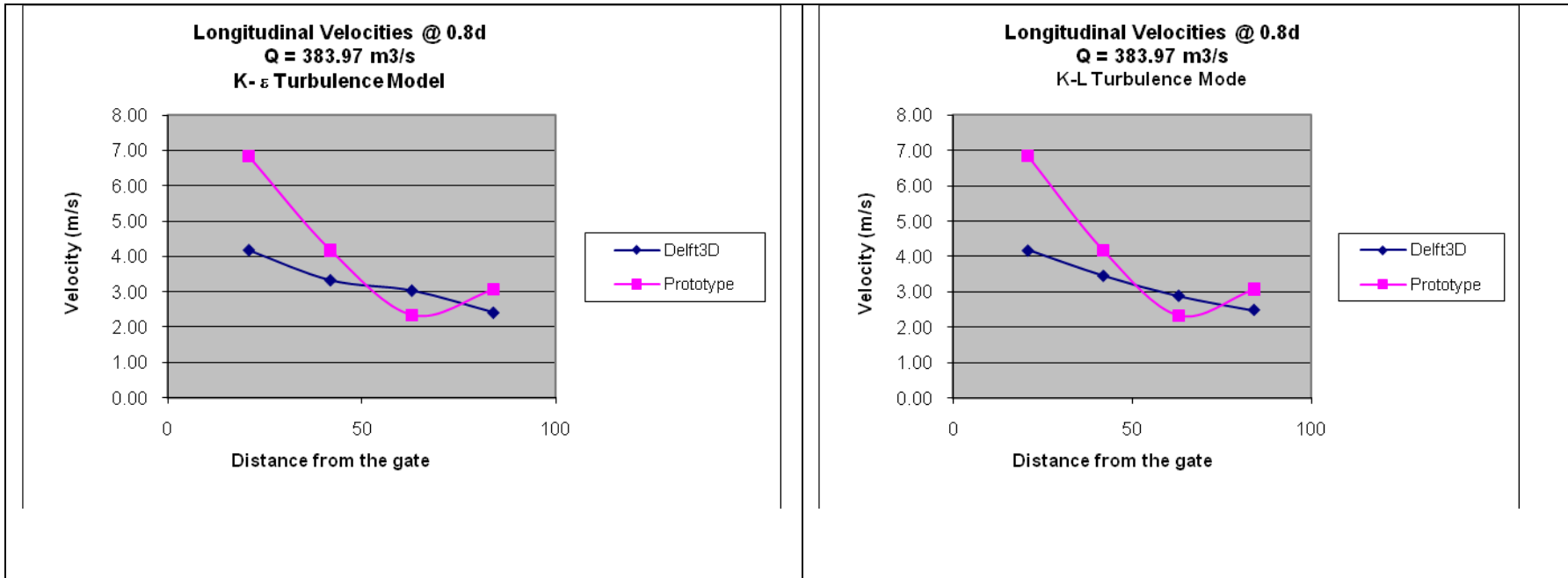
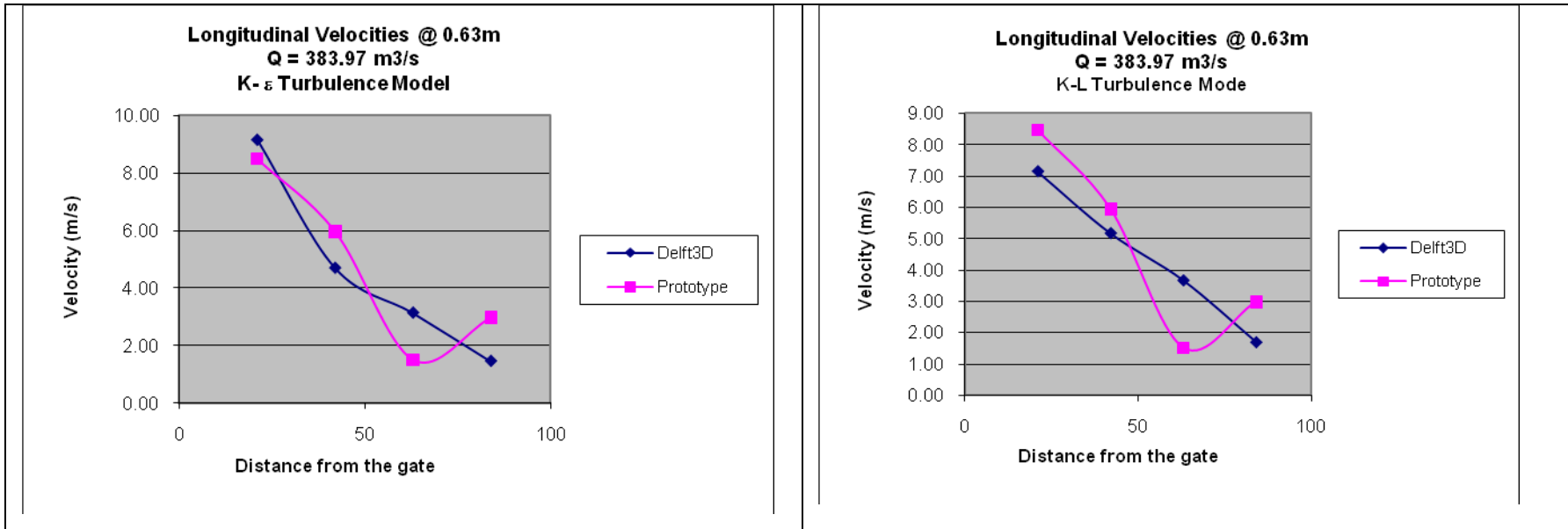


Table 4-25: Velocities in the longitudinal direction downstream the sill (for $Q = 383.97 \text{ m}^3/\text{s}$ only)







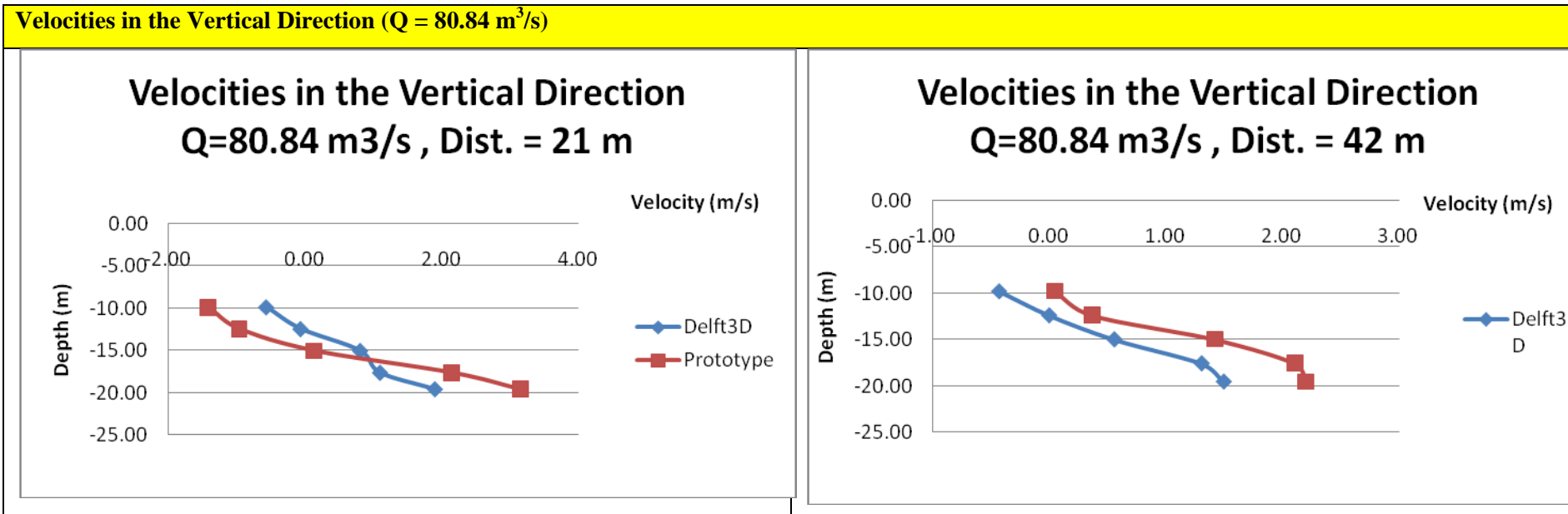


From the figures above it is remarkable that there is no significant change or improvement in the results after changing the turbulence model from K- ϵ to K-L model.

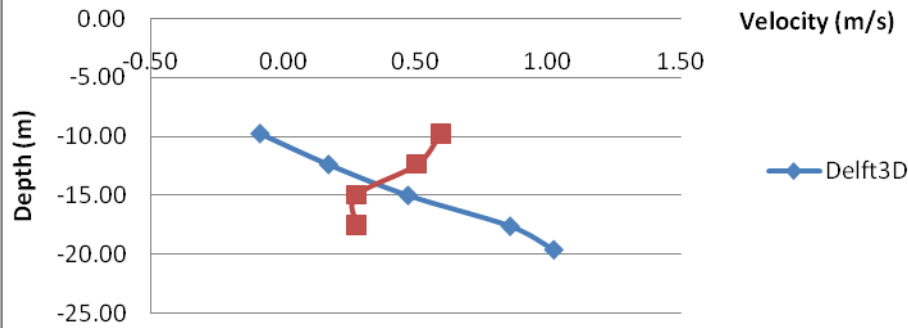
Velocities Profiles for all discharges

After studying Delft 3D sensitivity and determining the effective parameters (the roughness & the turbulence model) the velocity profiles in the vertical direction and the longitudinal velocities for different discharges were drawn using Excel sheets for Delft 3D and the Prototype, see tables 25 and 26.

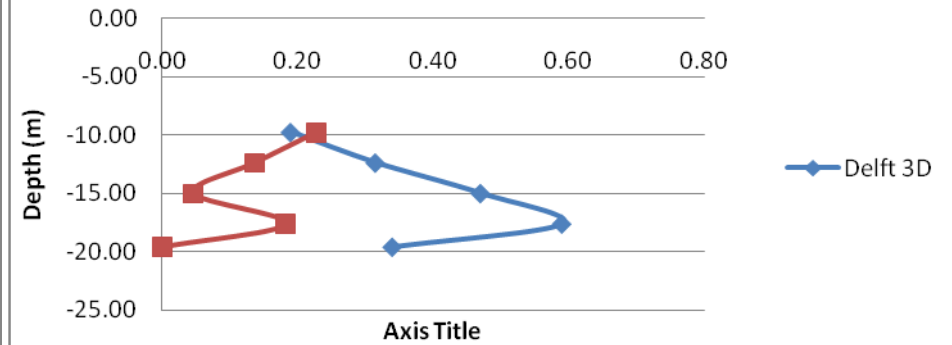
Table 4-26: the velocity profiles in the vertical direction



**Velocities in the Vertical Direction
Q=80.84 m³/s , Dist. = 63 m**

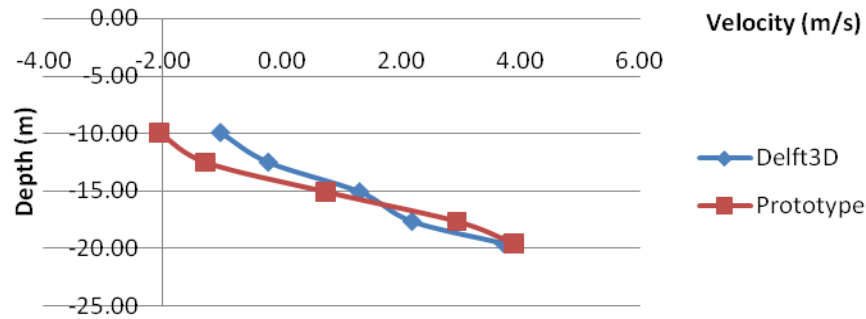


**Velocities in the Vertical Direction
Q=80.84 m³/s , Dist. = 84 m**

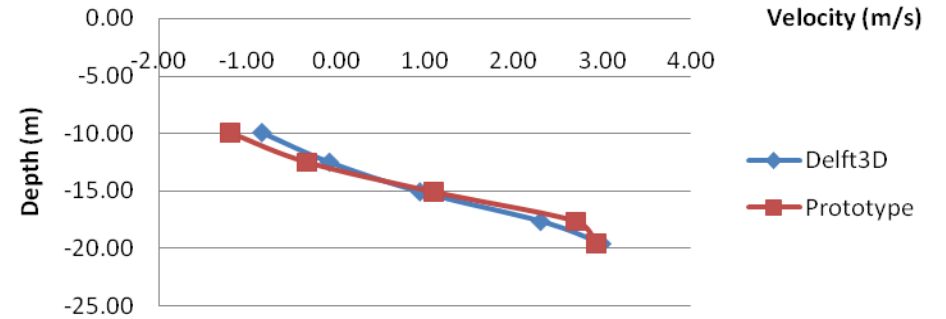


Velocities in the Vertical Direction (Q = 141.46 m³/s)

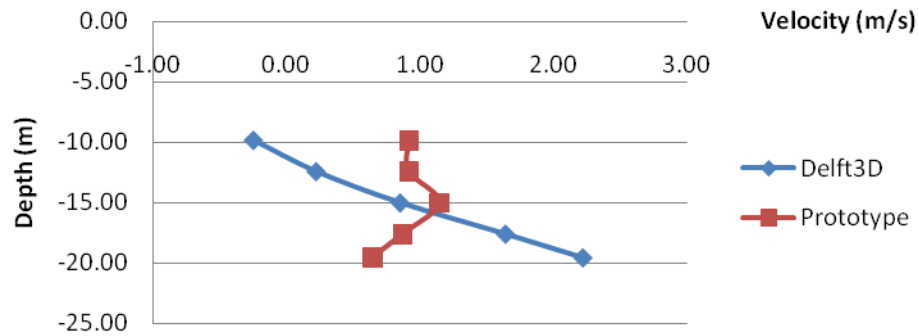
Velocities in the Vertical Direction
Q=141.46 m³/s , Dist. = 21 m



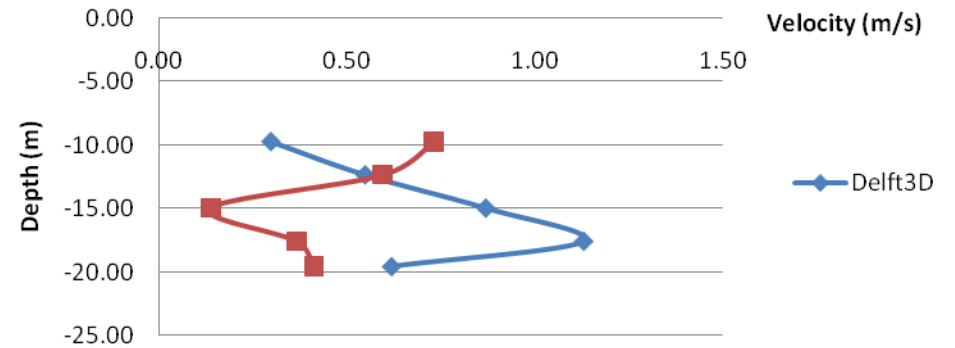
Velocities in the Vertical Direction
Q=141.46 m³/s , Dist. = 42 m



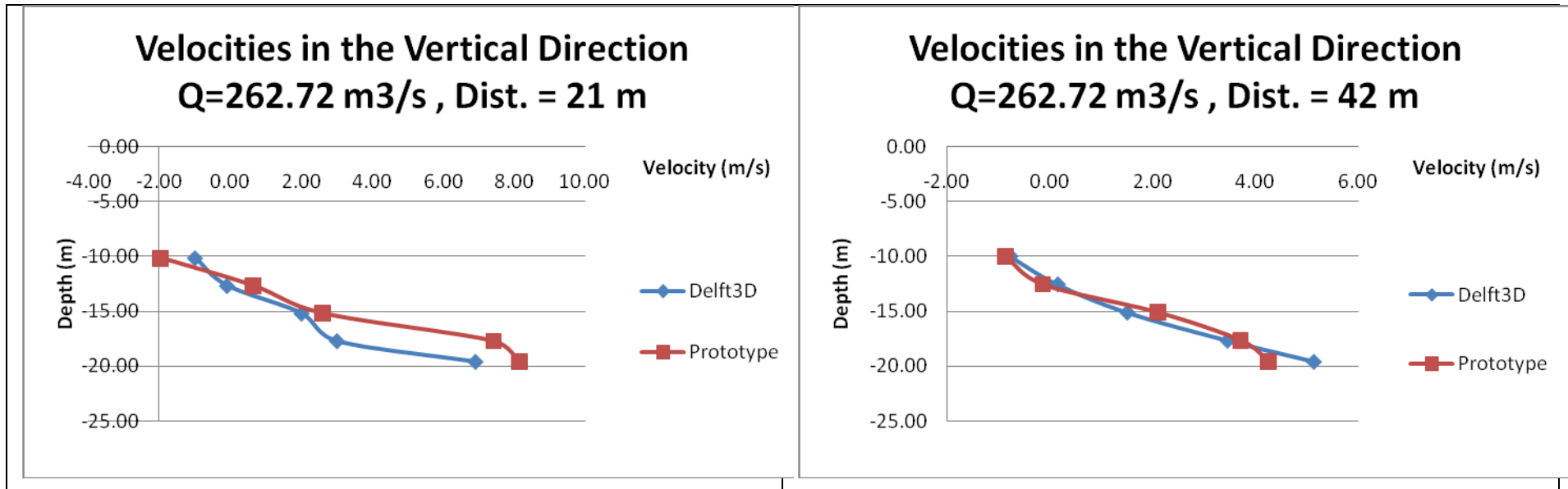
**Velocities in the Vertical Direction
Q=141.46 m³/s , Dist. = 63 m**



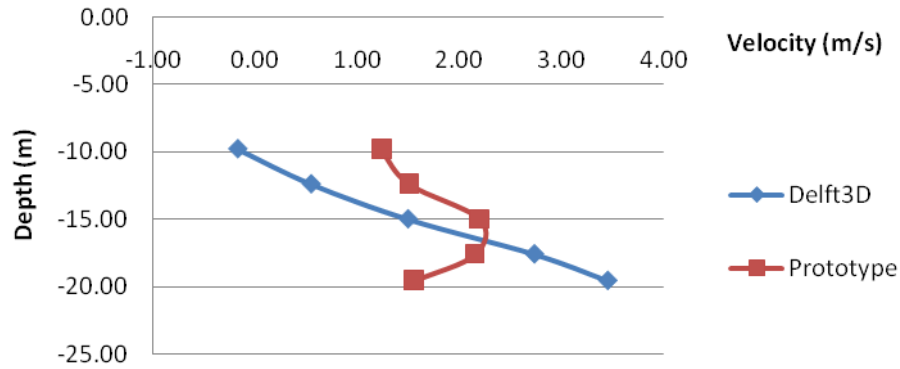
**Velocities in the Vertical Direction
Q=141.46 m³/s , Dist. = 84 m**



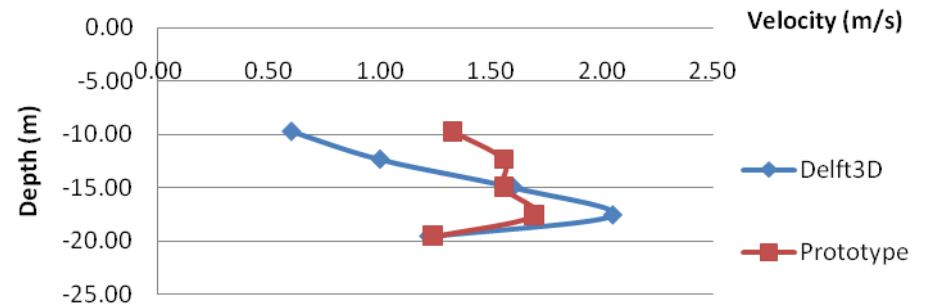
Velocities in the Vertical Direction (Q = 262.72 m³/s)



**Velocities in the Vertical Direction
Q=262.72 m³/s , Dist. = 63 m**

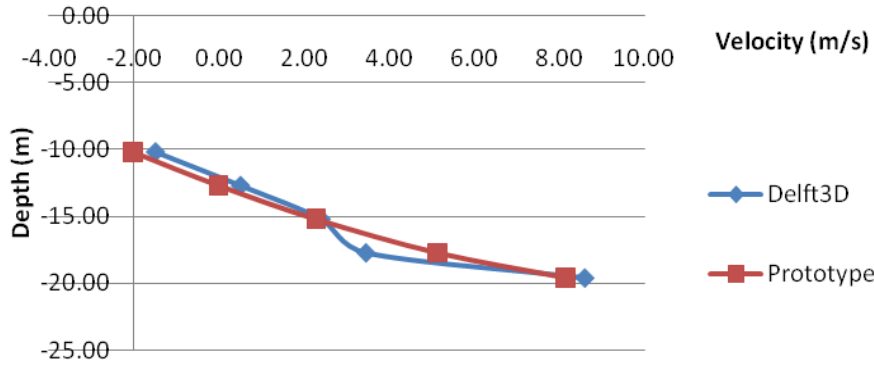


**Velocities in the Vertical Direction
Q=262.72 m³/s , Dist. = 84 m**

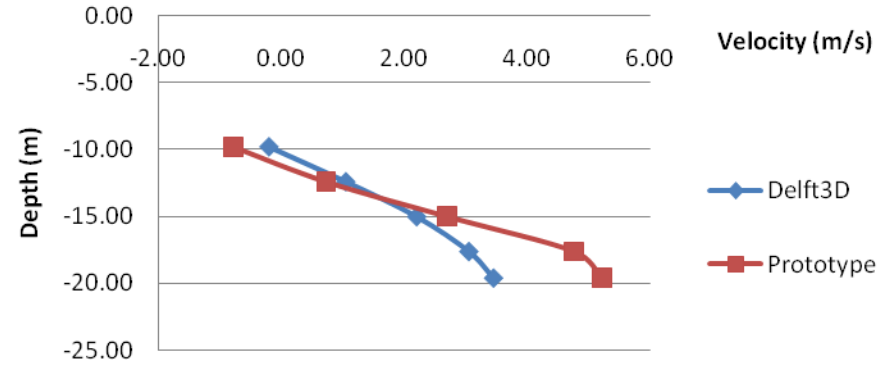


Velocities in the Vertical Direction (Q = 262.72 m³/s)

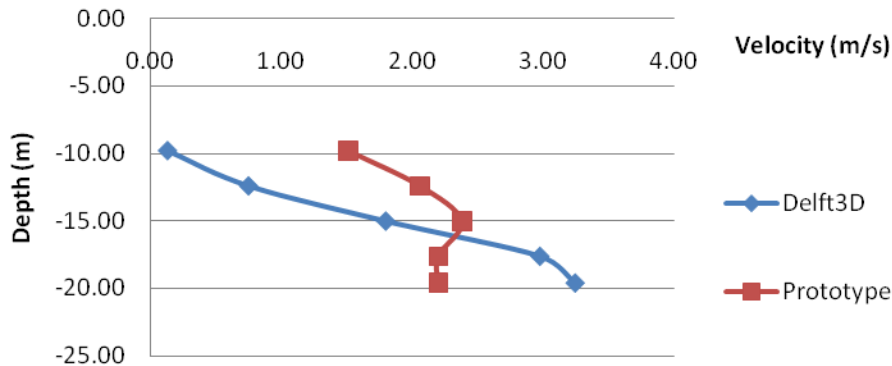
Velocities in the Vertical Direction
Q=323.35 m³/s , Dist. = 21 m



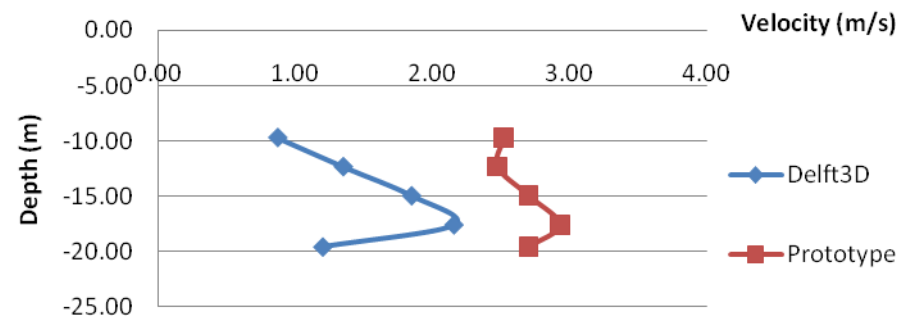
Velocities in the Vertical Direction
Q=323.35 m³/s , Dist. = 42 m



Velocities in the Vertical Direction
Q=323.35 m³/s , Dist. = 63 m

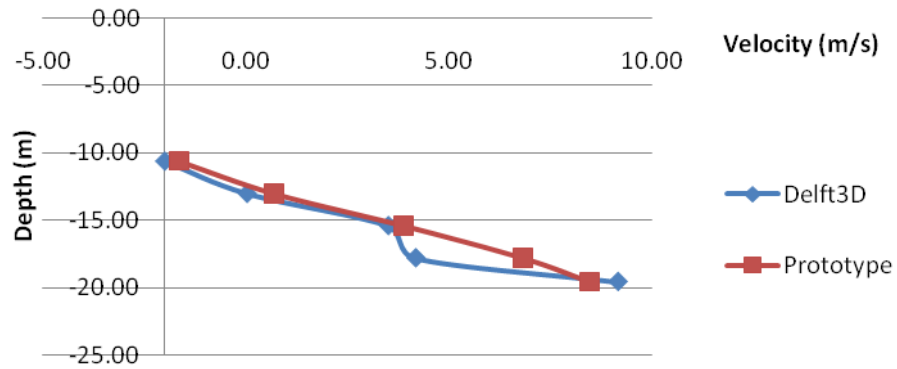


Velocities in the Vertical Direction
Q=323.35 m³/s , Dist. = 84 m

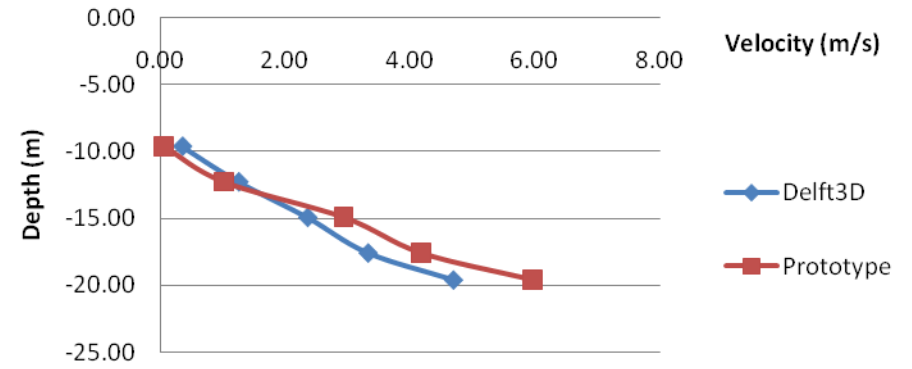


Velocities in the Vertical Direction ($Q = 383.97 \text{ m}^3/\text{s}$)

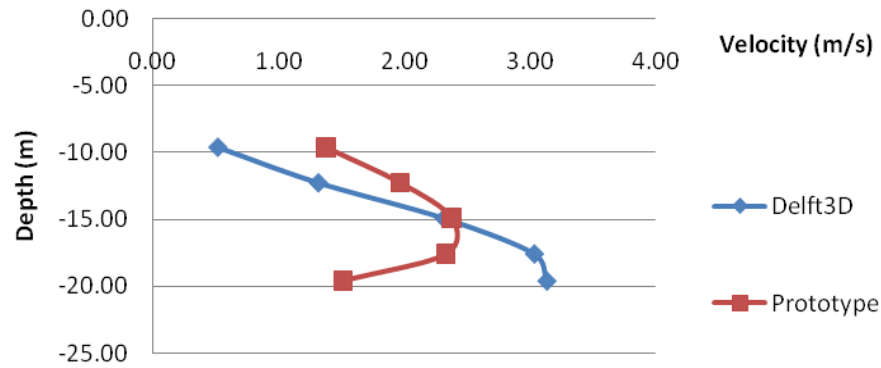
**Velocities in the Vertical Direction
 $Q=383.97 \text{ m}^3/\text{s}$, Dist. = 21 m**



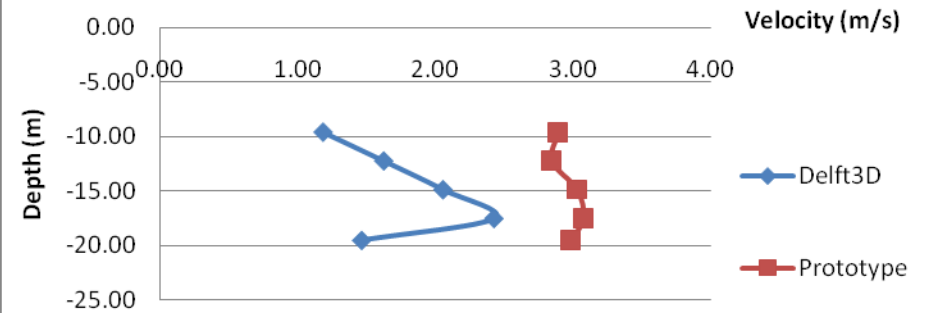
**Velocities in the Vertical Direction
 $Q=383.97 \text{ m}^3/\text{s}$, Dist. = 42 m**



Velocities in the Vertical Direction
Q=383.97 m³/s , Dist. = 63 m



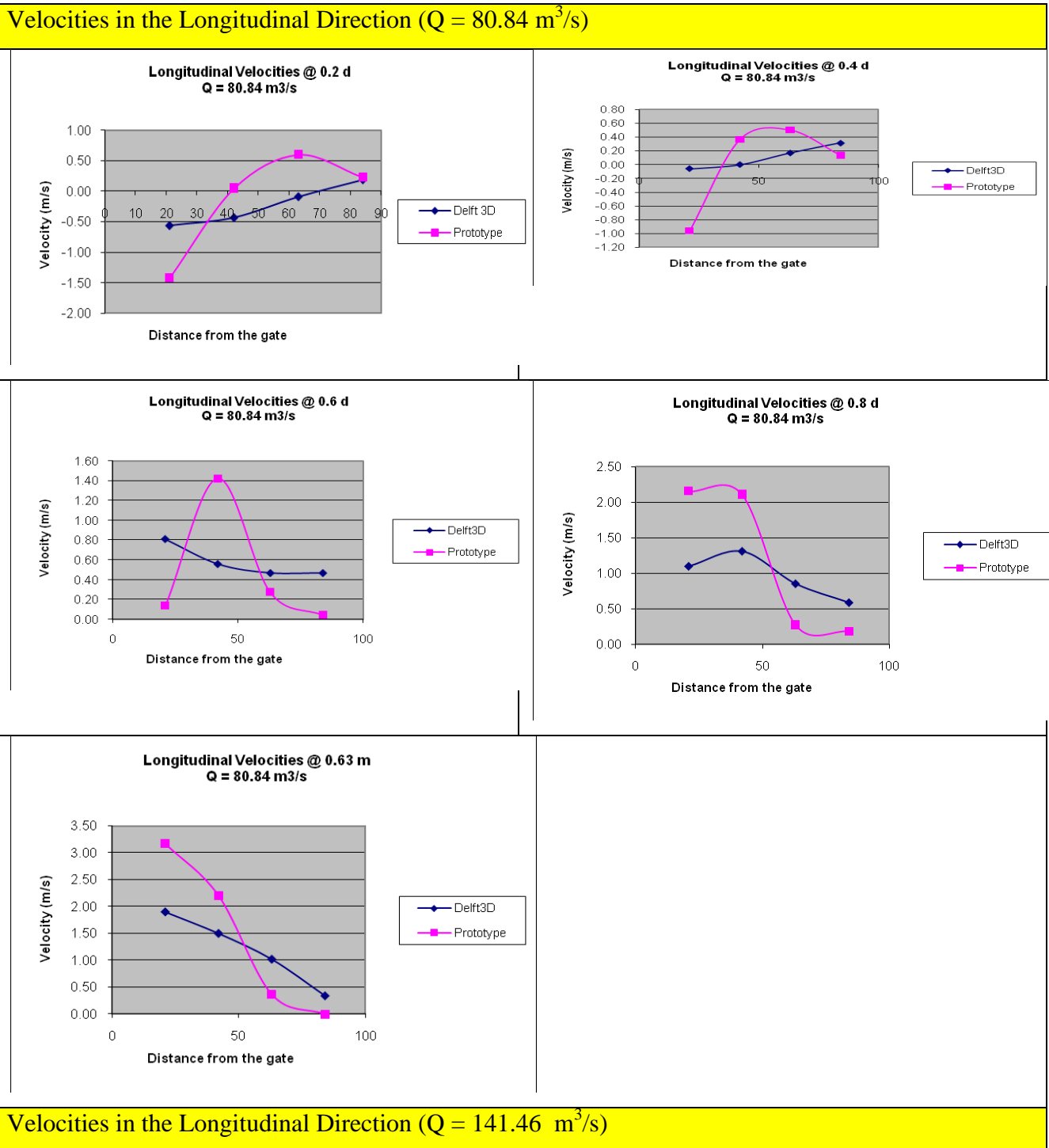
Velocities in the Vertical Direction
Q=383.97 m³/s , Dist. = 84 m

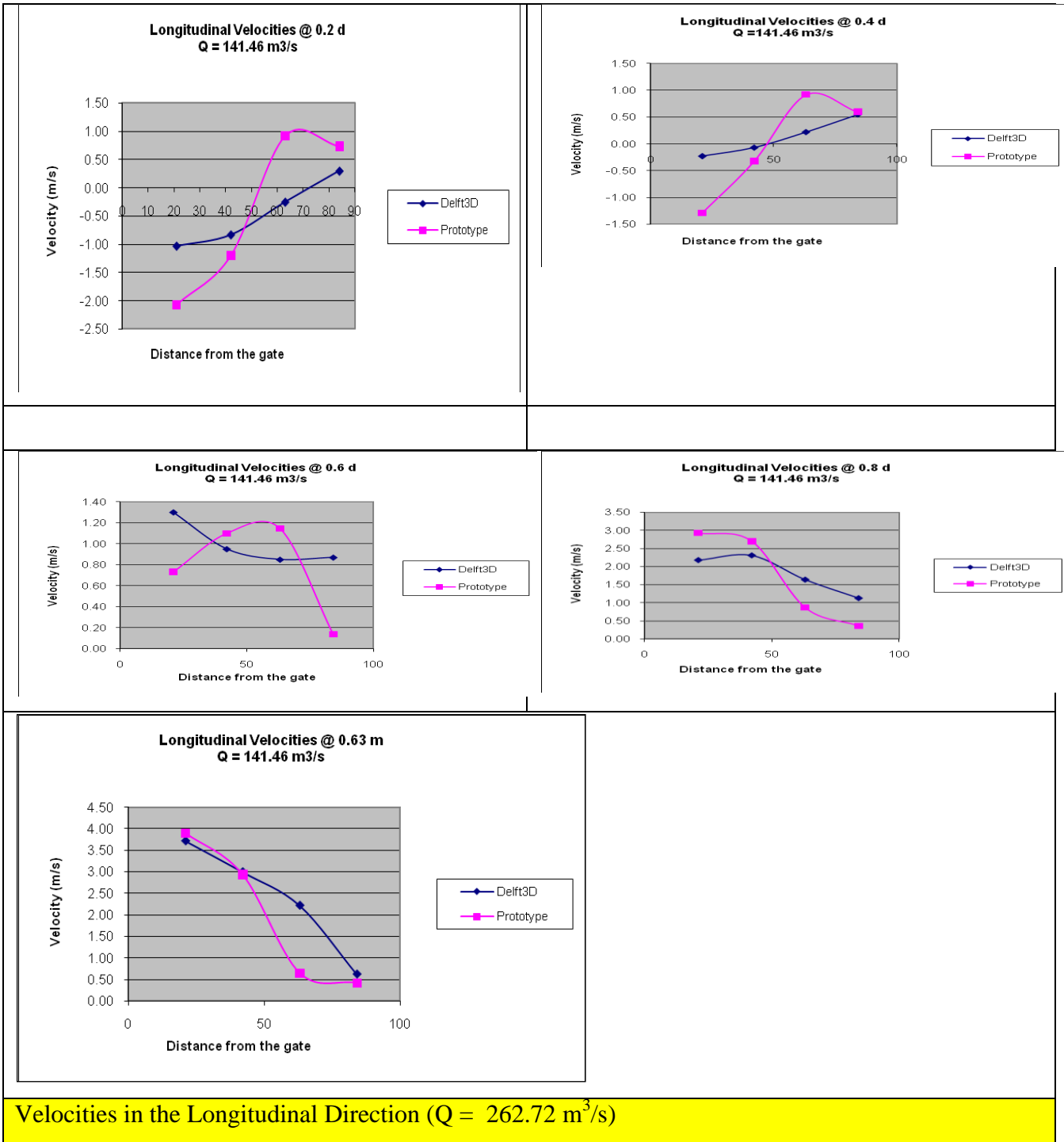


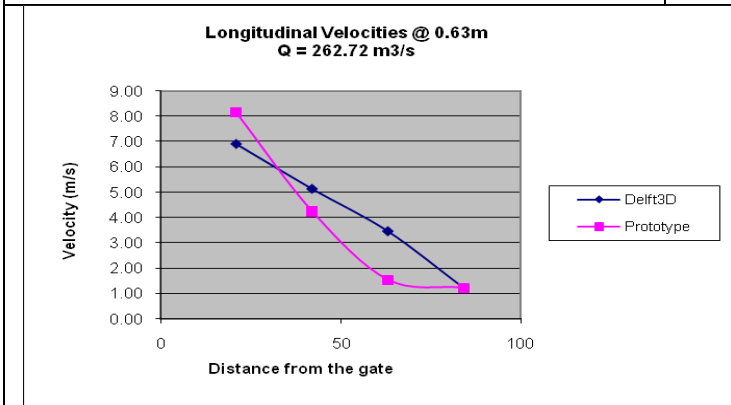
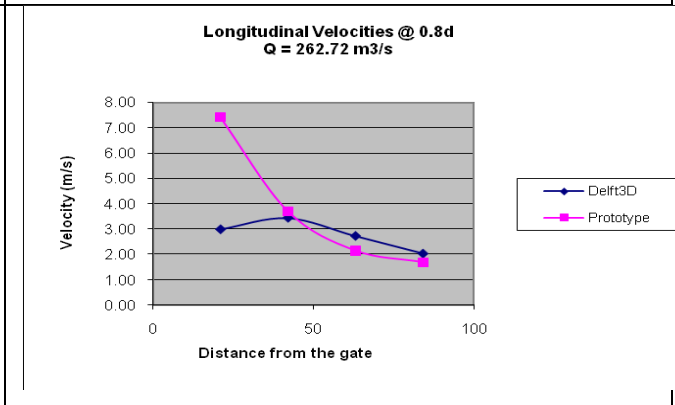
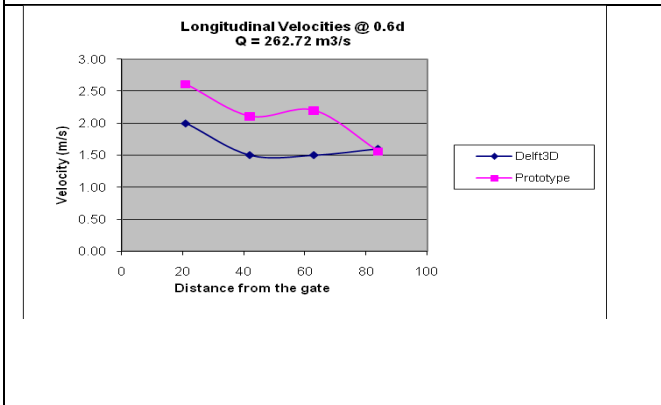
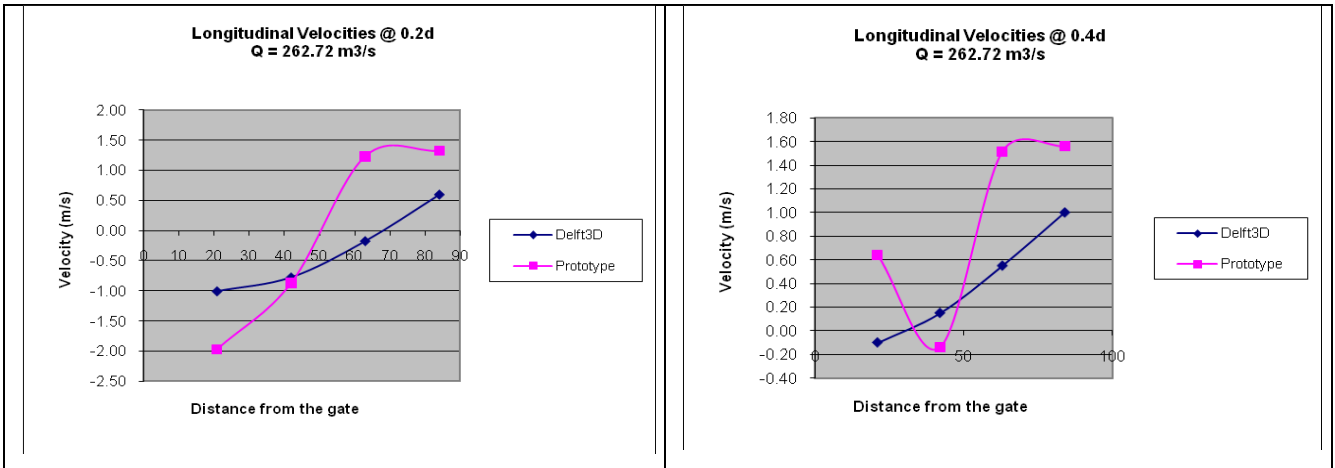
From the figures above it is remarkable that the velocity distributions from Delft 3D at distances 21 and 42 meters are more accurate than that ones at distances of 63 and 84 meters which are located out of the concrete area and near to the sloped area.

The following figures represent the longitudinal velocities along the sluiceway downstream the gated sill.

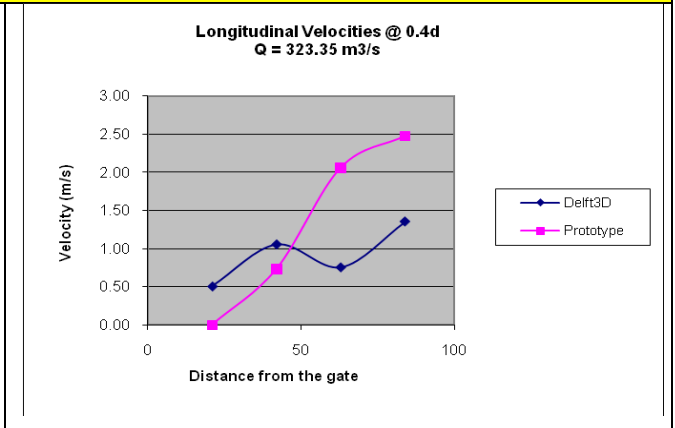
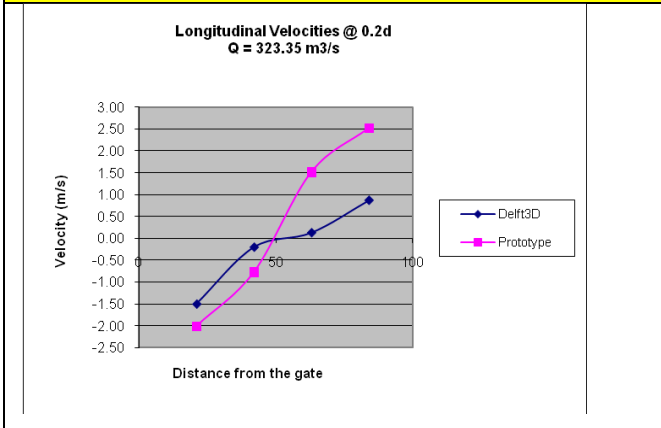
Table 4-27: Velocities in the Longitudinal Direction



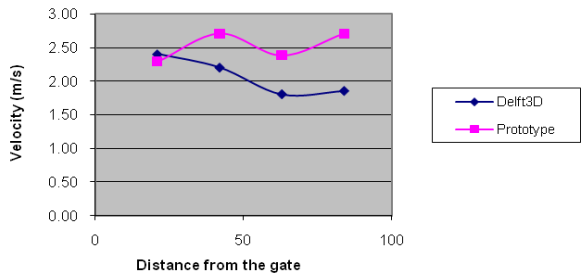




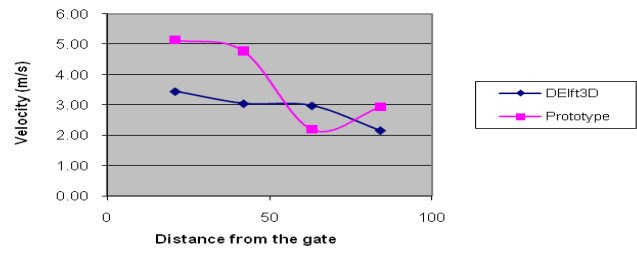
Velocities in the Longitudinal Direction (Q = 323.35 m³/s)



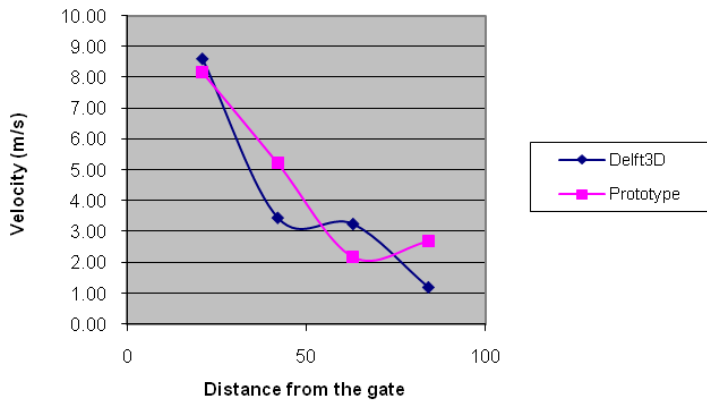
Longitudinal Velocities @ 0.6d
 $Q = 323.35 \text{ m}^3/\text{s}$



Longitudinal Velocities @ 0.8d
 $Q = 323.35 \text{ m}^3/\text{s}$

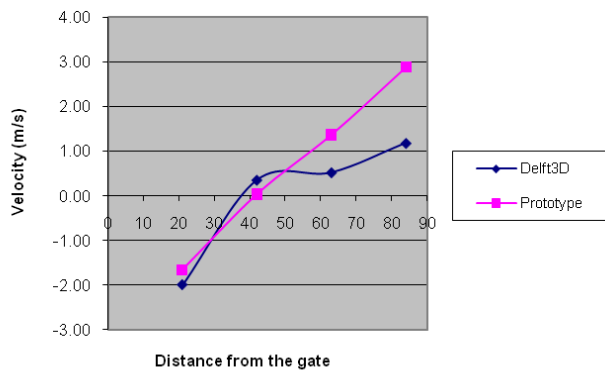


Longitudinal Velocities @ 0.63m
 $Q = 323.35 \text{ m}^3/\text{s}$

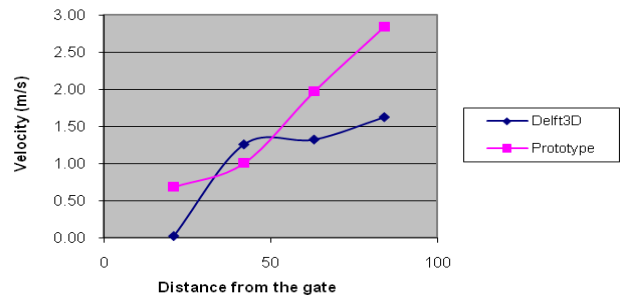


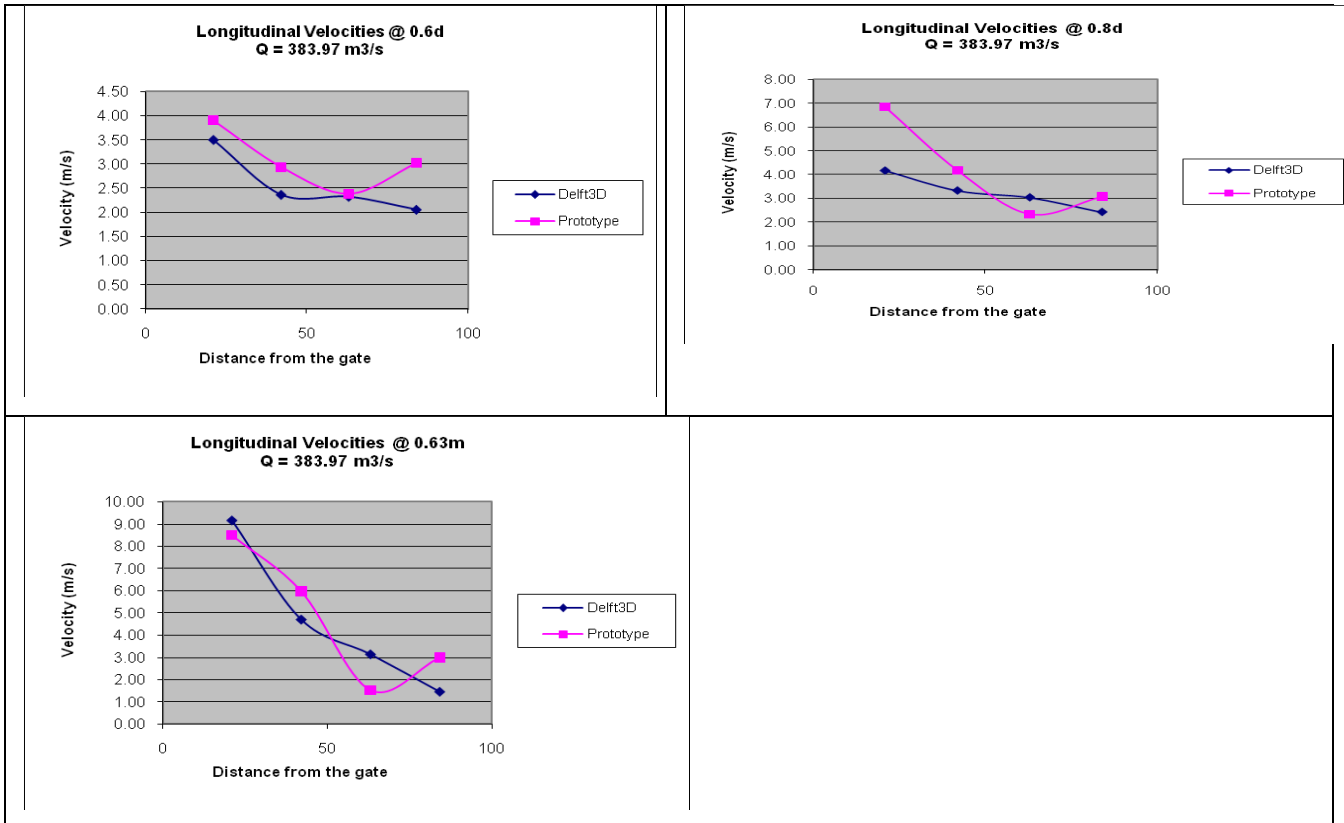
Velocities in the Longitudinal Direction ($Q = 383.97 \text{ m}^3/\text{s}$)

Longitudinal Velocities @ 0.2d
 $Q = 383.97 \text{ m}^3/\text{s}$



Longitudinal Velocities @ 0.4d
 $Q = 383.97 \text{ m}^3/\text{s}$





From figures above it is remarkable that the longitudinal velocities from Delft 3D near to the straight bed and close to the gated sill are more accurate than that ones which are near to the surface and far away from the gated sill.

The Submerged Hydraulic Jump using Barrier Option

The submerged hydraulic jump characteristics were studied using Delft 3D by applying the Barrier option to represent the gate effect. From the following figure it can be noticed that the dark blue area which located after the gate represents the negative velocities as shown on the velocity meter on the right side of the graph, this negative velocities indicate to the reverse flow occurrence or the submerged hydraulic jump existence, while the red areas indicate to the high velocities coming out from the gate.

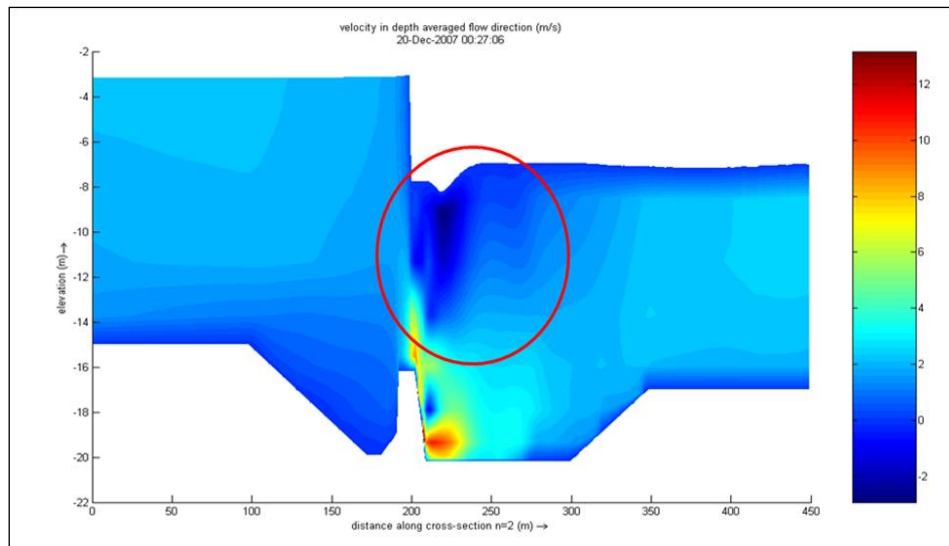


Figure 4-29: The submerged hydraulic jump

The submerged hydraulic jump length

The submerged hydraulic jump length was found from Delft 3D by using the longitudinal velocities charts at 0.2d from the water surface where it could be defined, approximately, as the length at which the velocity equal to zero which indicates the end of the submerged jump length. This procedure was checked first on the actual data of the prototype and it showed good accuracy (see figure 4-31). Figure 4-32 shows two examples on the procedure followed in finding out the jump length approximately.

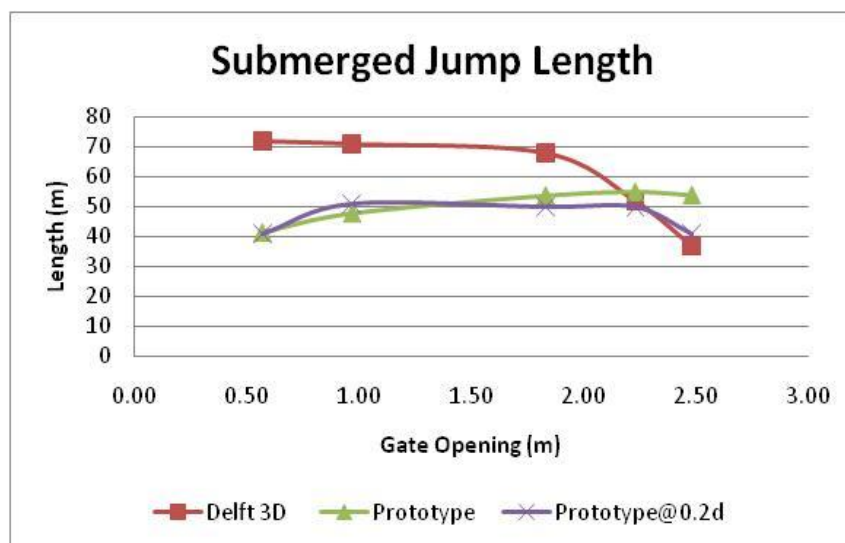


Figure 4-30: The submerged jump length

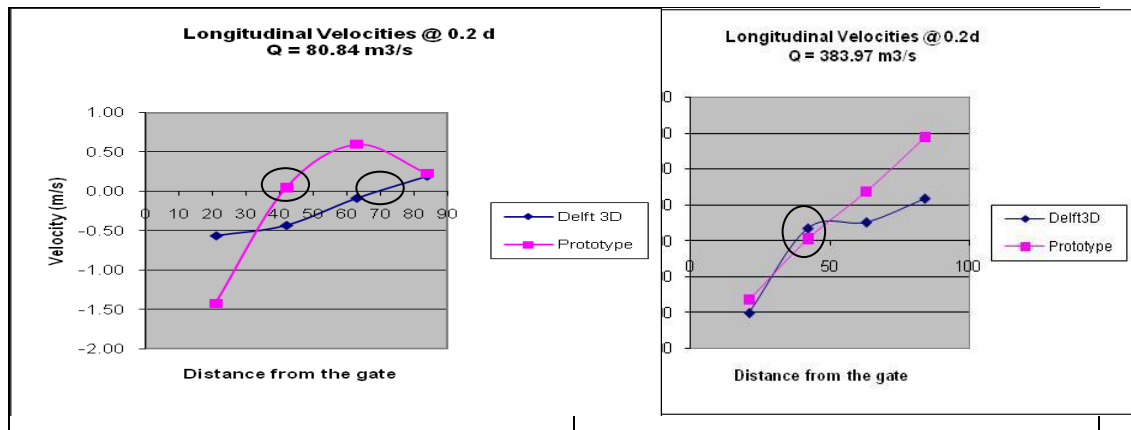


Figure 4-31: approximate estimation for the submerged jump length

The submerged hydraulic jump length was checked and calculated theoretically also using the following formulas:

$$L_{sj} = y_2(6.1+4.9 S) \quad (\text{Source: Atef Abd El-Hameed, MSc. Thesis})$$

Where

$$S : \text{Submergence Ratio} = \frac{y_t - y_2}{y_2}$$

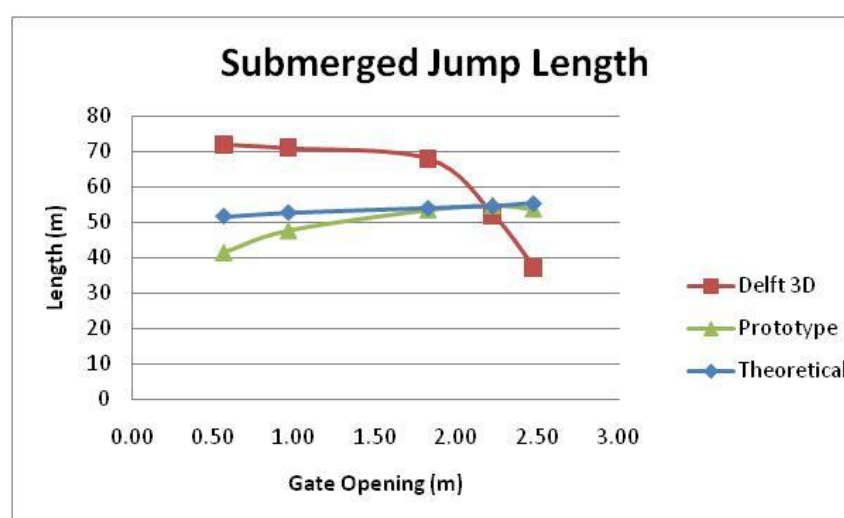
Table 4-28: calculation of the submerged jump length theoretically

Q (m ³ /s)	G.O. (m)	Hc (m)	Vc (m/s)	Fr	Y ₂ (m)	Y _t (m)	S	Lsj (m)
80.84	0.57	0.51	9.32	4.16	2.76	9.87	2.57	51.68
141.46	0.97	0.87	9.57	3.28	3.62	9.87	1.73	52.71
262.72	1.83	1.64	9.40	2.34	4.68	9.87	1.11	53.98
323.35	2.23	2.00	9.49	2.14	5.15	9.87	0.92	54.54
383.97	2.48	2.23	10.13	2.17	5.80	9.87	0.70	55.33

The following table presents a summary for all the values of the submerged hydraulic jump length from the prototype, the longitudinal velocities charts (at 0.2 d) and theoretically.

Table 4-29: a summary table for all the results regarding the jump length

Q (m ³ /s)	G.O. (m)	Yt (m)	Lsj (m) Prototype	Lsj (m) Prot. @ 0.2d	Lsj (m) Delft 3D	Lsj (m) Theoretically
80.84	0.57	9.87	41.37	41.00	72	51.68
141.46	0.97	9.87	47.67	51.00	71	52.71
262.72	1.83	9.87	53.55	50.00	68	53.98
323.35	2.23	9.87	54.81	50.00	52	54.54
383.97	2.48	9.87	53.76	41.00	37	55.33

**Figure 4-32:** the submerged jump length

From the previous figure it is clear that Delft 3D is not so accurate in finding out the submerged hydraulic jump length comparable with the prototype data, so it is recommended to carry out further deep studies in this field to improve the results.

5

DISCUSSION AND REMARKS

5.1 General

The local action research activity is mainly based on the development of research topic that represents high priority to many organizations sharing similar interest in the country level. This research topic connected about five research institution working in water related issue in Egypt. The main objectives are to strengthen country water research capacity on the basis of sharing professional experience in a collaborative manner, solving practical problem can be applied to any other basin country in the region and to facilitate building partnerships between water professionals, research and government institutions in trustful environment. The agreed research topic is "A Hybrid Approach to improve the design of stilling basin". This research intended to reach the optimum design for the stilling basin as an important component of any new barrages. However, to reach this objective via physical model will drastically increase the model cost. Therefore, the mathematical model will be used in conjunction with the physical model to attain the best results. Obtaining the suitable model to achieve the study goals is very complex in terms of lack of fund and capacity building. This model can represent a basic tool for capacity building.

Before explaining the outcome of this research, it is work noting the main comparison points for the physical and numerical models as well as their corresponding limitations

5.2 Comparison of Physical & Numerical models

Physical models provide an opportunity to observe the flow characteristics and to make measurements in limited locations. Velocity measurements in the stilling basin of the physical models are not obtainable due to excessive and complex structure of the turbulence. Three dimensional transient models provide another tool to describe, define and evaluate the flow characteristics within the stilling basin. Several models have been developed in that field like CFD (computational fluid dynamics) and Delft3D.

Numerical models can also be used to evaluate stilling basin modifications (deflectors, Baffle block removal, etc.). Physical modeling is an unalterable tool to guarantee economic and ecological design of complex hydraulic structures. Besides this "traditional" method, numerical modeling has become more and more important in the last few years. Powerful computers and improved mathematical algorithms supported this trend. Emphasis must be drawn to the fact that today numerical models are not able to compensate physical models. To simulate a three-dimensional flow field with computers under real state boundary conditions is impossible or better: unaffordable. It is for sure that engineers will go on using physical models in the near future, but with the support of numerical modeling to improve developing time, guarantee economic design and optimize the ecological value of the hydraulic structure. However, due to the complexity of the physical phenomenon related to energy dissipation and to the obvious three dimensional motion with high degree of turbulence, the use of mathematical models are subjected to further analyses. By using both the physical and numerical model a synergetic effect could be observed. The positive influences of numerical in combination with physical modeling are definitely an innovative way for engineers to develop hydraulic structures.

5.3 Limitations of the models

Most model studies involve simplifying assumptions with regard to the variables to be considered. Although the number of assumptions is frequently less stringent than that required for mathematical models, they

nevertheless introduce some uncertainty in the model design. Scale (physical) model will yield useful quantitative information about the characteristics of the prototype if it is completely similar to its prototype. Complete similarity can be obtained between the model and its prototype if the two systems are geometrically, kinematically and dynamically similar.

A true fact should be pointed out that there is no scale model is perfectly similar to its prototype. As it is already known that partial dynamic similarity or even partial geometric similarity should be satisfied. Consequently some discrepancy called scale effect between the results based on model study and prototype will always exist. The magnitude of scale effect can be assessing on the basis of experience and initial assumptions.

Table 5-1: Limitations of Physical and Numerical Models

Physical Model	Numerical Model
Model size (laboratory)	Storage capacity
Discharge (pumping capacity)	Computational speed
Energy head (pumping capacity)	incomplete set of equations
Model laws	Turbulence hypothesis
Minimum model scale	Accuracy of assumed relationships
Surface tension, viscosity, roughness	Availability of coefficients and initial
Model size and boundary conditions	Space and time resolution
Measuring methods	Numerical stability & boundary condition
Data collection	Convergence of the solution scheme

6

CONCLUSIONS AND RECOMMENDATIONS

6.1 Conclusions

General

It is obvious that the use of the numerical model became a useful tool in the engineering practice. However, careful analyze of the type of model used is still needed in several cases, such as the case of the rapid varied flow, to save time and to obtain the most reliable solutions. At the same time due to simplified calculation schemes, the use of complementary laboratory studies increases the reliability of the design solutions. The results of these studies cannot yet be overlooked.

Subsequently, the main conclusions and recommendations derived in this study are briefly presented as follows:

The hydraulic performance of the case study

1. Water drop over sill (53.45) is higher than that one over sill level (52.80).
2. The change in the sill levels has no significant influence on the upstream water levels.
3. The baffle blocks in case of the 3D model have no significant influence on the water levels or the head losses in case of fully open gate, nevertheless there is a slight increase in the head losses in case of partially open gates.
4. In case of fully open gate the total head losses are small in absolute values due to the relatively small crest height above the river bed.
5. Head losses are increasing with the discharge in case of fully open gate.
6. The head losses in case of partially open gates are much higher than in case of fully open gates due to the existence of the hydraulic jump. Moreover the losses are inversely proportional with the discharge in case of partially open gates.
7. The steady jump with energy dissipation between 45 and 70 % is limited to small gate openings, e.g. low discharges from 600 to 1700 m³/s.

The use of Delft 3D models and comparison with 2D Scale models

1. In general the numerical model proved to be efficient in studying the flow capacity of the structure analyzed in this study (the discharges and the corresponding upstream and downstream water levels and the average approach velocities).
2. 2DV Sigma grid is not sensitive w.r.t the bed changes (no significant changes in water levels) for discharges greater than 2000 m³/s.
3. 1D and 2DV (Z-Grid) have good correlations with the flume data in cases of the head loss and drop over the sill.
4. 2DV (Z-Grid) gives good results in case of study the velocity values near the horizontal uniform bed and steady flow (e.g. at the U/S & D/S gauge stations), 1D model has a good agreement with the flume data also nevertheless it gives slight higher values because it gives depth averaged velocities.
5. In case of partially open gate 1D Model gave good results for the calibration of the radial gate opening particularly with low discharges.
6. Z-Grid model is quite efficient in representing the submerged hydraulic jump.
7. In general the new option Barrier is reliable in calibrating the gate openings by changing the losses coefficient.

8. 2DV Z-grid combined with Barrier option gives good results for the velocity profiles in the vertical direction near the gate opening and less accuracy is obtained far downstream the gate. The reason of the low accuracy is that the velocity distribution drawn in the riprap area was drawn, in the flume model, after reaching the steady state condition of the local scour but it was assumed fixed bed in the numerical model).
9. Velocities in the longitudinal direction are more accurate near the bed than near the surface.
10. Due to the low accuracy near the surface the submerged hydraulic jump length obtained from Delft 3D is not so accurate.
11. Delft 3D does not show remarkable sensitivity w.r.t. the roughness or the turbulence module, in other words the results do not improve by changing the roughness or the turbulence module.
(Remark: it is logic that there is no significant changes in the results w.r.t. the turbulence module because it is an isotropic condition).

6.2 Recommendations

1. In general it is recommended to use Z-Grid (2DV) model to study water levels or head losses in case of fully open gates and to study the submerged hydraulic jump characteristics in case of partially open gates.
2. In cases of studying the flow processes in the normal conditions (partially open gates) 1D Model could be used efficiently to study water levels, water depths, head losses but in case of studying the velocities or Froude number it is recommended to calculate the velocity at the vena-contracta using the data (water depths and discharges) obtained from the 1D Model to calculate the velocities and Froude number at the vena-contracta.
3. Numerical models should be calibrated with scale models to be used in further applications for similar cases.
4. It is recommended to use Barrier option to study the gate opening calibration, velocities near the gate and velocities near the bed.
5. It is recommended to use K- ϵ turbulence model.
6. Further studies should be done on the hydraulic jump characteristics for submerged and free jumps.
7. A separate intensive studies should be carried out on the local scour downstream the stilling basins.

7 REFERENCES

- Abdel-Aal, G.M. (1995): Control of hydraulic jump in contracted streams by gradual expansion, PhD thesis, Faculty of Engineering Zagazig University.
- Abdel-Aal, G.M. (1999): Study of hydraulic jump in gradually expanding rectangular channels, *Scientific Bulletin*, Ain Shams University, Faculty of Engineering, 34(4), December, 339-351.
- Abdel-Aal, G.M. (2000): A study of stilling basin in non-prismatic channels, *Scientific Bulletin*, Faculty of Engineering, Ain Shams university, 35(1), March, 207-222..
- Abdel Azim, M. (2005), "Improving Stilling Basin Designs for the New Barrages on the Nile River", PhD. thesis, HRI -Egypt.
- Abd El Hameed, A. (1990), "Study of Submerged Flow Characteristics under Silled Sluice Gates", MSc. thesis, Ain Shams University.
- Abdel Wahab, A. (2002): Characteristics of flow in diverging stilling basins, PhD thesis, Faculty of Engineering, Zagazig university.
- Ahmed M. A., James F. R., Ghassan A. and Steven R. A. (1993): Characteristics of B-jump with different toe locations, *Journal Hydraulic Engineering.*, ASCE, 119(8), 938-948.
- Belanger J.B. (1828): Essay on the numerical solution of some problems relative the steady flow of water, Carilian-Goeury, Paris.
- Boris A. B. and Arthur E. M. (1935): The hydraulic jump in terms of dynamic similarity, Transactions, ASCE, 101, 630-680.
- Bradley, J. N. and Peterka, A. J. (1957): The hydraulic design of stilling basins, hydraulic jumps on a horizontal apron, *J. Hydr. Div.*, Proc. ASCE, 83(10), 1401- 1425.
- Bureau of Reclamation. (1955): Research studies on stilling basins, energy dissipaters, and associated appurtenance, U.S., Hydraulic Laboratory Report No. Hyd-339, June.
- Busnelli, M. M. (2001) Numerical Simulation of Free Surface Flows with Steep Gradients, PhD thesis, TUDelft, the Netherlands.
- Casulli, V., and Stelling, G. S. (1998) "Numerical Simulation of Three-Dimensional Quasi- Hydrostatic, Free-Surface Flows", ASCE J. Hydr. Eng., 124(7), 678-686.
- Casulli, V. (1999) A Semi-Implicit Finite Difference Method for non-Hydrostatic, Free-Surface Flows, Int. J. Num. Methods in Fluids, 30, 425-440.
- Chanson, H. (1999): The hydraulics of open channel flow: an introduction, Butterworth- Heinemann, London, UK.
- Chow, V. T. (1988): Open channel hydraulics, McGraw-Hill Book, Co. Inc. 21 printing, International Student edition, 393-438.
- Delft 3D Manual version 3.14, October 2007.

- Ead S. A. and Rajaratnam N. (2002): Hydraulic jump on corrugated beds, *J. Hydr. Eng.*, ASCE, 128(7), 656-663.
- Edward A. (1959): Hydraulic energy dissipaters, McGraw-Hill Book Co. Inc., New York, N.Y.
- Elzeir, M. A. (1996): Modeling Flow in Compound Channels, PhD thesis, K.U. Leuven, Belgium.
- Ferreri G. B., and Nasello C. (2002): Hydraulic Jumps at Drop and Abrupt Enlargement in Rectangular Channel, *J. Hydr. Res.*, IAHR, 40(4).
- Foster, J. W. and Shrinde, R. A. (1950): Control of hydraulic jump by sills, Transactions, ASCE, Vol. 155, 973-1022.
- France P. W. (1981): Analysis of the hydraulic jump within a diverging rectangular channel, Proc. Instn. Civil Engineers. Part 2, June, 71, 369-378.
- French R. H. (1986): Open channel hydraulics, McGraw-Hill.
- Giovanni B. F. and Carmelo N. (2002): Hydraulic jump at drop and abrupt enlargements in rectangular channel, *J. Hydr. Res.*, IAHR, 40(4), 491-505.
- Hager W.H. (1995): Cascades, drops, and rough channels, Energy Dissipaters. D. L. Vicher & W. H. Hager, 151-166. A. A. Balkema / Rotterdam/ Brookfield.
- Hager W. H. (1985): Hydraulic jump in non-prismatic rectangular channels, *J. Hydr. Res.*, IAHR, 23(1), 21-35.
- Hager, W. H. and Bretz, N. V. (1986): Hydraulic jumps at positive and negative steps, *J. Hydr. Res.*, IAHR, 24(4), 237-253, Discussion 25(3), 1987.
- Hager, W.H. and Sinniger, R. (1985): Flow characteristics of the hydraulic jump in a stilling basin with an abrupt bottom rise, *J. Hydr. Res.*, IAHR, 23(2), 101-113.
- Hager, W.H. (1992): Energy dissipaters and hydraulic jump, Kluwer Academic Publishers, Dordrecht, The Netherlands.
- Hager, W.H., Bremen, R. and Kawagoshi, N. (1990): Classical hydraulic jump: Length of roller, *J. Hydr. Res.*, IAHR, 28(5), 591-608.
- Hager, W.H., Li, D. (1992): Sill controlled energy dissipater, *J. Hydr. Res.*, IAHR, 30(2), 165-181.
- Herbrand K. (1973): The spatial hydraulic jump, *J. Hydr. Res.*, IAHR, 11(3), 205-218.
- Hirsch, C. (1990): Numerical Computation of Internal and External Flows, Vol. 2: Computational Methods for Inviscid and Viscous Flows, John Wiley & Sons, 691 pp.
- Hsu, E. (1950): Discussion of "Control of the hydraulic jump by sills," by Foster, J and Skrinde, R.A, Transactions of the ASCE, 115, 988-991.
- Huges, W. C. and Flack, J. E. (1984): Hydraulic jump properties over a rough bed, *J. Hydr. Eng.*, ASCE, 110(12), 1755-1771.
- Hydraulic Research Institute (1999), "New Naga Hammadi Barrage Hydraulic Model Investigations - Sluiceway Detail Model", HRI Quanater- Egypt.
- Hydraulic Research Institute (2007), "local action research project for strengthening the collaborative work between the Egyptian institutions working in the water sector", Quanater- Egypt.

- Jain, A.K. (1990): Fluid mechanics, Khanna Publishers, Delhi, India, Sixth Edition.
- Khalifa, A. M., and McCorquodale J. A. (1979): Radial hydraulic jump, *J. Hydr. Div.*, ASCE, 105(HY9), 1065-1078.
- MacCorquodal, J. A., and Mohamed M. S. (1994): Hydraulic jumps on adverse slopes, *J. Hydr. Res.*, 32(1), 119-130.
- McCorquodal, J. A. and Khalifa, A. M. (1983): Internal flow of the hydraulic jump, *J. Hydr. Engrg.*, ASCE, 109(6), 684- 701.
- McCorquodal, J. A. (1986): Hydraulic jumps and internal flows, Encyclopedia of fluid mechanics, Gulf Publishing Co., Houston, Texas, 122-137.
- Michelle M., Antonio P., and Hubert C. (2003): Tailwater level effects on flow conditions at an abrupt drop, *J. Hydr. Res.*, IAHR, 41(1), 39-51.
- Mohammed A. H.S. (1991): Effect of roughened-bed stilling basin on length of rectangular hydraulic jump, *J. Hydr. Engrg.*, ASCE, 117(1), 83-93.
- Negm, A.M. (2000): Hydraulic performance of rectangular and radial stilling basins, Advances in Hydro-Science and Eng. Proc., 26-29, Seoul-Korea.
- Negm, A. M. (2000): Semi-theoretical approach for detecting of cavitatoin at steps in horizontal stilling basins-hydraulic jump type, Al-Azhar Eng. Sixth International Conference, Sept. 1-4, 167-176.
- Nettleton, P. C. and McCorquodal J. A. (1983): Radial stilling basin with baffles, Proceeding Canadian Society for Civil Engineering Montreal, Canada, 561-580.
- Ohtsu, I and Yasuda, Y. (1990): Transition from supercritical to subcritical flow at an abrupt drop, *J. Hydr. Res.*, IAHR, 29(3), 309-328.
- Ohtsu, I., and Yasuda, Y. (1991): Hydraulic jump in sloping channel, *J. Hydr. Engrg.*, ASCE, 117(7), 905-921.
- Owais, T. M. (1983): Lecture notes on open channel flow and hydraulic modeling, Vol. I, Second Edition, Faculty of Engineering, Zagazig University.
- Quraishi, A. A. and Al-Brahim, A. M. (1992): Hydraulic jump in sloping channel with positive or negative step, *J. Hydr. Res.*, IAHR, 30(6), 769-782.
- Patankar, S. V. and Spalding D. B. (1972) "A Calculation Procedure for Heat, Mass, and Momentum Transfer in Three-Dimensional Parabolic Flows", *Int. J. Heat Mass Transfer*, 15, 1787-1806.
- Rageh, O.S. (1999): Effect of baffle blocks on the performance of radial hydraulic jump, Proc. 4th Int. Water Technology Conf. (IWTC99), Alex., Egypt, 255-269.
- Rouse, H. and Simon, I. (1957): History of hydraulics, Dover Publications, Inc. New York.
- Shri Ram C. (2003): Direct equation for hydraulic jump elements in rectangular horizontal channel, *J. Irrig. & Drain.*, ASCE, 129(4), 291-294.
- Shukry, A., Elkhawalka, S. and Elganaini, M. (1987): Regulators and barrages, Irrigation and Hydraulics department, Faculty of Engineering, Ain Shams University, Cairo, Egypt.
- Stansby, P. K., and Zhou, J. G. (1998): Shallow-Water Flow Solver with non-hydrostatic Pressure: 2D Vertical Plane Problems, *Int. J. Num. Methods in Fluids*, 28, 541-563.
- Stefano P. and Alssandro P. (2000): Limiting and sill-controlled adverse-slope hydraulic jump, *J. Hydr. Engrg.*, ASCE, 126(11), 847-851.

- Stelling, G.S. and Duinmeijer, S.P.A., (2003), "A staggered conservative scheme for every Froude number in rapidly varied shallow water flows", *International Journal for Numerical Methods in Fluids*. No. 43.
- Subramania K. (1982): *Flow in open channel*, McGraw Hill Publishing Company, New Delhi, India.
- Toch, A. (1955), "Discharge characteristics of tainter gates", *Transactions, ASCE* 120, pp. 290-300.
- Toro, E. F. (1997): *Riemann Solvers and Numerical Methods for Fluids Dynamics*, Springer, 592 pp.
- Vreugdenhil, C. B. (1994): *Numerical Methods for Shallow Water Flow*, Kluwer Academic Publishers, Dordrecht, 262 pp.
- Wafaie, E. M. (1990): *Design of roughened bed radial stilling basins applied to Egyptian practice*, PhD, Faculty of Engineering, Ain Shams University, Cairo, Egypt.
- Wesseling P. (2001): *Principles of Computational Fluid Dynamics*, Springer, 644 pp.

List of Research Group Members

Name	Organization
Dr. Ahmed Sayed Mohamed Ahmed	Hydraulics Research Institute
Dr. Abdelazim M. Ali	Hydraulics Research Institute
Dr. Ahmed El-Belasy	Hydraulics Research Institute
Dr. Mohamed Roushdy	Hydraulics Research Institute
Eng. Mohamed Bahgat	Hydraulics Research Institute
Eng. Abdelhamid Abdelhaq	Hydraulics Research Institute
Prof. Dr. Karima Attia	Nile Research Institute
Dr. Medhat Aziz	Nile Research Institute
Eng. Mohamed Ali Hamed	Nile Research Institute
Eng. Heba El Sersawi	Nile Research Institute
Prof. Dr. Sonia El-Serafy	Ain Shams University
Eng. Peter Ryad	Ain Shams University
Prof. Dr. Moahmed Sobeih	Menofia University
Dr. Essam El-Din	Menofia University
Prof. Dr. Mohamed El-Zeir	Menia University

Full Profiles of Research Group Members are available on: *The Nile Basin Knowledge Map*

<http://www.NileBasin-Knowledgemap.com>

A Hybrid Approach to Improve the Design of Stilling Basin

In the framework of activating and improving the collaboration between local institutions in each Nile Basin Countries, the Nile Basin Capacity Building Network (NBCBN) has initiated and supports a research program with a so-called local action research project that has been activated during the workshop organized in Cairo from 5-7 March 2007. Amongst this program is to strengthening the collaborative work between the Egyptian institutions working in the water sector. The involved Egyptian institutions are : Ain Shams University, Hydraulics Research Institute, National Water Research Center, Menia University, Menofia University Nile Research Institute, National Water Research Center

The research point was properly selected to meet the most critical research interest for most of the involved institutions in order to make sure that the professional experience of the above mentioned institutions are fully utilized. It is intended that the selected research topic represents a practical problem that can be applied to many of the Nile Basin Countries. This includes the design of an energy dissipating structure which is called the stilling basin. The research topic pertaining to stilling basin has been described in the research methodology that is divided into stages. These stages are to: Provide an overview on the stilling basin, collect the available data, construct and conduct a physical model study, develop or adopt a numerical model. The developed or adopted numerical model would eventually be utilized to investigate the flow field in the stilling basin and derive the flow conditions that will be employed in designing the stilling basin.